BRNO UNIVERSITY OF TECHNOLOGY
VYSOKÉ UČENÍ TECHNICKÉ V BRNĚ

FACULTY OF ELECTRICAL ENGINEERING AND COMMUNICATION
DEPARTMENT OF RADIO ELECTRONICS

FAKULTA ELEKTROTECHNIKY A KOMUNIKAČNÍCH TECHNOLOGIÍ
ÚSTAV RADIOELEKTRONIKY

MODELS OF CONTROL CHANNELS IN THE LTE SYSTEM

DOCTORAL THESIS
DIZERTAČNI PRÁCE

AUTHOR Ing. JIŘÍ MILOŠ
AUTOR PRÁCE

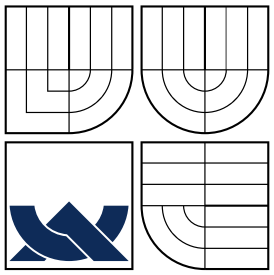

BRNO UNIVERSITY OF TECHNOLOGY
VYSOKÉ UČENÍ TECHNICKÉ V BRNĚ

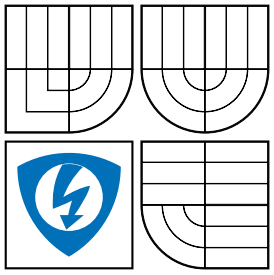

FACULTY OF ELECTRICAL ENGINEERING AND COMMUNICATION
DEPARTMENT OF RADIO ELECTRONICS

FAKULTA ELEKTROTECHNIKY A KOMUNIKAČNÍCH TECHNOLOGIÍ
ÚSTAV RADIOELEKTRONIKY

MODELS OF CONTROL CHANNELS IN THE LTE SYSTEM

MODELY ŘÍDICÍCH KANÁLŮ SYSTÉMU LTE

DOCTORAL THESIS
DIZERTAČNI PRÁCE

AUTHOR
AUTOR PRÁCE
Ing. JIŘÍ MILOŠ

SUPERVISOR
VEDOUCÍ PRÁCE
prof. Ing. STANISLAV HANUS, CSc.

BRNO 2014

ABSTRACT

The doctoral thesis is focused on a signal processing in the LTE physical control channels and performance analysis of control information transmission according to receiving conditions. The thesis is divided into two parts. The first part deals with simulation of the transmission of control information in baseband. The created simulators for uplink and downlink are presented. The simulations are performed for all possible system settings and various channel models. The MIMO influence on a quality of control information reception under fading channels is also presented. The second part of the thesis is focused on LTE utilization in shared channel ISM (2.4 GHz). The basic LTE application concept for ISM band is presented. This concept is fundamental to created simulation scenario. The chapter also presents the LTE and Wi-Fi coexistence simulator in 2.4 GHz ISM passband. The coexistence simulation are presented according to simulation scenario and the results are shown. The simulated coexistence analysis results are verified in laboratory environment. The comparison of the simulated and the measured coexistence analysis results is crucial for further optimization of the coexistence simulator. Recommendations for optimal and reliable operation of LTE are specified according to the simulated and the measured results. Recommendations should be useful to the reliable transmission of LTE control information in bad receiving conditions.

KEYWORDS

LTE, physical layer, control channels, simulator, MATLAB, interference, ISM band

ABSTRAKT

Dizertační práce se zabývá zpracováním signálu fyzických řídicích kanálů systému LTE a vyšetřováním bitové chybovosti při přenosu řídicí informace z vysílače do přijímače v závislosti na podmínkách příjmu. Práce je rozdělena do dvou hlavních částí. První část práce je zaměřena na simulaci přenosu řídicí informace LTE v základním pásmu. Jsou zde prezentovány vytvořené simulátory řídicích kanálů ve směru uplink i downlink. Simulace jsou provedeny pro všechny druhy nastavení systému a základní modely přenosového prostředí. Jsou zde popsány výsledky vlivu použití MIMO technologií na kvalitu příjmu řídicí informace především v únikových kanálech. Druhá část práce je zaměřena na možnost nasazení systému LTE ve sdíleném pásmu ISM (2.4 GHz). Jsou zde představeny základní koncepce použití, na jejichž základě je vytvořen scénář simulací. Kapitola dále popisuje tvorbu simulátoru koexistence LTE a systému Wi-Fi v přeneseném pásmu ISM 2.4 GHz. Jsou zde uvedeny výsledky simulací koexistence LTE a rušivého systému Wi-Fi provedených dle vytvořeného scénáře. Výsledky simulací koexistence LTE a Wi-Fi jsou ověřeny měřením v laboratorních podmínkách. Toto porovnání je důležité z hlediska optimalizace simulátoru koexistence. Dle výsledků obou typů simulací a měření jsou stanovena provozní doporučení, která mají přispět k bezpečnému a spolehlivému vysílání a příjmu řídicích informací LTE i při nepříznivých podmínkách příjmu.

KLÍČOVÁ SLOVA

LTE, fyzická vrstva, řídicí kanály, simulátor, MATLAB, interference, ISM pásmo

DECLARATION

I declare that I have written my doctoral thesis on the theme of "Models of control channels in the LTE system" independently, under the guidance of the doctoral thesis supervisor and using the technical literature and other sources of information which are all quoted in the thesis and detailed in the list of literature at the end of the thesis.

As the author of the doctoral thesis I furthermore declare that, as regards the creation of this doctoral thesis, I have not infringed any copyright. In particular, I have not unlawfully encroached on anyone's personal and/or ownership rights and I am fully aware of the consequences in the case of breaking Regulation § 11 and the following of the Copyright Act No. 121/2000 Coll., and of the rights related to intellectual property right and changes in some Acts (Intellectual Property Act) and formulated in later regulations, inclusive of the possible consequences resulting from the provisions of Criminal Act No. 40/2009 Coll., Section 2, Head VI, Part 4.

Brno ....
(author's signature)

BIBLIOGRAPHIC CITATION

MILOŠ, J. *Models of control channels in the LTE system*. Doctoral thesis. Brno: Brno University of Technology, Faculty of Electrical Engineering and Communication, 2014. pp. 109.

ACKNOWLEDGEMENT

I would like to express my gratitude to my supervisor prof. Ing. Stanislav Hanus, CSc., for his advice, invaluable guidance and help throughout my research. I would also thank to Ing. Otto Vodvářka from Rohde & Schwarz – Praha, s.r.o., who lent me the R&S FSW26 signal analyzer.

Last but not least, I would like to thank Gabriela and my family for their endless encouragement and patience throughout my studies.

Brno ....
(author's signature)

Faculty of Electrical Engineering
and Communication
Brno University of Technology
Technicka 12, CZ-61200 Brno
Czech Republic

http://www.six.feec.vutbr.cz

ACKNOWLEDGEMENT

The described research was performed in laboratories supported by the SIX project; the registration number CZ.1.05/2.1.00/03.0072, the operational program Research and Development for Innovation. A support of the project Systems of Wireless Internet Communication (SYWIC) LD11081 in frame of COST IC 0906 action is also gratefully acknowledged.

Brno ....

(author's signature)

EVROPSKÁ UNIE
EVROPSKÝ FOND PRO REGIONÁLNÍ ROZVOJ
INVESTICE DO VAŠÍ BUDOUCNOSTI

To my beloved Gabriela and my parents

CONTENTS

LIST OF FIGURES

LIST OF TABLES

1 INTRODUCTION

A growing number of users and the actual demand for mobile applications and multimedia services require an intelligent user equipment (UE) as well as general innovation of cellular networks. The current second and third generation cellular networks (GSM, UMTS or their following WCDMA versions based on the IP protocol – HSxPA, HSPA+) will not be able to cover increasing user traffic. Due to these circumstances, the 3GPP organisation[1] developed a new communication standard whose overall system capacity and given services, satisfy the requirements of present-day cellular network users [1]. Performance requirements for the new cellular network were primarily *peak data rate* (100 Mbps instantaneous in downlink, 5 bps/Hz and 50 Mbps instantaneous in uplink 2.5 bps/Hz, both within 20 MHz system bandwidth), *control plane capacity* (minimally 200 users per cell within a 5 MHz bandwidth allocation), *user plane latency* (less than 5 ms), *user throughput*, *spectrum efficiency*, *mobility* (E-UTRAN optimized for mobile speed from 0 to 15 km/h; mobile speed from 15 to 120 km/h shall be supported with a high performance; mobility with speed between 120 and 350 km/h is preserved), *spectrum flexibility*, *coexistence and interworking with other wireless standards* (mainly with 3GPP Radio Access Technology) and *low complexity* [2]. A number of these contradictory targets were implemented and the developed cellular standard is called the Long Term Evolution (LTE).

The LTE is a cellular network standard, which is still inherent to the third generation of these networks. Some sources provide information that LTE is one of the fourth generation cellular network standards. A full-featured standard of the fourth generation is the LTE-Advanced. Despite the fact that the LTE Physical Layer Release 8 was published in December 2008, it is still necessary to investigate the LTE system and make it perfect not only due to the increasing demands for services but also due to the question of overall system performance and security [3]. The above mentioned targets together with demands for system performance and security are achievable by sufficient and robust signal processing of control information on a physical layer. Unfortunately, there is inadequate attention in creating physical control channel models and their consecutive performance analysis. A proper control information signal processing analysis and interpretation of its results may help to optimize overall system performance. Also a study of the LTE coexistence with other cellular or wireless standards is necessary. A growing trend of releasing LTE to the former analog TV frequency bands or ISM bands brings a significant need for coexistence analyses especially in the field of control information or physical control channel performance.

[1]The 3rd Generation Partnership Project (3GPP) - a project where six organisations unified to create cellular communication standards, see http://www.3gpp.org.

1.1 Overview of the LTE Physical Layer

Former cellular networks e.g. GSM, UMTS or HSxPA, HSPA+ requires Signal to Noise Ratio (SNR) or Signal to Interference Ratio (SIR) margins of 20–30 dB for good voice quality [4]. LTE has a different approach to reduce fading. The LTE physical layer transmission scheme in both directions (uplink and downlink) is based on the Orthogonal Frequency Division Multiplex (OFDM) technique due to its robustness to frequency-selective fading, similar as in WiMAX or WLAN standards. In downlink, LTE uses Orthogonal Frequency Division Multiple Access (OFDMA) [5,6]. This technique takes advantages of a basic OFDM with the possibility of user division in the frequency and time domain. This feature together with effective channel estimation provides the possibility of effective channel equalization for every single user and scheduling (it is provided by higher layers).

In uplink, LTE uses Single Carrier-Frequency Division Multiple Access (SC-FDMA) based on Discrete Fourier Transform (DFT) spreading. The SC-FDMA transmission scheme was chosen due to its very low Peak to Average Power Ratio (PAPR) of the transmitted signal [7]. Single-carrier based transmission techniques allows more efficient utilization of the power amplifier. As a disadvantage, in contrast to using OFDMA in downlink, there can be less resistance towards frequency-selective fading. Another advantage is the possibility of a scalable bandwidth allocation in LTE which is easily applicable in OFDM based systems.

Also using multiple antennas at the base station (BS) and UE makes a high performance system. The multiple antenna technique is used in different configurations in LTE [7]. The receive diversity technique is a relatively old and utilized way to improve reception in uplink. Multiple antennas on the transmitter side are used for transmit diversity technique and also beamforming as an addition. In LTE, receive and transmit diversity techniques are used in LTE especially in control channels. The closed and open loop spatial multiplexing technique is used in traffic channels only [5].

The LTE physical layer uses a wide range of channel coding types from simple codes with very low computational complexity to highly efficient and complex channel codes. In traffic channels the Turbo codes and Convolutional codes are preferred and in control channels are used specially varied types of block codes [8]. The phase shift keying (BPSK, QPSK) and quadrature amplitude modulations (16QAM, 64QAM) are used as a modulation schemes. Using the 64QAM modulation scheme in uplink depends on the category of UE (cat. 5 is necessary in this case). As was mentioned before, LTE allows a scalable bandwidth allocation. System bandwidths are in a range from 1.4 MHz to 20 MHz. This feature together with both frequency division duplex (FDD) and time division duplex (TDD), enables to use a frequency band of former cellular systems.

The LTE downlink has a triplet of traffic physical channels; Physical Downlink Shared Channel (PDSCH), Physical Broadcast Channel (PBCH) and Physical Mul-

ticast Channel (PMCH). Traffic physical channels are not a subject of the doctoral thesis and they are mentioned here only for completeness. Their detailed description and use will be mentioned only when necessary. LTE downlink also has a triplet of control channels; Physical Control Format Information Channel (PCFICH), Physical Hybrid ARQ Indicator Channel (PHICH) and Physical Downlink Control Channel (PDCCH).

In uplink, the Physical Uplink Shared Channel (PUSCH) and Physical Uplink Control Channel (PUCCH) are available. Control information in uplink is transmitted using both PUSCH and PUCCH [5, 8]. Moreover, there is a Physical Random Access Channel (PRACH) which is used only for random access to the network. It transmits a special signal based on Zadoff-Chu sequences. PRACH is not a subject of the doctoral thesis.

A detailed description of transmitted control information in downlink and uplink, signal processing in mentioned physical control channels and performance or coexistence analysis results will be presented in the following chapters.

1.2 State of the Art

Analysis of the physical layer signal processing and creation of related mathematical models are very important parts of design and performance tests in cellular or wireless communication standards. Performance or coexistence analysis results are necessary during the design process, testing and optimization process in the area of cellular or wireless communication standards. As a result of computer technology, mathematical models are created. Analysis of these models provides a relatively accurate description of behavior of investigated standards in actual conditions, and financial costs are minimal as well. For better precision of mathematical models, there is the possibility of additional measurements of previous simulated models on real devices in the laboratory or real conditions. This useful feedback renders high precision to create mathematical computer models of the investigated system.

A description of the actual state of LTE control channel performance or coexistence analysis results as well as measurement results or available LTE simulators are described in this section.

Present Situation and Tendency

The LTE physical layer performance or coexistence analysis is mainly focused on the area of traffic channels. Performance analysis of LTE transmission schemes (OFDMA, SC-FDMA) is presented in [9–11] with concentration on PAPR, spectral efficiency and available resource allocation differences. Rezaei compares LTE and Mobile WiMAX considering multiple antenna technology [12].

Performance analysis of LTE downlink physical traffic channels in general is discussed by Elnashar [13] with a comparison of LTE in Band-3 (1800 MHz) and HSPA+ both for 20 MHz system bandwidth and Mehlführer [14] with a complex throughput analysis considering multiple antenna technology for all possible Channel Quality Indicator (CQI) settings. This paper also describes the LTE Link Level Simulator developed at Vienna University of Technology [15], see below. There are a lot of resources which deal with LTE traffic physical channels performance analyses primarily in downlink. These references were used during the analysis of signal processing and optimization process of LTE downlink control channel models.

The performance analysis of downlink physical control channels (PCFICH, PDCCH and PHICH) is mentioned in [16] only on a theoretical base. Article [17] examines a similar problem which presents PDCCH performance analysis results in an AWGN channel model and describes PDCCH implementation in FPGA. The performance analysis of PHICH LTE-FDD control channels was presented in [16] on a theoretical base only. Link level performance results of PHICH for physical antenna port in the Vehicular A channel model were published in [18].

For link level performance analysis of control information, it is necessary to analyze and further optimize the process of the LTE uplink physical layer signal processing chain. Control information in LTE uplink can be transmitted via both

PUCCH and PUSCH. Throughput performance analysis results in LTE uplink traffic channels are described in [19]. Performance analysis of the traffic data transmission using the Physical Uplink Shared Channel (PUSCH) under various environment conditions is described in [20, 21]. This analysis of the PUSCH performance is provided without the possibility of transmitting signal information via this physical channel. In [22], the block error rate (BLER) performance analysis results only for PUCCH format 2A/2B are presented. A new multiuser receiver is proposed in [23], as an addition, the PUCCH format 1 signal processing is described and performance results for PUCCH format 1 are presented. Article [24] discusses detailed signal processing of CQI transmission via PUCCH (format 2) and performance analysis results for PUCCH format 2 along with proposing a complex-field coding scheme to improve performance. Khan [25] mentions performance analysis of the PUSCH channel for traffic data only depending on the transmission environment and type of mapping. Donthi [26] discusses closed-form expressions for the throughput of achieved by CQI feedback mechanism in LTE and determined that the frequency resolution of the CQI incurs a loss in throughput in downlink direction. As in downlink, these references were used during the analysis of signal processing and optimization process of LTE uplink control channel models.

Simulation Model Types and Environment

From the overall network architecture point of view, there are two basic types of simulation; system level and link level [27]. *System level simulation (SLS)* covers a complete network. It considers more devices, which communicate simultaneously. This property allows the eventuality of coexistence analysis, intercell or intracell interference analysis. In most events, this type of simulation uses only general models of investigated devices. In the case of *Link level simulation (LLS)*, only single link (single BS and UE) is simulated. Only a pair of users is considered (transmitter and receiver) within the cell. In general, it is not used for intercell or intracell coexistence analysis for its own network, but it is possible in specific events. However, the Link level simulation uses detailed mathematical models of investigated network devices.

The most important output of the performance analysis are graphs of the bit and block error rate (BER, BLER) and graphs of system throughput. This analysis is provided in dependence on quality of transmission channel environment and other system parameters. There are two ways of throughput or error rate evaluation.

- **Error rate evaluation through traffic simulation** – the first way to evaluate error rate is traffic simulation from transmitter to receiver using a mathematical model of transmission environment and through the comparison of transmitted and received data. Error rate analysis using this technique is reliable and accurate for varied wireless standards. A disadvantage of this technique is the large time demand in the case of low error rates ($< 10^{-6}$).

– **Semi-analytical error rate evaluation** – it is an alternative way to simulate the technique mentioned above. Some types of communication systems could calculate error rate results much faster than the traffic simulation technique, which works only with simulation data. The semi-analytical method uses a combination of traffic simulation and mathematical analysis. A disadvantage of this method is the impossibility of using all types of communication systems [28].

As a base for communication system analysis, a lot of simulation tools or environments could be used. There are commercial or free software tools. Some of them are universal which also works for technical computation in general, and others are profiled only for creating communication system models.

– **MATLAB & Simulink** – is an interactive software environment and a scripting programming language of fourth generation. Its main advantage is great universality for mathematical computing and a number of specialized toolboxes (including Communication System Toolbox and Signal Processing Toolbox) with a large function library. In the last versions of MATLAB the toolbox for parallel computing was included. Other advantages of this tool in the area of mobile communication simulations is the number of specialized literature and high-quality help tool. Simulink is a superstructural tool of MATLAB, which is a component of MATLAB installation. Simulink is used for real-time simulation of systems.

– **Octave** – is a free alternative to MATLAB. The principles of working with Octave are similar. The advantage is that Octave is licensed under GPL and is partially compatible with MATLAB. The disadvantage could be fewer libraries and functions.

– **IT++** – is a free licensed library (GPL) of C++. It contains functions and classes for signal processing in communication standards. An advantage is the speed of computation.

– **Opnet Modeler** – is a programming tool for design, simulation and analysis of large communication networks. Its main advantage is an efficiency and functioning. Using a graphical environment, it is possible to create a model of any network architecture. The main utilization is for traffic simulation mainly in upper layers. It is not suitable for physical layer simulations. An interesting possibility is the so-called acceleration of network traffic, where the network behavior may be simulated within a few months. The benefit is the availability of large libraries.

– **Python & SimPy** - Python is a widely used general-purpose, high-level programming language. Its design philosophy emphasizes code readability, and its syntax allows programmers to express concepts in fewer lines of code than would be possible in languages such as C. With the SimPy package,

there is the possibility of simple implementation and simulation of complex real system. Python & SimPy is licensed as open source.

Presently, there are a lot of free or commercial software tools for simulating and analysing an LTE system. The LTE Link level simulator - downlink [15], developed in Vienna University of Technology, is in practice a direct 3GPP standard compliant implementation of the LTE downlink physical layer procedures (segmentation, channel coding, MIMO, transmit signal generation, pilot patterns, channel estimation, synchronization sequences). Implementation complexity and simulation time are high. The simulator is implemented using MATLAB environment and several functions are implemented in C and transformed to MATLAB MEX-files. The simulator is licensed under GPL.

Wojtowicz's openLTE simulator [29] is an open source implementation of 3GPP LTE standard. OpenLTE is focused only on downlink and is implemented in Octave. The LTE simulator (LTE-Sim) [30], developed at the Technical University of Bari, also has open source code. LTE-Sim is a System level simulator supporting higher layers and configuration of network management. Four kinds of network nodes UE, evolved NodeB (eNB), Home eNB (HeNB) and Mobility Management Entity/Gateway (MME/GW) are modeled.

Steepest Ascent[2] company produced a 3G Evolution Lab - 3G FDD Toolbox and Blockset which is a commercial software simulation tool which includes relevant libraries. The library provides a convenient means of creating simulations of 3GPP LTE and signal transmissions from either BS or UE. All relevant parameters can be configured manually. The library also includes individual subcomponents to allow the use of certain subsystems. Only the Steepest Ascent 3G Evolution Lab includes control channels in both downlink and uplink directions [31].

[2]Steepest Ascent has been acquired by MathWorks, the maker of MATLAB & Simulink mathematical computing software. Effective October 16, 2013, the functionality of Steepest Ascent LTE Toolbox and LTE-Advanced Toolbox and Blockset is available in LTE System Toolbox, a new MathWorks product for simulating the physical layer of LTE and LTE-Advanced wireless communication systems (MATLAB 2013a/b).

2 AIMS OF THE DOCTORAL THESIS

The LTE physical control channel plane was chosen because there are only a few articles or case studies which examine or analyze the topic. The physical control plane should be investigated to a greater extent. Note that in general, the presented results in cited articles do not consider comprehensive analysis and fading channel models. The link level simulation and error rate or error vector magnitude evaluation (performance and coexistence analysis) through the traffic simulation are chosen for the thesis. A high precision of examined blocks in the physical control channel signal processing chain was preferred. For expected precision of the performance analysis results and also for adjacent channel coexistence analysis the link level analysis is much more suitable than system level analysis.

As a base link level simulator in downlink direction, the Link level simulator, developed at Vienna University of Technology was chosen[1]. In the simulator, the physical control channels were missing. For completing the mentioned simulator, the physical control channels were created and included. The Viennese simulator is free for non-commercial academic use.

In uplink, a Link level simulator developed at the Department of radio electronics of Brno University of Technology is also available. Unfortunately, its unpreparedness for implementing physical control channels and overall confusing structure lead to the decision about creation of the author's own LTE physical control channel simulator in uplink with all possible features.

The MATLAB environment was chosen as a simulation tool. According to above mentioned information and with consideration to all possible options and methods, there is a summarization of main aims of the doctoral thesis.

1. Creation of specific mathematical models of the physical control channels in the Long Term Evolution system in both directions (downlink and uplink) and their implementation into the Link level simulator, developed in Vienna University of Technology (downlink only).

2. Simulation of the control information transmission from transmitter to receiver by using various system settings and various channel models. Simulation of the control information transmission from transmitter to receiver using varied system settings under interferences according to defined scenario.

3. Provide control measurement if any. Determine the set of system recommendations for optimal control information transmission.

The aims are elaborated in the following chapters.

[1] In 2010, cooperation was initiated between the Institute of Telecommunications, Vienna University of Technology and the Department of Radio Electronics, Brno University of Technology on creating LTE uplink and downlink link level simulators.

3 LTE PHYSICAL LAYER

In this chapter, the uplink and downlink LTE physical layer (PHY) with emphasis on physical control channels features, parameters and description of signal processing and the created mathematical models is presented. Mathematical models are created and evaluated in the MATLAB environment due to its comprehensiveness, flexibility, available toolboxes and prime debugging tools. Signal processing on the receiver side of LTE is not presented in 3GPP standards,thus a model of the receiver part, which is completely created by the author, is described in detail. In Section 3.1, the common characteristics of LTE physical layer is described and a general block scheme of the used simulator is presented. Section 3.2 describes the control information signal processing in uplink physical channels with emphasis on each used format and modulation scheme. Settings of UCI performance analysis simulations and its results are also presented. Downlink physical control channels signal processing and performance analysis results are presented in Sec. 3.3. Afterwards, this chapter is summarized in Sec. 3.4.

3.1 Common Characteristics

The Long Term Evolution physical layer (PHY) is defined for both the paired spectrum for Frequency Division Duplex (FDD) and unpaired spectrum for Time Division Duplex (TDD). LTE FDD is intended for use in the former 2.5G and 3G cellular network bands in the whole world. In November 2007, the ITU-R World Radiocommunication Conference (WRC-07) established a new spectrum for International Mobile Telecommunications (IMT) as an addition to former 2.5G and 3G cellular network bands [32]. This frequency band bring a risk of collisions with terrestrial television broadcast (DVB-T, DVB-T2) which uses the same frequency bands. LTE TDD (or TD-LTE) also has some advantages and using FDD or TDD LTE depends on local conditions and necessities. The complete LTE FDD frequency bands are listed in Tab. 3.1.

For FDD, pairs of frequency sub-bands are defined, while for TDD only one compact band is defined. Some of the frequency bands overlap. LTE frequency bands are defined all over the world. The mentioned frequency bands are different in each country and are defined by national frequency tables. In Europe, the band numbers 3,7,8 and 20 are used for LTE FDD and band numbers 33, 34 and 38 are used for LTE TDD. However, this dissertation is focused on the LTE FDD operation only. The LTE TDD attributes are not discussed. The channel raster is 100 kHz for all bands, which means that the carrier center frequency must be an integer multiple of 100 kHz [33]. In contrast, the channel raster of the UMTS is an integer multiple of 200 kHz.

Tab. 3.1: LTE FDD bands and frequencies

LTE FDD band number	Frequency range – uplink [MHz]	Frequency range – downlink [MHz]	Frequency bandwidth [MHz]	Duplex pair space [MHz]	Uplink/Downlink sub-band space [MHz]
1	1920–1980	2110–2170	60	190	130
2	1850–1910	1930–1990	60	80	20
4	1710–1755	2110–2155	45	400	355
5	824–849	869–894	25	45	20
6	830–840	875–885	10	35	25
7	2500–2570	2620–2690	70	120	50
8	880–915	925–960	35	45	10
9	1749.9–1784.9	1844.9–1879.9	35	95	60
10	1710–1770	2110–2170	60	400	340
11	1427.9–1452.9	1475.9–1500.9	20	48	28
12	698–716	728–746	18	30	12
13	777–787	746–756	10	–31	41
14	788–798	758–768	10	–30	40
15	1900–1920	2600–2620	20	700	680
16	2010–2025	2585–2600	15	575	560
17	704–716	734–746	12	30	18
18	815–830	860–875	15	45	30
19	830–845	875–890	15	45	30
20	832–862	791–821	30	–41	71
21	1447.9–1462.9	1495.9–1510.9	15	48	33
22	3410–3500	3510–3600	90	100	10
23	2000–2020	2180–2200	20	180	160
24	1625.5–1660.5	1525–1559	34	–101,5	135,5
25	1850–1915	1930–1995	65	80	15

The basic time period of one time sample T_s which is necessary to define the time domain field in LTE is given by the equation (3.1).

$$T_\mathrm{s} = \frac{1}{15000 \times 2048} = 3.2552 \cdot 10^{-8}\,\mathrm{s}. \tag{3.1}$$

Uplink and downlink transmission in the time domain is organized into *radio frames*. The radio frame duration $T_\mathrm{rf} = 10\,\mathrm{ms}$. LTE PHY supports two types of radio frames, Type 1 which is used for FDD and Type 2 which is used for TDD. The radio frame consists of 10 *subframes*. The subframe duration T_sf equals 1 ms. Two *slots* create a single subframe ($T_\mathrm{slot} = 0.5\,\mathrm{ms}$).

The duration of each above mentioned time element is defined as a multiple of the number of time samples and T_s. For a single radio frame $T_\mathrm{rf} = 307200 \times T_\mathrm{s} = 10\,\mathrm{ms}$, for one subframe $T_\mathrm{sf} = 30720 \times T_\mathrm{s} = 1\,\mathrm{ms}$, and for one slot $T_\mathrm{slot} = 15360 \times T_\mathrm{s} = 10\,\mathrm{ms}$. The radio frame includes 20 slots. The slots are numbered from 0 to 19. The subframe is defined as two consecutive slots.

For transparent composition of all physical channels and physical signals (reference and synchronization signals), LTE defines the time-frequency *resource grid*. Radio frame structure 1, which is used in FDD, and the uplink/downlink resource grid is illustrated in Fig. 3.1. This solution is suitable in terms of allocation of physical channel and signal resources and their flexible change. The structure of the resource grid in uplink and downlink is similar. On the x-axis is time (SC-FDMA or OFDMA), on the y-axis is frequency (subcarriers).

The smallest unit in the resource grid is the *resource element*. The resource element represents a single modulation symbol sample in the model. Each resource element is unambiguously identifiable by a pair of indices (k, l), where k represents the resource element position in the frequency domain and l represents its position in the time domain. The resource element corresponds to the SC-FDMA or OFDMA symbol. A *resource block* is used for easily describing the resource grid. The resource block is defined by 1 slot in the time domain and set of subcarriers $N_{\mathrm{sc}}^{\mathrm{RB}}$ in the resource block in the frequency domain. All possible resource block configurations are listed in Tab. 3.2.

The number of resource elements in one resource block is given by the system configuration, defined by equation (3.2).

$$N_{\mathrm{RE}}^{\mathrm{RB}} = N_{\mathrm{symb}} N_{\mathrm{sc}}^{\mathrm{RB}}, \tag{3.2}$$

where N_{symb} is the number of SC-FDMA or OFDMA symbols in the resource block. A configuration with normal cyclic prefix length and frequency spacing $\Delta f_{\mathrm{sc}} = 15\,\mathrm{kHz}$ is assumed. The number of resource elements in the resource block is

$$N_{\mathrm{RE}}^{\mathrm{RB}} = N_{\mathrm{symb}} N_{\mathrm{sc}}^{\mathrm{RB}} = 12 \times 7 = 84.$$

Each resource element represents a complex-valued modulation symbol according to used modulation scheme. The SC-FDMA or OFDMA modulation symbol duration T_{symb} is defined as

$$T_{\mathrm{symb}} = T_{\mathrm{cp}} + T_{\mathrm{mb}}, \tag{3.3}$$

where T_{cp} is the cyclic prefix (CP) duration and T_{mb} is the SC-FDMA/OFDMA symbol main body duration. Note that the first symbol in the time slot for normal

Tab. 3.2: Physical resource block parameters

Direction	Cyclic prefix length	Frequency spacing	$N_{\mathrm{sc}}^{\mathrm{RB}}$	N_{symb}
Uplink	Normal	$\Delta f_{\mathrm{sc}} = 15\,\mathrm{kHz}$	12	7
	Extended	$\Delta f_{\mathrm{sc}} = 15\,\mathrm{kHz}$	12	6
Downlink	Normal	$\Delta f_{\mathrm{sc}} = 15\,\mathrm{kHz}$	12	7
	Extended	$\Delta f_{\mathrm{sc}} = 15\,\mathrm{kHz}$	12	6
	Extended	$\Delta f_{\mathrm{sc}} = 7.5\,\mathrm{kHz}$	24	3

Tab. 3.3: List of supported LTE system frequency bandwidths

	System bandwidths (B_{sys})					
	1.4 MHz	3 MHz	5 MHz	10 MHz	15 MHz	20 MHz
Resource block number (N_{RB})	6	15	25	50	75	100
Number of subcarriers (N_{sc})	72	180	300	600	900	1200
Used bandwidth - B_{UL} [MHz]	1.095	2.715	4.515	9.015	13.515	18.015
Used bandwidth - B_{DL} [MHz]	1.08	2.7	4.5	9.0	13.5	18.0

Note: the center subcarrier (DC in baseband) is transmitted in uplink only.

CP length is larger that the remaining symbols in the slot. This feature achieves better protection of information transmitted in the first symbol in the subframe. In the first symbol, the physical control channel information is usually transmitted [5].

A scalable frequency channel bandwidth is a significant feature of LTE [3]. In LTE, six supported frequency channel bandwidths are defined as given in Tab. 3.3. Due to a larger system bandwidth, a higher system throughput can be reached. The system configurations with a lower frequency channel bandwidth are compatible with frequency bands of former cellular networks. In this thesis, only the system bandwidth $B_{\mathrm{sys}} = 1.4\,\mathrm{MHz}$ is considered due to lower overall complexity of the physical layer model and thus lower time consumption for providing simulations.

The used frequency bandwidth in both directions is given by multiplying the number of subcarriers N_{sc} by the frequency spacing of adjacent orthogonal subcarriers Δf_{sc}.

The value of subcarrier spacing equalling 15 kHz was adopted for easy cooperation with former WCDMA and HSPA systems. If we consider possible FFT size (N_{FFT}) as a power of two and base subcarrier spacing value, the base chip rate $f_{\mathrm{cr}} = 3.84\,\mathrm{MHz}$, which corresponds to the WCDMA and HSPA system chip rate.

The above mentioned time and frequency parameters are necessary in order to create a mathematical model of the physical layer and for calculating the theoretical probability of error in OFDM-based communication systems.

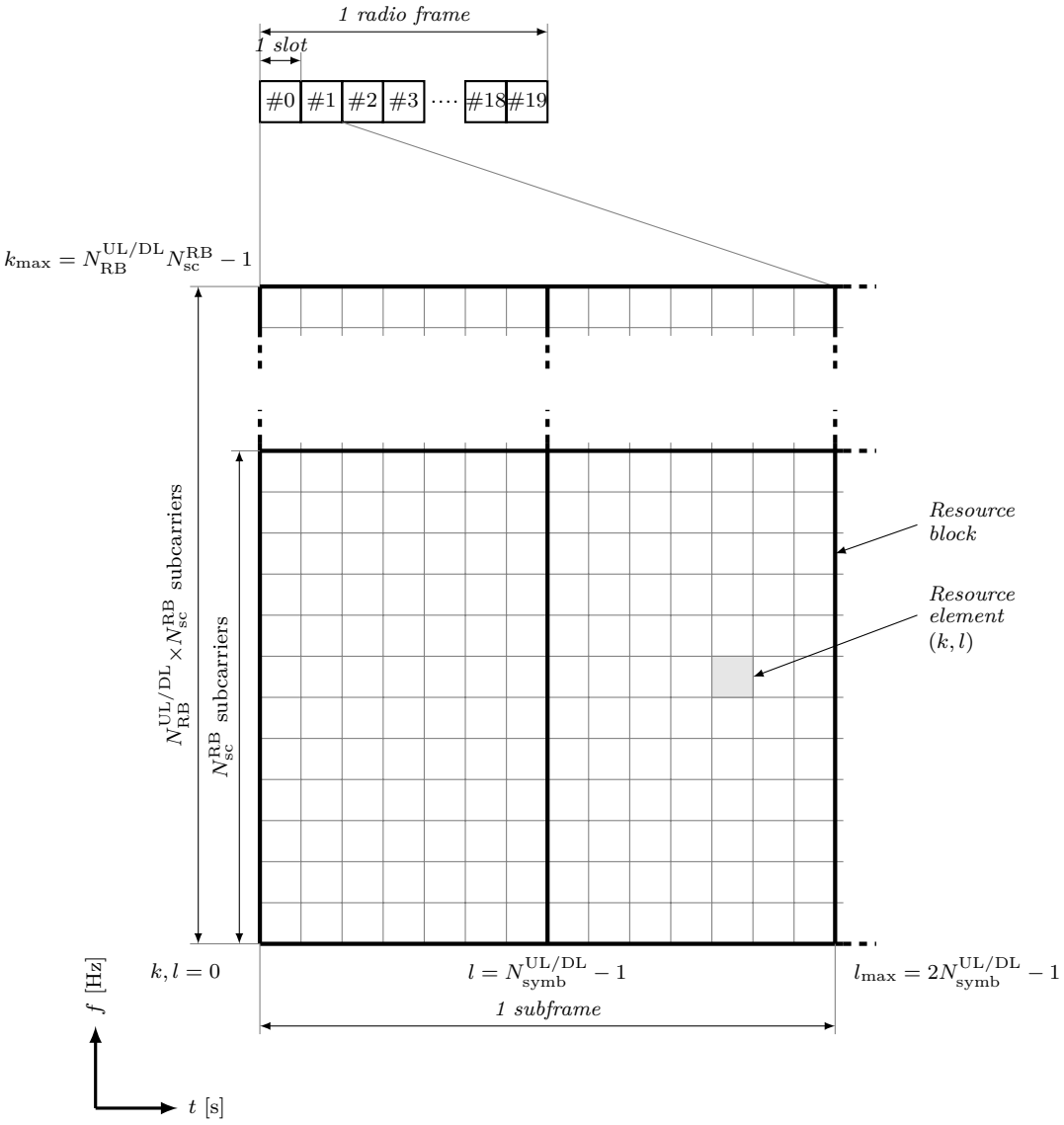

Fig. 3.1: Radio frame - Type 1 and time-frequency resource grid

General Link Level Simulator Scheme

Each baseband link level uplink control information simulator was developed in MATLAB[1] environment. The common general block scheme of control information simulator for all physical control channels in uplink and downlink[2] is depicted in Fig. 3.2.

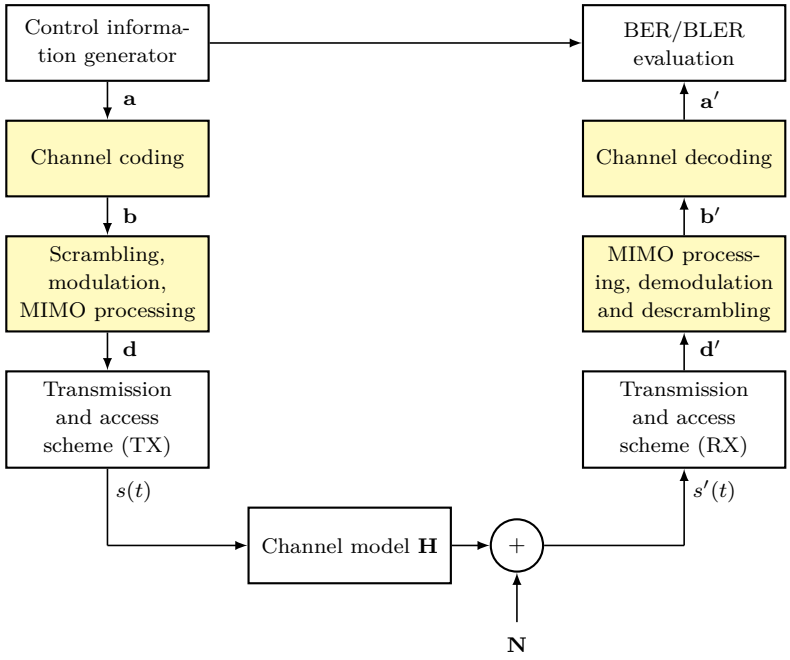

Fig. 3.2: General control information link level performance analysis model scheme

First, in this general structure, randomly generated control information $\mathbf{a} = [a_0, a_1, \ldots, a_{A-1}]$ for single subframe leads to a channel coding block [8]. Here, A denotes the length of the control information codeword. The randomization process of control information generation is achieved by the MATLAB `RandStream` function [34]. Channel coding, scrambling, modulation and MIMO processing is different for each physical channel and is discussed separately in detail (yellow labeled blocks). Notice that in LTE uplink the MIMO operation is not explicitly defined. Only receive diversity is modeled in LTE uplink. The vector of channel coded bits $\mathbf{b}$ is then scrambled with a cell-specific pseudo-random sequence $\mathbf{c}$ and a scrambled vector of bits $\widetilde{\mathbf{b}}$ is created according to

$$\widetilde{\mathbf{b}} = \mathbf{b} \oplus \mathbf{c}, \tag{3.4}$$

[1]Presented LTE uplink and downlink link level models are created and evaluated in MATLAB 8.0.0.783 (R2012b) environment.

[2]In the case of downlink, general Link level LTE downlink simulator [15] was created at Vienna University of Technology. Due to the fact that control channels are missing in the simulator, they were created and implemented by the author.

where **c** is the cell-specific pseudo-random sequence which is different in each LTE physical channel [5]. Cell-specific pseudo-random sequences **c** are used in LTE to minimize inter-cell interference. When the received data is descrambled using a different sequence than in the transmitted side, we obtain only an incorrect signal such as noise.

After the scrambling process, modulation is performed and the vector of complex-valued symbols **d** is created. The symbol alphabet of modulation symbols is different in LTE physical control channels and formats. In the transmission and access scheme, modulated symbols **d** are mapped into the time-frequency resource grid (see Fig. 3.1) and SC-FDMA or OFDMA signal processing operations are performed to make the baseband signal $s(t)$ [5].

As was mentioned above, the SC-FDMA transmission and access scheme was chosen for LTE uplink [7, 32, 35]. The main reasons for using SC-FDMA are low Peak to Average Power Ratio (PAPR), low sensitivity to carrier frequency offset and linear distortion. The model of SC-FDMA/OFDMA transmission and access scheme is depicted in Fig. 3.3.

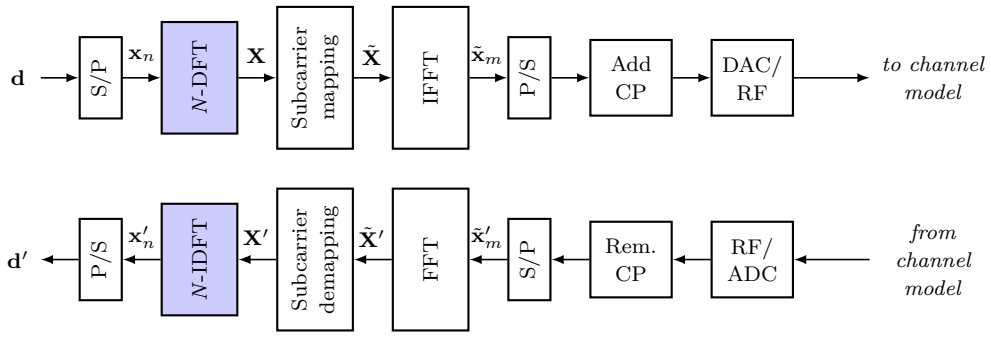

Fig. 3.3: General SC-FDMA/OFDMA signal processing chain

White labeled blocks are common for both SC-FDMA and OFDMA, blue labeled blocks are only in the SC-FDMA signal processing chain. The row vector of input complex-valued samples (modulation symbols) **x** is split into N parallel streams $\mathbf{x}_n = \mathbf{x}^{\mathrm{T}}$, and N-point Discrete Fourier Transform (DFT) is performed. The localized mapping scheme is only used to map subcarriers $\left(\mathbf{X} \Rightarrow \tilde{\mathbf{X}}\right)$ in LTE uplink. In localized mapping, the DFT outputs are mapped to a subset of consecutive subcarriers thereby confining them to only a fraction of the system bandwidth.

After N-point DFT operation, the vector of mapped subcarriers $\tilde{\mathbf{X}}$ is led to the Inverse Fast Fourier Transform (IFFT) signal processing block where it is transformed into the time domain $\tilde{\mathbf{x}}_m$. Zero subcarriers, DC subcarrier and the reference signal is also added in this block. Parameters of SC-FDMA used in LTE uplink are listed in Tab. 3.4. The parallel stream $\tilde{\mathbf{x}}_m$ is transposed to a vector of complex-valued samples, and cyclic prefix (CP) is added according to Tab. 3.4.

The fading channel is realized using a Tapped delay line (TDL) model with AWGN added in terms of a set SNR value [36, 37]. Parameters of fading channel models used in this thesis are listed in Tab. A.1 and A.2. The channel model is fully described via the matrix of channel coefficients

$$\mathbf{H} = \begin{bmatrix} h_{k_{\max},1} & h_{k_{\max},2} & \cdots & h_{k_{\max},l_{\max}} \\ h_{k_{\max}-1,1} & h_{k_{\max}-1,2} & \cdots & h_{k_{\max}-1,l_{\max}} \\ \vdots & \vdots & \ddots & \vdots \\ h_{2,1} & h_{2,2} & \cdots & h_{2,l_{\max}} \\ h_{1,1} & h_{1,2} & \cdots & h_{1,l_{\max}} \end{bmatrix},$$

where each channel coefficient $h_{k,l}$ corresponds to a resource element, see Fig. 3.1. In OFDM-based communication systems, it is necessary to provide channel estimation and equalization. Channel estimation is not provided in the presented uplink and downlink simulators and the model always works with perfect knowledge of the matrix of channel coefficients $\mathbf{H}$ during a single subframe period.

After the signal is transferred to RF and passes through the channel model $\mathbf{H}$ and AWGN (here depicted as $\mathbf{N}$), it is added according to the SNR value set at the beginning of the simulation, the signal $s'(t)$ is led to the SC-FDMA receiver part. At first, the signal is down-converted in the RF/ADC block and CP samples are removed. After that, signal samples are transposed to a column vector and the FFT operation is performed. Signal samples are led to the subcarrier demapping block where traffic and control data samples are picked up from the resource grid and the N-IDFT operation is performed. Finally, parallel-to-serial conversion is performed. Demodulation and descrambling processes are then provided and the vector of modulated and scrambled bits $\mathbf{d}'$ enters the demodulation, descrambling and channel decoding blocks.

The OFDMA transmission and access scheme is used in LTE downlink. The main advantages of OFDMA are flexibility of deployment across various frequency

Tab. 3.4: SC-FDMA/OFDMA parameters (for $\Delta f_{\text{sc}} = 15\,\text{kHz}$)

System bandwidths B_{sys}	Sampling frequency	N_{FFT}	Cyclic prefix			
			normal		extended	
[MHz]	[MHz]		T_{cp} [µs]	samples	T_{cp} [µs]	samples
1.4	1.92	128	4.69/5.21	9/10	16.67	32
3	3.84	256	4.69/5.21	18/20	16.67	64
5	7.68	512	4.69/5.21	36/40	16.67	128
10	15.36	1024	4.69/5.21	72/80	16.67	256
15	23.04	1536	4.69/5.21	108/120	16.67	384
20	30.72	2048	4.69/5.21	144/160	16.67	512

bands, averaging interferences from neighboring cells, enables Single Frequency Network (SFN) coverage, and the possibility of using the frequency diversity technique by spreading the carriers all over the used spectrum. The main disadvantage of OFDMA is its higher sensitivity to frequency offset and phase noise [38]. The OFDMA signal processing chain is depicted in Fig. 3.3. Only white labeled blocks are used in OFDMA. The row vector of input complex-valued modulated symbols $\mathbf{d}$ is mapped to the resource grid $\tilde{\mathbf{X}}$ and IFFT is performed, and vector $\tilde{\mathbf{x}}_m$ is formed. Zero subcarriers and the reference signal is also added in this block. Then, the column vector of complex-valued samples in time domain $\tilde{\mathbf{x}}_m$ is split into the row vector and CP samples are added according to the system configuration (see Tab. 3.4). Receiver operations are provided in the same way as in the case of SC-FDMA except for the N-IDFT operation.

The transmission and access scheme will also be mentioned in the physical control channel description. The multiantenna technique is also adopted in LTE standard [5] and it is used in control information signal processing. Due to large variances in using this technique in the uplink and downlink direction, it will be described in detail in the relevant physical control channel description.

After the signal passes through the transmission channel model with the matrix of channel coefficients $\mathbf{H}$ and AWGN is added in terms of a predefined value of SNR, the signal $s'(t)$ is led to the receiver. Here, inverse SC-FDMA or OFDMA operations are performed and received modulating symbols $\mathbf{d}'$ are picked from the resource grid. Demodulation and descrambling processes are then provided and the vector of demodulated and descrambled bits $\mathbf{b}'$ enter the channel decoding block.

After the channel decoding process, the decoded bits $\mathbf{a}' = \left[a'_0, a'_1, \ldots, a'_{A-1}\right]$ are compared with the corresponding vector of bits $\mathbf{a}$ and Bit error rate (BER) or Block error rate (BLER) is then evaluated. The value of BER for given SNR is evaluated according to

$$\mathrm{BER} = \frac{\sum_{i=0}^{A-1} (a_i \oplus a'_i)}{A}. \tag{3.5}$$

The value of BLER for given SNR is defined as the ratio of the number of erroneous blocks to the number of all transmitted blocks.

In all figures with performance analysis results in the AWGN channel model, the theoretical bit error probability P_b for SC-FDMA or OFDMA transmission access scheme will be plotted (without considering channel coding). It helps with the correctness of provided simulations. Generally, in LTE BPSK, QPSK, 16QAM and 64QAM, modulation schemes are defined [5]. Bit error probability of PSK modulation schemes is computed according to

$$P_\mathrm{b} = \frac{1}{2}\mathrm{erfc}\left(\sqrt{\frac{E_\mathrm{b}}{N_0}}\right), \tag{3.6}$$

where erfc () is the complementary error function, E_b is signal energy per bit and N_0 is noise power spectral density.

Bit error probability of 16QAM modulation scheme is computed according to

$$P_{\mathrm{b}} = \frac{3}{2k}\mathrm{erfc}\left(\sqrt{\frac{kE_{\mathrm{b}}}{10N_0}}\right), \tag{3.7}$$

where $k = \log_2 M$ and M are the number of constellation points in the modulation scheme. For 64QAM is defined

$$P_{\mathrm{b}} = \frac{2}{k}\left(1 - \frac{1}{\sqrt{M}}\right)\mathrm{erfc}\left(\sqrt{\frac{3k}{2(M-1)}\frac{E_{\mathrm{b}}}{N_0}}\right). \tag{3.8}$$

For OFDM-based transmission and access schemes we can write the relation between SNR and bit energy to noise power spectral density ratio

$$\frac{E_{\mathrm{b}}}{N_0} = \frac{S}{N}\frac{B}{f_{\mathrm{b}}}\frac{N_{\mathrm{sc}}}{N_{\mathrm{FFT}}}\frac{T_{\mathrm{d}}}{T_{\mathrm{d}} + T_{\mathrm{cp}}}k, \tag{3.9}$$

where f_{b} is codeword bit rate and T_{d} is duration of examined data symbols.

3.2 Uplink Control Information Transmission

This section discusses in detail the description of uplink control information (UCI) signal processing in LTE uplink physical layer with emphasis on describing channel coding. UCI performance analysis results are also presented. LTE uplink physical layer includes several types of traffic and control physical channels and physical signals. Mapping of transport channels to physical channels in uplink is shown in Fig. 3.4.

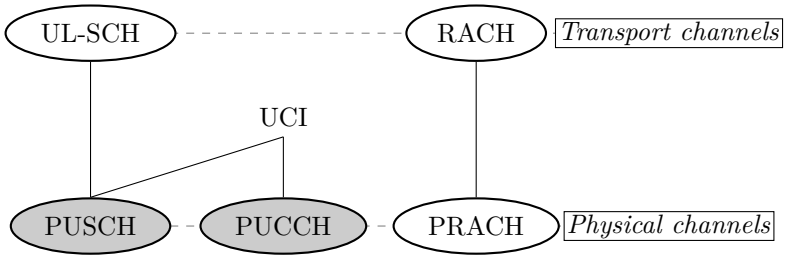

Fig. 3.4: Mapping transport to physical channels in LTE uplink

As shown, it is obvious that there is a triplet of physical channels, Physical Uplink Shared Channel (PUSCH), Physical Uplink Control Channel (PUCCH) and Physical Random Access Channel (PRACH). As was mentioned, PRACH is not investigated in this thesis due to the fact that there is no possibility to determine the bit or block error rate. Uplink Control Information (UCI) is transmitted via PUCCH and PUSCH, which is primarily used for transmitting uplink traffic data [8]. In this section, control information transmission via PUCCH and PUSCH is presented.

3.2.1 Physical Uplink Control Channel

Transferring UCI in the case of a large number of UE and a short UCI codeword is provided by PUCCH. Note that PUSCH and PUCCH are never transmitted in the same subframe. UCI is transmitted via PUCCH in the case where UE has no traffic data to transfer to the BS. PUCCH uses at least 2 resource blocks on the edge of the resource grid (in frequency domain). UCI consists of three types of control information; Channel quality information, Scheduling Request (SR) and Uplink Hybrid Automatic Repeat Request (HARQ) acknowledged or non-acknowledged information [1]. Note that SR information is transmitted via PUCCH only. Channel quality information is also divided to the following components: Channel Quality Indicator (CQI), Precoding Matrix Indicator (PMI) and Rank Indicator (RI). The CQI and PMI are usually grouped together into a single CQI/PMI codeword. The CQI carries information about the current channel state which is measured by UE. The PMI provides feedback information to the BS about the set of precoding weights for BS when closed-loop spatial multiplexing or multiuser MIMO transmission modes are

used [39]. The RI gives feedback to the BS about the number of transport blocks for transmission to the BS [40]. Other control information in uplink is a Hybrid Automatic Repeat Request Indicator (HARQ-ACK). The HARQ-ACK indicator is used for reporting acknowledged or non-acknowledged information about previous data transferred on the Physical Downlink Shared Channel (PDSCH). Here, an HARQ-ACK indicator equalling one means successful data transfer.

PUCCH Link Level Model

PUCCH has six transmission formats: format 1, 1A, 1B, 2, 2A and 2B [8]. These formats are defined by the type of transmitted information. The scheduling request is transmitted via PUCCH, format 1. The modulation scheme for SR is not defined. The SR requirement from UE is given only by power emissions in the control region in the resource grid. PUCCH format 1A/1B transmits a one or two-bit HARQ-ACK codeword which is modulated using the BPSK or QPSK modulation scheme. PUCCH format 2 carries CQI/PMI and RI information. The format 2 codeword has a length from 4 to 11 bits. It uses the QPSK modulation scheme. In the case of format 2A/2B codeword, one or two bit HARQ-ACK information is only added to format 2. In the case of format 2A, a one bit HARQ-ACK codeword is modulated using BPSK and in the case of format 2B, a two bit HARQ-ACK codeword is modulated using QPSK [5]. A complete list of available PUCCH formats, modulation schemes and transmitted control information is presented in Tab. 3.5. Overall PUCCH channel coding, scrambling and modulation model in the transmitter is depicted in Fig. 3.5.

PUCCH format 1 gives UE an alternative method to require a scheduling grant. PUCCH format 1 is used in the case of network overloading and when PRACH signalization is not successful. In format 1A/1B, a one or two-bit HARQ-ACK codeword is transmitted. First, HARQ-ACK is multiplexed with an SR, if necessary. A multiplexed vector of bits $\mathbf{b} = [b(0), \ldots, b(M_{\text{bit}} - 1)]$ is modulated using QPSK (format 1B) or BPSK (format 1A), see Fig. 3.6.

Tab. 3.5: List of PUCCH formats

Format	Modulation scheme	Number of bits per subframe	Type of transmitted control information
1	Not available	Not available	SR
1A	BPSK	1	HARQ-ACK
1B	QPSK	2	HARQ-ACK
2	QPSK	20	CQI/PMI, RI
2A	QPSK and BPSK	21	CQI/PMI, RI and HARQ-ACK
2B	QPSK and BPSK	22	CQI/PMI, RI and HARQ-ACK

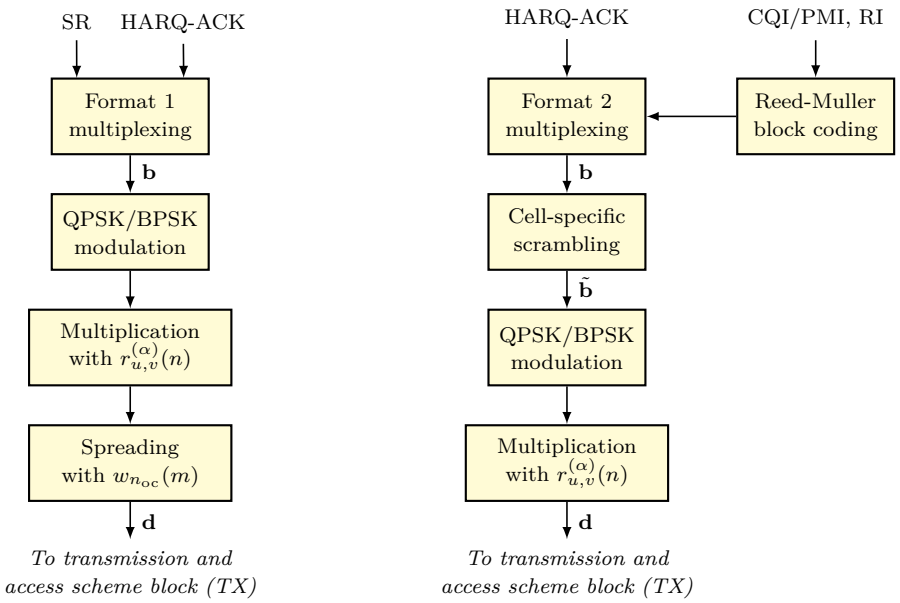

(a) Format 1/1A/1B (b) Format 2/2A/2B

Fig. 3.5: Block scheme of PUCCH channel coding, scrambling and modulation model

Modulated symbol $d(0)$ is multiplied using Zadoff-Chu $r_{u,v}^{(\alpha)}(n)$ sequence of length $N_{\text{seq}}^{\text{PUCCH}} = 12$, according to

$$y(n) = d(0) r_{u,v}^{(\alpha)}(n), \qquad n = 0, 1, \ldots, N_{\text{seq}}^{\text{PUCCH}} - 1, \tag{3.10}$$

where $r_{u,v}^{(\alpha)}(n)$ is defined as

$$r_{u,v}^{(\alpha)}(n) = \mathrm{e}^{\mathrm{j}\alpha n}\, \bar{r}_{u,v}(n), \qquad 0 \leq n < N_{\text{seq}}^{\text{PUCCH}}, \tag{3.11}$$

where α is cyclic shift and $\bar{r}_{u,v}$ is a base sequence [5]. The cyclic shift α varies between slots and symbols. The r sequences are used for minimizing cross-correlation between different user signals in a cell [41].

Next, the complex-valued signal $y(n)$ is spread with orthogonal sequence $w_{n_{\text{oc}}}(m)$ to separate users mapped into the same resources, and the matrix of mapped complex-valued symbols $\mathbf{z}$ is created according to (3.12)

$$z_1(m' N_{\text{SF}}^{\text{PUCCH}} N_{\text{seq}}^{\text{PUCCH}} + m N_{\text{seq}}^{\text{PUCCH}} + n) = S(n_{\text{s}}) w_{n_{\text{oc}}}(m) y(n), \tag{3.12}$$

where

$$\begin{aligned} m &= 0, 1, \ldots, N_{\text{SF}}^{\text{PUCCH}} - 1, \\ n &= 0, 1, \ldots, N_{\text{seq}}^{\text{PUCCH}} - 1, \\ m' &= 0, 1, \end{aligned}$$

$N_{\text{SF}}^{\text{PUCCH}}$ is the PUCCH spreading factor, $S(n_{\text{s}})$ is the scrambling sequence defined in [5], n_{s} is the slot number and n_{oc} is the orthogonal sequence index. The parameter

Tab. 3.6: Orthogonal sequences $w_{n_{\mathrm{oc}}}$ for PUCCH format 1A/1B

Sequence	$w_{n_{\mathrm{oc}}} = [w(0), \ldots, w(N_{\mathrm{SF}}^{\mathrm{PUCCH}} - 1)]$	
index n_{oc}	$N_{\mathrm{SF}}^{\mathrm{PUCCH}} = 4$	$N_{\mathrm{SF}}^{\mathrm{PUCCH}} = 3$
0	$[+1, +1, +1, +1]$	$[+1, +1, +1]$
1	$[+1, -1, +1, -1]$	$\left[+1, \mathrm{e}^{\mathrm{j}2\pi/3}, \mathrm{e}^{\mathrm{j}4\pi/3}\right]$
2	$[+1, -1, -1, +1]$	$\left[+1, \mathrm{e}^{\mathrm{j}4\pi/3}, \mathrm{e}^{\mathrm{j}2\pi/3}\right]$

$N_{\mathrm{SF}}^{\mathrm{PUCCH}}$ equals 4 or 3 (if the Sounding reference signal is transmitted in subframe). Possible orthogonal sequences $w_{n_{\mathrm{oc}}}$ are listed in Tab. 3.6. If we consider $d(0)$ as a base modulation symbol, overall spreading factor for PUCCH format 1A/1B equals 96. Position of complex-valued vector $\mathbf{z}_1$ in the resource grid after mapping process is depicted in Fig. 3.8. Here, each complex-valued sample of $y(n)$ is spread by $w_{n_{\mathrm{oc}}}$ to four symbols in each slot, thus additional frequency diversity is performed.

Format 2, CQI/PMI and RI, is channel coded using the $(20, A)$ Reed-Muller code, where A is the length of input codeword in bits [8]. When channel coding is performed, the output sequence $\mathbf{b} = [b(0), b(1), \ldots, b(19)]$ of 20 bits in length is scrambled using a cell-specific pseudo-random sequence $\mathbf{c}$ according to (3.4). The block of scrambled bits $\widetilde{\mathbf{b}} = \left[\tilde{b}(0), \tilde{b}(1), \ldots, \tilde{b}(19)\right]$ is modulated using QPSK modulation as is depicted in Fig. 3.6 and results in the vector of complex-valued symbols $\mathbf{d} = [d(0), d(1), \ldots, d(9)]$. Each complex-valued symbol $d(0), d(1), \ldots, d(9)$ is multiplied with a cyclically shifted length $N_{\mathrm{seq}}^{\mathrm{PUCCH}} = 12$ sequence $r_{u,v}^{(\alpha)}(n)$ according to

$$z_2(N_{\mathrm{seq}}^{\mathrm{PUCCH}} n + i) = d(n) \cdot r_{u,v}^{(\alpha)}(i), \tag{3.13}$$

where $n = [0, 1, \ldots, 9]$, $i = \left[0, 1, \ldots, N_{\mathrm{sc}}^{\mathrm{RB}} - 1\right]$ and $N_{\mathrm{sc}}^{\mathrm{RB}}$ is a resource block size in the frequency domain, expressed as the number of subcarriers (here $N_{\mathrm{sc}}^{\mathrm{RB}} = N_{\mathrm{seq}}^{\mathrm{PUCCH}}$). Sequence $r_{u,v}^{(\alpha)}(n)$ is defined by (3.11).

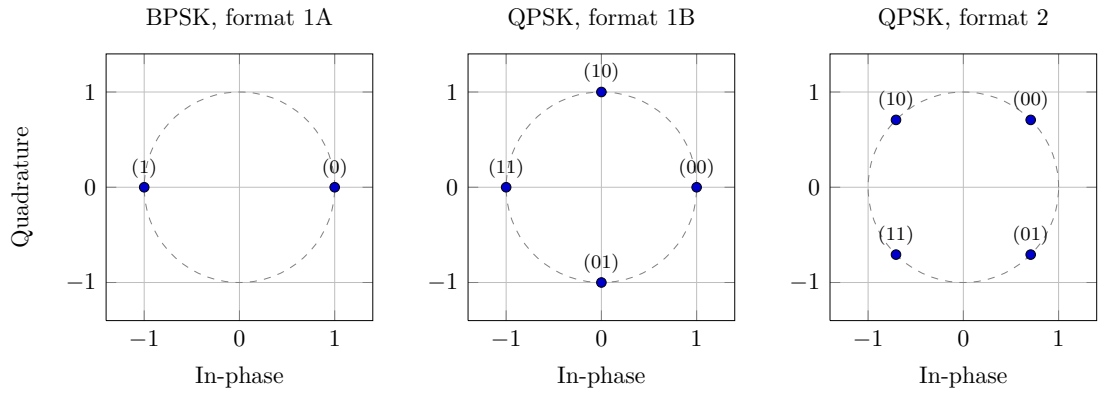

Fig. 3.6: Modulation schemes for PUCCH formats 1A/1B and format 2

For PUCCH formats 2A and 2B, the bits $b(20), \ldots, b(M_{\text{bit}} - 1)$ are modulated in the same way as in the case of PUCCH format 1A and 1B resulting in modulation symbol $d(10)$ as is depicted in Fig. 3.6. Note, that PUCCH format 2A (BPSK) and 2B (QPSK) are used only for normal CP length. The vector of complex-valued symbols $\mathbf{z}_2$ is mapped to the edge of the resource grid in a similar way as in the case of format 1A/1B (see Fig. 3.8). In the case of PUCCH format 2A/2B, these modulation symbols are mapped instead of reference signals (RS) to the column $l = \{5, 12\}$. After the resource mapping process, IFFT is performed. After the addition of a cyclic prefix (CP), the signal in the time domain enters the transmission channel.

When the signal passes through the transmission channel $\mathbf{H}$, it leads to receiving antennas. In LTE uplink, MIMO is not explicitly defined [5]. Due to this circumstance, only the receiving diversity (RxD) technique is used. First, in the receiver, CP is removed and FFT is performed. Block schemes of PUCCH demodulation, de-

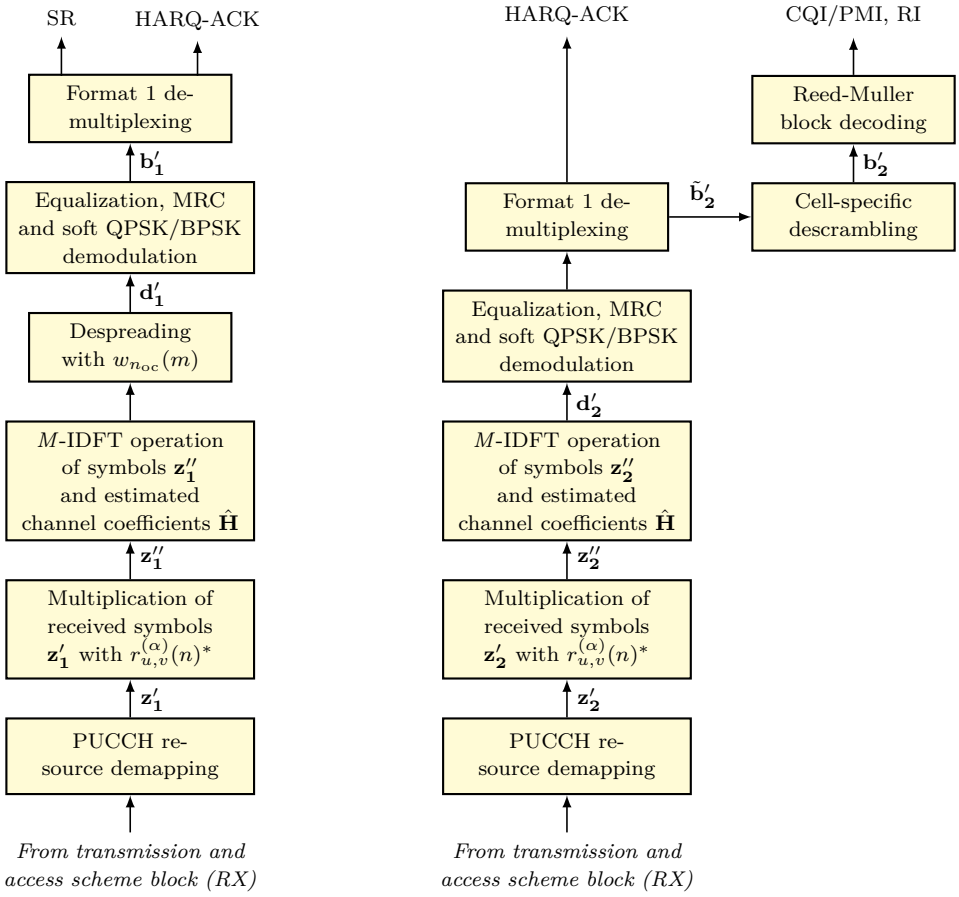

(a) Format 1/1A/1B (b) Format 2/2A/2B

Fig. 3.7: Block scheme of PUCCH channel decoding, descrambling and demodulation model

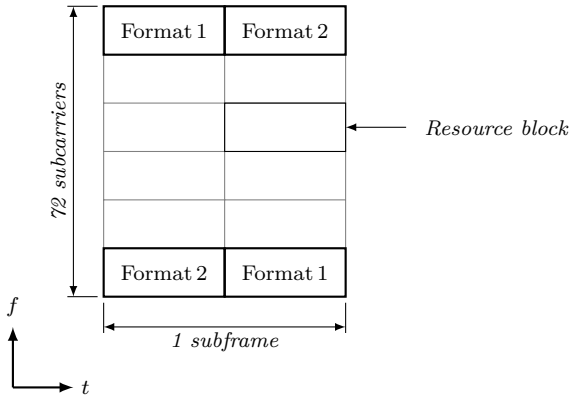

Fig. 3.8: Example of PUCCH mapping into time-frequency resource grid, (B = 1.4 MHz)

scrambling and channel decoding is depicted in Fig. 3.7. PUCCH resources $\mathbf{z}'_1$ and $\mathbf{z}'_2$ are picked-up (demapped) from the resource grid and the corresponding signal is multipled using the Zadoff-Chu sequence $r_{u,v}^{(\alpha)}(n)^*$ according to

$$\begin{aligned} \mathbf{d}'_1 &= IDFT\{\mathbf{z}''_1\} = IDFT\left\{\mathbf{z}'_1\mathbf{r}_{u,v}^{(\alpha)*}\right\}, \\ \mathbf{d}'_2 &= IDFT\{\mathbf{z}''_2\} = IDFT\left\{\mathbf{z}'_2\mathbf{r}_{u,v}^{(\alpha)*}\right\}, \end{aligned} \tag{3.14}$$

where $\mathbf{d}'_1$ is a vector of received complex-valued symbols corresponding to PUCCH format 1A/1B and $\mathbf{d}'_2$ is a vector of received complex-valued symbols corresponding to PUCCH format 2, 2A/2B. IDFT of length equalling 12 is provided with the despread signal and the signal of individual users is separated. Simultaneously, the same operations on the receiving side are provided with the corresponding estimated channel coefficients $\hat{\mathbf{H}}$. Channel coefficients which correspond with PUCCH are arranged into the matrix of channel coefficients matched to each receive antenna $\hat{\mathbf{H}}_{\mathrm{PUCCH}} = \left[\hat{\mathbf{h}}_0, \hat{\mathbf{h}}_1, \ldots, \hat{\mathbf{h}}_{R_{\mathrm{PUCCH}}-1}\right]$, where R_{PUCCH} is the number of PUCCH received symbols. In the case of format 2/2A/2B QPSK or BPSK, equalization of received modulation symbol with Maximal Ratio Combining (MRC) is provided in terms of

$$\tilde{d}'_x = \frac{\mathbf{d}'_x \cdot \hat{\mathbf{h}}_x^H}{\hat{\mathbf{h}}_x^H \cdot \hat{\mathbf{h}}_x}, \tag{3.15}$$

where $\tilde{d}'_x$ is the equalized single modulation symbol after the Maximal ratio combining process, $\mathbf{d}'_x = \left[d_x^{(1)}, \ldots, d_x^{(N_{\mathrm{RX}})}\right]$ is the vector of received modulation symbols corresponding to each receive antenna, $\hat{\mathbf{h}}_x = \left[h_x^{(1)}, \ldots, h_x^{(N_{\mathrm{RX}})}\right]$ is the vector of estimated channel coefficients corresponding to the vector of received symbol $\mathbf{d}'_x$ and each receive antenna, and N_{RX} is the number of receive antennas.

Soft demodulation of modulated symbol in receiver $\tilde{d}'$ with coordinates (x, y)

using the log-likelihood ratio (LLR) algorithm is provided according to

$$L(b) = \log\left(\frac{\sum\limits_{s\in S_0} \mathrm{e}^{-\frac{1}{\sigma^2}\left((x-s_x)^2+(y-s_y)^2\right)}}{\sum\limits_{s\in S_1} \mathrm{e}^{-\frac{1}{\sigma^2}((x-s_x)^2+(y-s_y)^2)}}\right) \tag{3.16}$$

and its approximate version respectively

$$L(b) = -\frac{1}{\sigma^2}\left[\min_{s\in S_0}\left((x-s_x)^2+(y-s_y)^2\right) - \min_{s\in S_1}\left((x-s_x)^2+(y-s_y)^2\right)\right], \tag{3.17}$$

where b is transmitted bit, σ^2 is noise variance of baseband signal, S_0 is ideal constellation point with bit 0 at the given bit position, S_1 is ideal constellation point with bit 1 at the given bit position, s_x is in-phase coordinate of ideal constellation point and s_y is quadrature coordinate of ideal constellation point.

For PUCCH format 2 and 2A/2B, CQI/PMI, RI and HARQ-ACK bits are demultiplexed after demodulation, if necessary. After that, cell-specific descrambling is provided in terms of (3.4). The CQI/PMI, RI bits are decoded using the Reed-Muller block decoder. Due to the fact that the punctured version of Reed-Muller block coding is used in LTE uplink, a matched filter as the simplest and fastest block decoder is used for decoding. The receiver knows all possible sets of channel coding block output codewords and finds maximal correspondence in the received codeword. Note, that a matched filter is used in all block channel decoding in LTE [8, 42] and presented link level models. The format 1A/1B signal separated by the user is despread with orthogonal sequences and equalized using MRC receive diversity technique (3.15) soft demodulated according to (3.16) and (3.17) respectively.

Performance Analysis Results of UCI Transmission via PUCCH

Performance analysis was performed for all possible PUCCH formats except format 1. The number of subframes N_{subf} equals 50000 due to the reference BER/BLER level equalling 10^{-3}. The reference level was determined according to the required target quality for LTE uplink control information reception [43]. The AWGN channel model was only used in simulations, thus the channel coefficient matrix $\mathbf{H}$ has all coefficients equalling 1. Simulations assume perfect knowledge of the transmission channel model and a single UE and single BS within a cell.

In Fig. 3.10, the BER of HARQ-ACK information transmitted via PUCCH format 2A and 2B in the AWGN channel model for various numbers of receiving antennas is shown. It is obvious that transmitting HARQ-ACK using PUCCH format 1A/1B has a lower BER. The difference between the SNR value of format 1A and 2A, when BER equals the BER reference level 10^{-3}, is 6.3 dB. Using four receiving antennas adds a diversity gain equalling 6 dB in comparison to the SISO mode. The difference between the theoretical value for uncoded BPSK in SC-FDMA and simulated BER value for PUCCH format 2A with one transmitting and one receiving antenna equals 5.5 dB, for format 2B, the difference equals 8.5 dB.

Tab. 3.7: PUCCH simulation parameters

Parameters	Description
Frame structure	FDD
Number of transmitted subframes	50000
System bandwidth	1.4 MHz
Cyclic prefix (CP)	normal
Subcarrier spacing	15 kHz
Channel estimation	perfect knowledge
Demodulation method	Soft-decision (LLR)
Antenna configuration [$N_{TX} \times N_{RX}$]	1×1, 1×2, 1×4

Bit error rate results of CQI/PMI, RI codeword transmitted using PUCCH format 2 are presented in Fig. 3.11. These simulations were provided only with a CQI codeword of 4 bits in length. The difference between the SNR value of format 2 for the SISO antenna mode and the mode with 4 receiving antennas, when BER equals the BER reference level 10^{-3}, is 6 dB. The difference between the theoretical value of uncoded QPSK modulation scheme in SC-FDMA and simulated BER value for PUCCH format 2 with one transmitting and one receiving antenna equals 7.4 dB. If we compare the simulation results of transmitting control information using format 2 and 2B, there is no marked difference between their curves and reference values.

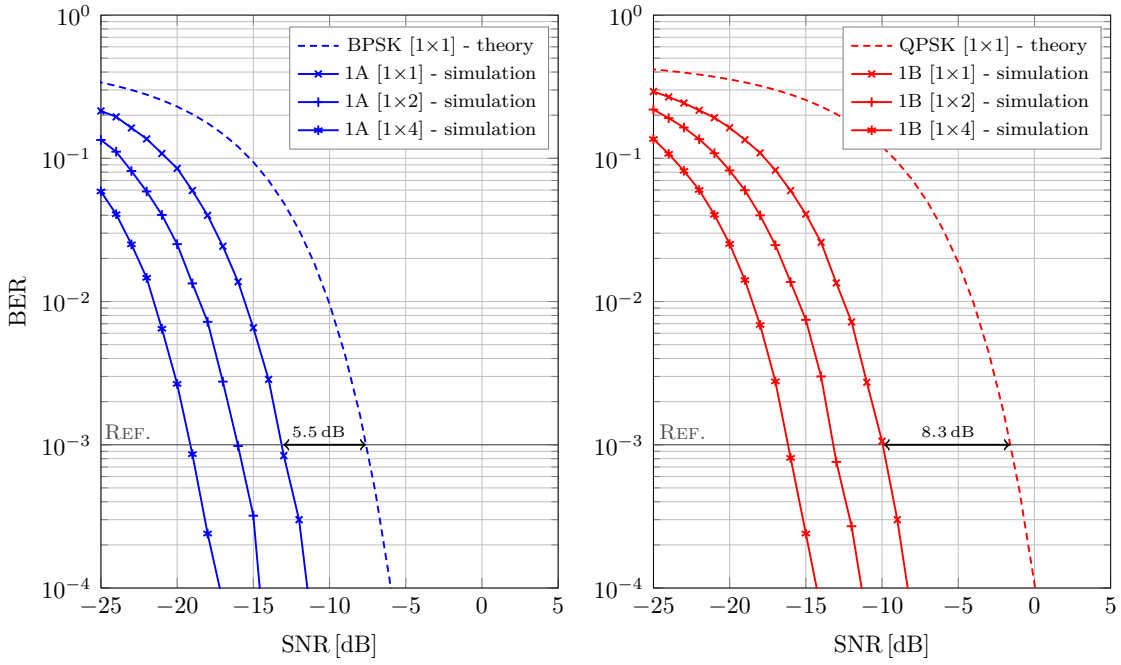

Fig. 3.9: BER of HARQ-ACK information transmitted using PUCCH, format 1A (left) and format 1B (right) in AWGN channel, various antenna modes

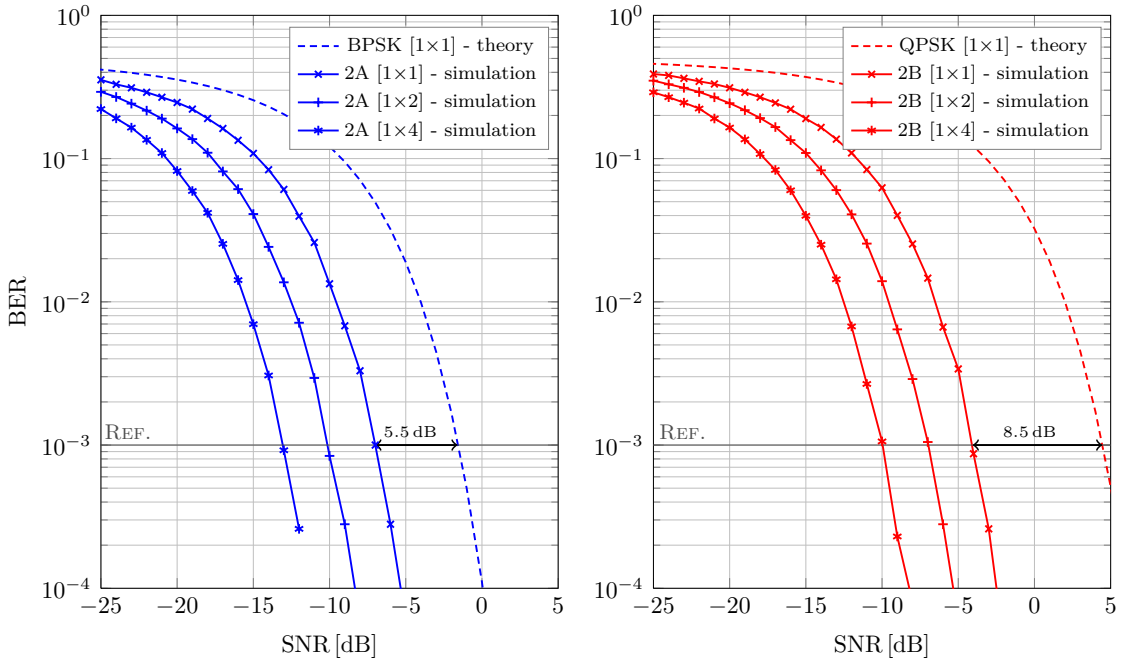

Fig. 3.10: BER of HARQ-ACK information transmitted using PUCCH, format 2A (left) and format 2B (right) in AWGN channel, various antenna modes

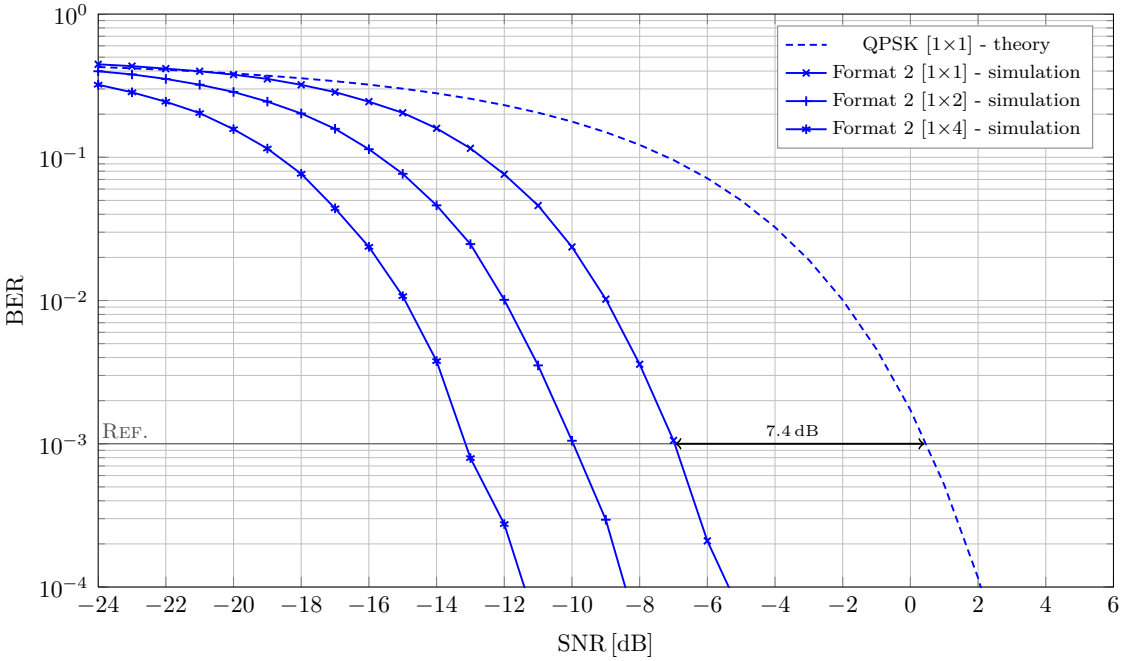

Fig. 3.11: BER of CQI/PMI and RI information transmitted using PUCCH format 2 in AWGN channel for various antenna configurations

3.2.2 Physical Uplink Shared Channel

As was mentioned in LTE uplink, channel quality information includes three components, Channel Quality Indicator (CQI), Precoding Matrix Indicator (PMI) and Rank Indicator (RI). The necessity of these components depends on the used transmission mode in downlink. If MIMO transmission mode is used, RI and PMI information are necessary. The knowledge about channel state (CQI) is essential primarily in the closed-loop MIMO system mode. The CQI message is triggered if the CQI request field in the Physical Downlink Control Channel (PDCCH) message, Downlink Control Indicator (DCI), format 0 is set to a value of 1. The CQI value defines the Modulation and Coding Scheme [1, 44].

The HARQ-ACK indicator is not included into CQI/PMI/RI modes and done separately. The HARQ-ACK indicator could be one or two-bit information depending on the number of transmitted codewords in downlink. All of mentioned signal information can be transmitted periodically (every 2–160 ms) or aperiodically on request of the BS. The minimum aperiodic reporting interval is 1 ms (one subframe). Aperiodic reporting is always scheduled by the BS (scheduling grant). This type of reporting is set by BS in Radio Resource Control information (RRC). Aperiodic CQI/PMI and RI reporting types can be Wideband feedback, BS-configured sub-band feedback and UE-selected sub-band feedback according to system settings [1].

PUSCH Link Level Model

PUSCH control information channel coding, scrambling and modulation model on the transmitting side is depicted in Fig. 3.12. If the length of CQI/PMI is less than 12 bits, only $(32, O)$ Reed-Muller channel coding is performed. Here O is the length of CQI/PMI input codeword. The vector of channel coded bits is labeled as $\mathbf{Q}_{\mathrm{CQI}}^{(2)}$. If the length of CQI/PMI is greater than 11 bits, convolutional coding with code rate equalling 1/3 is used. Generating polynomials of the used convolutional coder is defined according to

$$\begin{aligned} G_0{=}&x^6 + x^4 + x^3 + x + 1, \\ G_1{=}&x^6 + x^5 + x^4 + x^3 + 1, \\ G_2{=}&x^6 + x^5 + x^4 + x^2 + 1. \end{aligned} \tag{3.18}$$

Then, the rate matching operation is executed [8]. In the rate matching block, the vector of coded bits are interleaved using the Quadratic Permutation Polynomial technique and redundant bits are removed. Permutation is provided in terms of permutation pattern. In the receiver, it is necessary to calculate the position of dummy bits in the interleaver matrix. The vector of channel coded and rate matched bits is labeled as $\mathbf{Q}_{\mathrm{CQI}}^{(1)}$.

When CQI/PMI channel coding is performed, the vector $\mathbf{Q}_{\mathrm{CQI}}^{(1)}$ or $\mathbf{Q}_{\mathrm{CQI}}^{(2)}$ is then multiplexed with the vector of bits from the application data branch $\mathbf{F}$. Multiplexing is executed sequentially, according to

$$\mathbf{G} = \begin{bmatrix} \mathbf{Q}_{\mathrm{CQI}}^{(1)}, \mathbf{F} \\ \mathbf{Q}_{\mathrm{CQI}}^{(2)}, \mathbf{F} \end{bmatrix} \begin{array}{l} \text{for Convolutional coding,} \\ \text{for Reed-Muller coding.} \end{array} \tag{3.19}$$

The vector of multiplexed bits $\mathbf{G} = [g_0, g_1, \ldots, g_{H-1}]$, where H is the number of multiplexed bits, is regrouped into a set of column vectors $\mathbf{G}_{\mathrm{tmp}}$. Here, each column represents a single modulation symbol represented in bits as illustrated in (3.20).

$$\mathbf{G}_{\mathrm{tmp}} = \begin{bmatrix} g_0 & g_{Q_m} & \cdots & g_{H-Q_m} \\ g_1 & g_{Q_m+1} & \cdots & g_{H-Q_m+1} \\ \vdots & \vdots & \ddots & \vdots \\ g_{Q_m-1} & g_{2Q_m-1} & \cdots & g_{H-1} \end{bmatrix}. \tag{3.20}$$

The number of rows equals $Q_m = \log_2 M = \{2, 4, 6\}$ according to the used modulation scheme in PUSCH, where M is the number of bits per single modulation symbol in modulation scheme (QPSK, 16QAM and 64QAM). Each column vector of the pre-interleaving matrix $\mathbf{G}_{\mathrm{tmp}}$ is put into the interleaving matrix $\mathbf{K}$ row by row. Afterwards, RI and HARQ-ACK channel coded bits are inserted into $\mathbf{K}$ to predefined positions. The RI channel coded bits $\mathbf{Q}_{\mathrm{RI}}$ are always inserted into column numbers $\{1, 4, 7, 10\}$, the HARQ-ACK channel coded bits $\mathbf{Q}_{\mathrm{HARQ}}$ are always inserted into

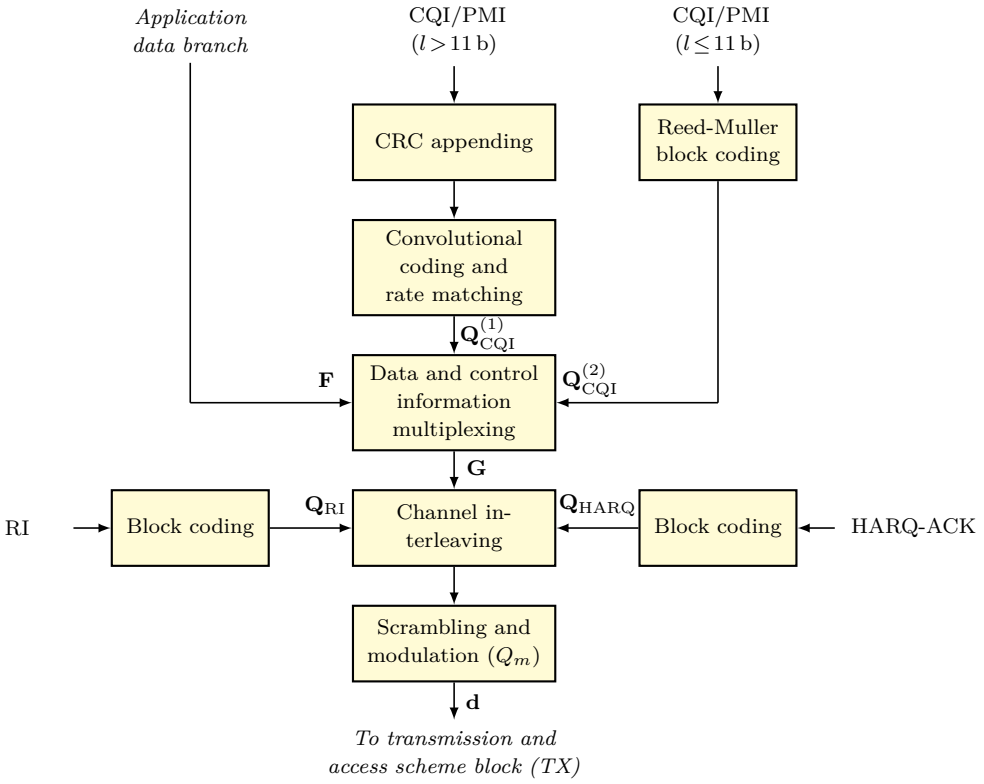

Fig. 3.12: Block scheme of PUSCH channel coding, scrambling and modulation model

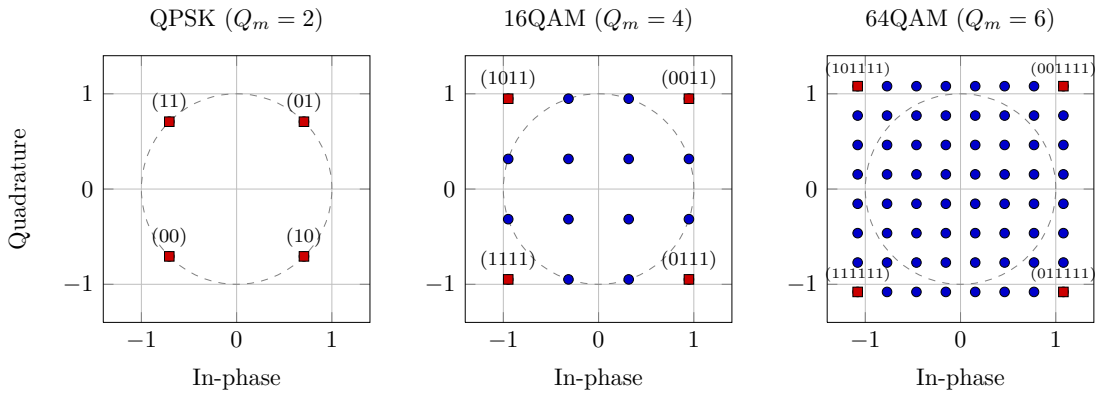

Fig. 3.13: PUSCH modulation schemes and position of RI and HARQ-ACK symbols using the placeholder technique

column numbers $\{2, 3, 8, 9\}$ (in the case of normal cyclic prefix) [8]. HARQ-ACK bits are situated close to Demodulation Reference Symbols (DMRS). Due to this fact, channel estimation of HARQ-ACK symbols is more accurate than in the case of RI symbols. The output vector of the interleaver is read column by column. The example of interleaver matrix $\mathbf{G}_{\text{tmp}}$ and mapping in the resource grid is depicted in Fig. 3.14.

In the case of transmitting RI and HARQ-ACK information, block channel coding is provided. RI and HARQ-ACK channel coding is provided in the way described in Tab. 3.8 and Tab. 3.9. Here, O_1 and O_2 are RI or HARQ-ACK input bits, $O_2 = O_1 \oplus O_2$, x is the so-called placeholder bit and y is the repetition placeholder bit. The placeholder technique is used in RI and HARQ-ACK channel coding for maximizing the Euclidean distance of symbols in modulation scheme [45]. The placeholder technique for HARQ-ACK and RI symbols in modulation schemes QPSK, 16QAM and 64QAM is illustrated in Fig. 3.13. The HARQ-ACK and RI symbols are always placed in the corner of the modulation scheme. The vector of RI channel coded bits is labeled as $\mathbf{Q}_{\text{RI}}$ and the vector of HARQ-ACK channel coded bits is labeled as $\mathbf{Q}_{\text{HARQ}}$.

Tab. 3.8: Channel coding of 1-bit RI or HARQ-ACK input message

Q_m	Coded RI or HARQ-ACK codeword
2	$[O_0, y]$
4	$[O_0, y, x, x]$
6	$[O_0, y, x, x, x, x]$

Tab. 3.9: Channel coding of 2-bit RI or HARQ-ACK input message

Q_m	Coded RI or HARQ-ACK codeword
2	$[O_0, O_1, O_2, O_0, O_1, O_2]$
4	$[O_0, O_1, x, x, O_2, O_0, x, x, O_1, O_2, x, x]$
6	$[O_0, O_1, x, x, x, x, O_2, O_0, x, x, x, x, O_1, O_2, x, x, x, x]$

The interleaved bits are then scrambled using a cell-specific pseudo-random sequence [5]. Due to using the placeholder technique, RI and HARQ-ACK bits must not be scrambled. Scrambled bits are modulated using QPSK, 16QAM or 64QAM which forms complex-valued symbols. The next step is to transform DFT precoding for PAPR reduction as is described in (3.21).

$$z(l\cdot M_{\mathrm{sc}}^{\mathrm{PUSCH}}+k)=\frac{1}{\sqrt{M_{\mathrm{sc}}^{\mathrm{PUSCH}}}}\sum_{i=0}^{M_{\mathrm{sc}}^{\mathrm{PUSCH}}-1}d(l\cdot M_{\mathrm{sc}}^{\mathrm{PUSCH}}+i)\mathrm{e}^{-\mathrm{j}\frac{2\pi k}{M_{\mathrm{sc}}^{\mathrm{PUSCH}}}}, \qquad (3.21)$$

$$k=0,\ldots,M_{\mathrm{sc}}^{\mathrm{PUSCH}}-1,$$
$$l=0,\ldots,\tfrac{M_{\mathrm{symb}}}{M_{\mathrm{sc}}^{\mathrm{PUSCH}}}-1.$$

Here $M_{\mathrm{sc}}^{\mathrm{PUSCH}}$ is the scheduled bandwidth for PUSCH transmission, expressed as the number of subcarriers and M_{symb} is the number of modulation symbols. The DFT size should be a multiple of 2,3 or 5 so that an efficient mixed-Radix DFT algorithm can be used [7].

The DFT precoded symbols are mapped into a resource grid and Demodulation Reference Signal (DMRS) and Sounding Reference Signal (SRS) are added (see Fig. 3.14). Afterwards, an SC-FDMA signal is formed and cyclic prefix (CP) is added. After the signal passes through the channel, which is described by the matrix of complex-valued channel coefficients $\mathbf{H}$, and AWGN is added, the signal enters the receiver.

In the receiver, which is depicted in Fig. 3.15, the CP is removed and inverse SC-FDMA operations are performed. Next, signal samples are equalized using the estimated channel coefficient matrix $\hat{\mathbf{H}}$. In the case of using more than a single receiving antenna, Maximal Ratio Combining (MRC) is performed according to (3.15). Executing the inverse DFT operation transforms the signal to the time domain. After the Soft-demodulation process (3.16) and (3.17), the vector of demodulated bits is descrambled using the same pseudo-random sequence as in the transmitter and is written to the deinterleaving matrix $\mathbf{K}'$ column by column. The position of placeholder bits x should be known in the receiver. These bits must not be descrambled. RI and HARQ-ACK coded bits are picked from the matrix, block decoding is executed and the RI or HARQ-ACK codeword is obtained.

Deinterleaved bits are read row by row from the matrix and CQI/PMI coded bits and application data is then separated. In the case of using Convolutional coding,

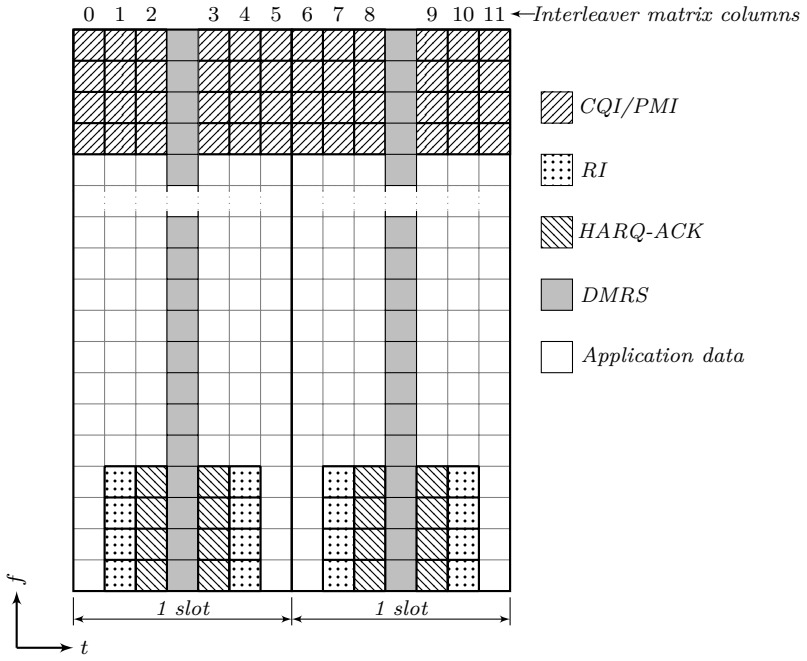

Fig. 3.14: Position of multiplexed and interleaved PUSCH symbols in the interleaving matrix $\mathbf{K}$, $Q_m = 4$ (Demodulation Reference Signal is depicted here due to better transparency)

rate dematching and Viterbi decoding is executed. In the end, the CRC appendix is removed and the CQI/PMI codeword is obtained. In the case of using Reed-Muller coding, only block decoding is executed and the CQI/PMI codeword is obtained.

Performance Analysis Results of UCI Transmission via PUSCH

Performance analysis was performed for all possible PUSCH configurations. The number of subframes N_{subf} equals 20000 due to the reference BER/BLER level equalling 10^{-3}. The reference level was determined according to the required target quality for LTE uplink control information reception [43]. PUSCH simulation parameters are listed in Tab. 3.10. Simulations were provided in AWGN and some characteristic fading channel models, which are described using the Tapped delay line model (see Tab. A.1 and A.2). Simulations assume perfect knowledge of the transmission channel model and a single UE and single BS within a cell. The abovementioned Control information generator supplies the simulator with randomly generated Uplink Control Information (CQI/PMI, RI and HARQ-ACK) according to simulation settings.

The CQI/PMI BER performance results under AWGN channel conditions are shown in Fig. 3.16. These simulations were performed for both types of channel coding, Reed-Muller and convolutional coding, and using all possible modulation schemes. In the case of Reed-Muller coding, CQI/PMI input codeword length is

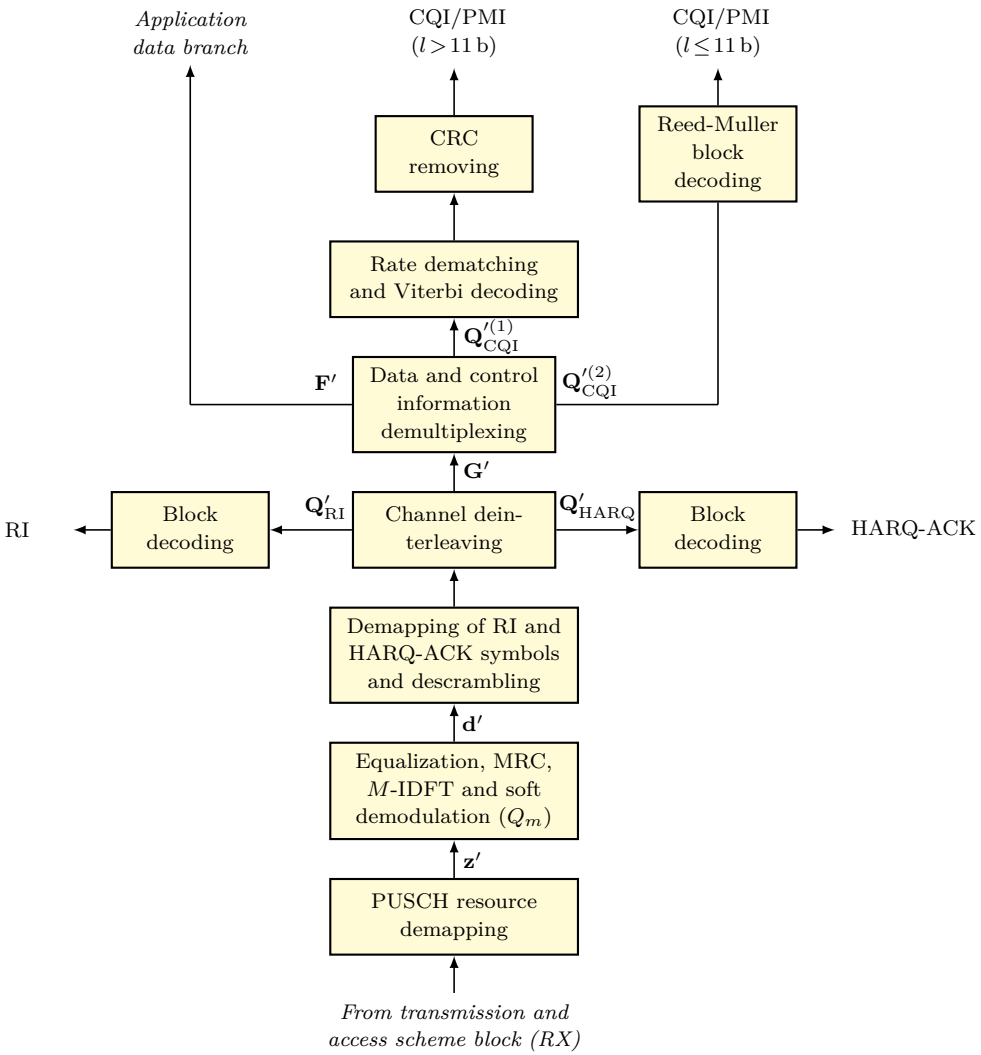

Fig. 3.15: Block scheme of PUSCH channel decoding, descrambling and demodulation model

4 bits. In the case of convolutional coding, the CQI/PMI input codeword has variable length. The value of SNR at which BER reaches the reference level are listed transparently in Tab. 3.11. From the results, it is obvious that Reed-Muller coding has a gain approximately equalling 3 dB to convolutional coding for the QPSK modulation scheme.

The HARQ-ACK or RI BER results are shown in Fig. 3.17. The results are depicted for both possible lengths of input codeword. These simulations are also provided for all possible modulation schemes. From the figure, it is obvious that coding of a 2-bit codeword in length, is more efficient than coding of a 1-bit codeword in length. The difference between the SNR value of 2-bit codeword coding and 1-bit codeword coding when BER equals the BER reference level 10^{-3} is 2.7 dB for the 64QAM modulation scheme. The lowest BER value is achieved when UCI is

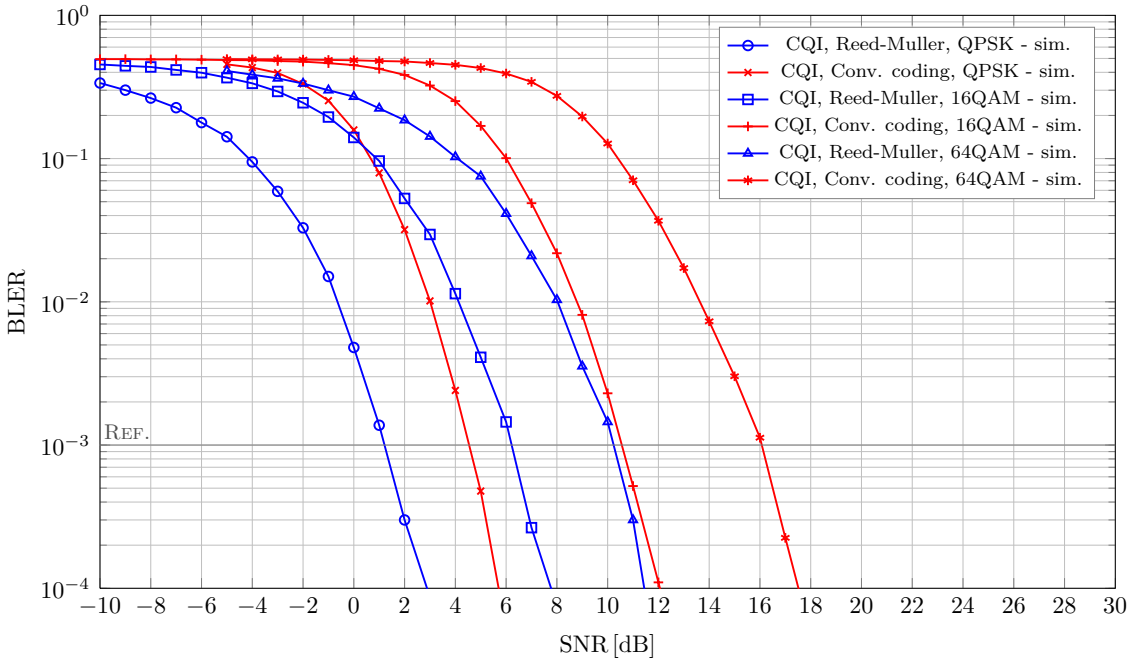

Fig. 3.16: BER of CQI/PMI information coded using Reed-Muller and conv. coding in AWGN channel, SISO antenna mode

transmitted using the 64QAM modulation schemes due to maximizing the Euclidean distance in the modulation scheme (see Fig. 3.13).

All simulations in fading channel models (Pedestrian A, Vehicular A) were performed only for the QPSK modulation scheme. In Fig. 3.18 the BER of CQI/PMI in Pedestrian A (PedA) channel model is shown. Simulations were performed for both types of channel coding and a number of receive antennas $N_{\mathrm{RX}} = \{1, 2, 4\}$. Summarized SNR values at which BER reaches the reference level of 10^{-3} for PedA are listed in Tab. 3.12. The SNR value at which the BER curve reaches the refer-

Tab. 3.10: PUSCH simulation parameters

Parameters	Description
Frame structure	FDD
Number of transmitted subframes	20000
System bandwidth	1.4 MHz
Cyclic prefix (CP)	normal
Subcarrier spacing	15 kHz
Channel estimation	perfect knowledge
Demodulation method	Soft-decision (LLR)
Antenna configuration [$N_{\mathrm{TX}} \times N_{\mathrm{RX}}$]	1×1, 1×2, 1×4

Tab. 3.11: SNR values at which BER reaches the reference level 10^{-3} in the AWGN channel

	CQI/PMI		HARQ-ACK, RI	
	Reed-Muller	Convolutional	1 bit	2 bits
QPSK	1.3 dB	4.5 dB	9.7 dB	6.5 dB
16QAM	6.2 dB	10.5 dB	7.3 dB	4.4 dB
64QAM	10.2 dB	16.1 dB	5.8 dB	3.1 dB

ence level, when the SISO antenna mode is used, is 24 dB for Reed-Muller coding and 28.5 dB for convolutional coding (the SNR value for convolutional coding is estimated from the trend of the curve). Both curves belong to the SISO antenna mode and have a typical shape for channels with Rayleigh PDF. Using two receive antennas gives a diversity gain in the SISO antenna mode of 7 dB for Reed-Muller coding and 11.7 dB for convolutional coding. Using four receive antennas improves reception by 8 dB approximately.

The BER of HARQ or RI in the PedA channel model for the QPSK modulation scheme is shown in Fig. 3.19. The results show the dependency of length of input codeword and the used antenna scheme. In PedA fading channel models, there are not marked differences between the curves for 1 bit and 2 bit HARQ or RI codeword.

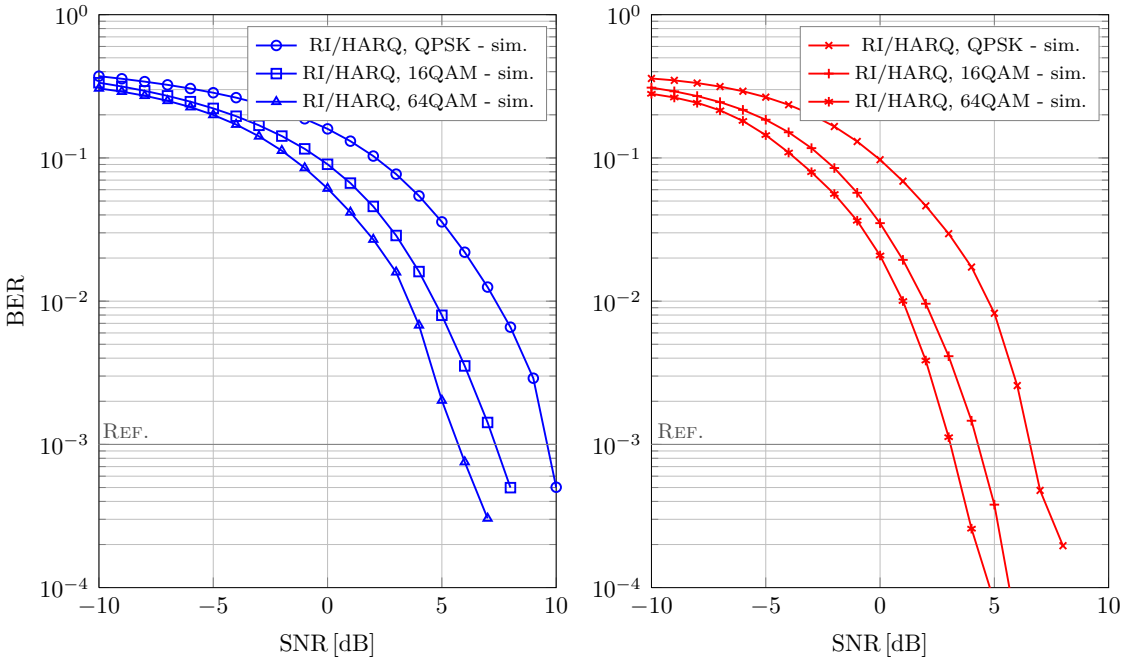

Fig. 3.17: BER of RI or HARQ-ARQ information transmitted via PUSCH, 1 bit codeword (left) and 2 bit codeword (right) in AWGN channel, SISO antenna mode

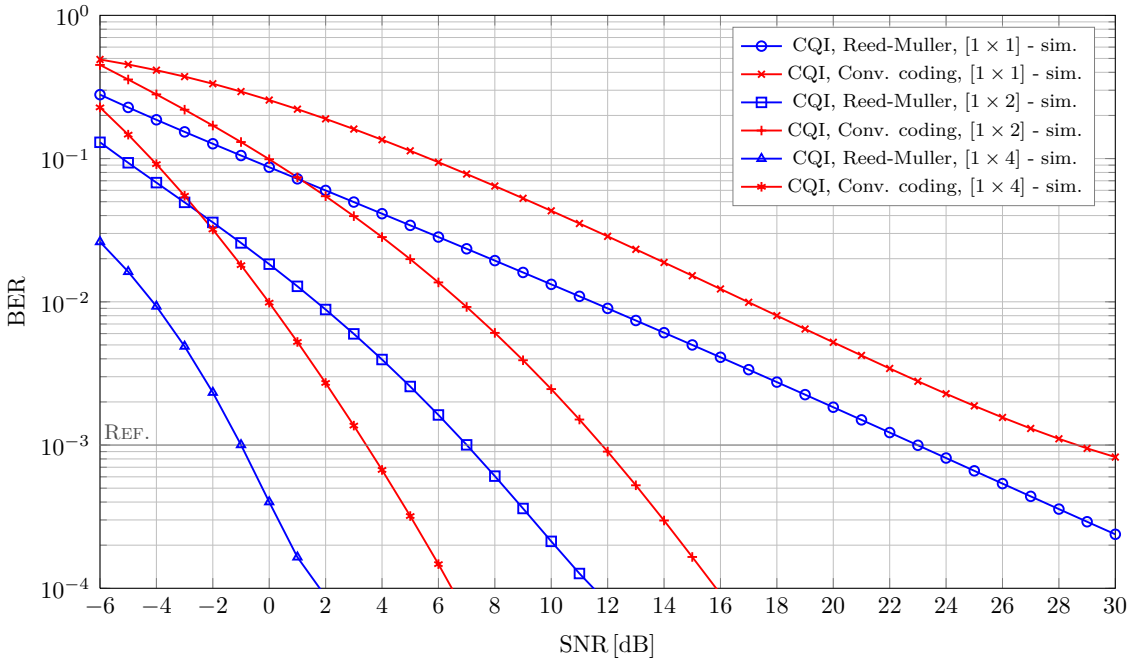

Fig. 3.18: BER of CQI/PMI information coded using Reed-Muller and Convolutional coding for the QPSK modulation scheme and different antenna configurations, in PedA channel

The BER results of CQI/PMI codeword transmission in the Vehicular A channel model are shown in Fig. 3.20. In the case of the SISO antenna mode, the results are worse by 0.5 dB for Reed-Muller coding and by 1.5 dB for convolutional coding if compared with Pedestrian A results. If we use receive diversity, the differences between the VehA and PedA SNR value at which BER reaches the reference level are less or equal to 1 dB.

The BER of HARQ or RI in VehA channel model for the QPSK modulation scheme and different antenna configurations is shown in Fig. 3.21. The BER results of HARQ or RI in the VehA fading channel model is similar to corresponding results in PedA especially in the case of using receive diversity. The summarized SNR values at which BER reaches the reference value are in Tab. 3.13.

Tab. 3.12: SNR values at which the BER reaches the reference level 10^{-3} in Pedestrian A channel, QPSK

	CQI/PMI		HARQ-ACK, RI	
	Reed-Muller	Convolutional	1 bit	2 bits
[1×1]	24.0 dB	28.5 dB	28.1 dB	25.7 dB
[1×2]	7.0 dB	11.7 dB	13.6 dB	11.8 dB
[1×4]	−1.0 dB	3.2 dB	7.0 dB	4.5 dB

Tab. 3.13: SNR values at which the BER reaches the reference level 10^{-3} in Vehicular A channel, QPSK

	CQI/PMI		HARQ-ACK, RI	
	Reed-Muller	Convolutional	1 bit	2 bits
[1×1]	23.6 dB	29.0 dB	30.0 dB	28.7 dB
[1×2]	5.6 dB	10.1 dB	13.5 dB	10.7 dB
[1×4]	−1.6 dB	2.4 dB	6.7 dB	3.5 dB

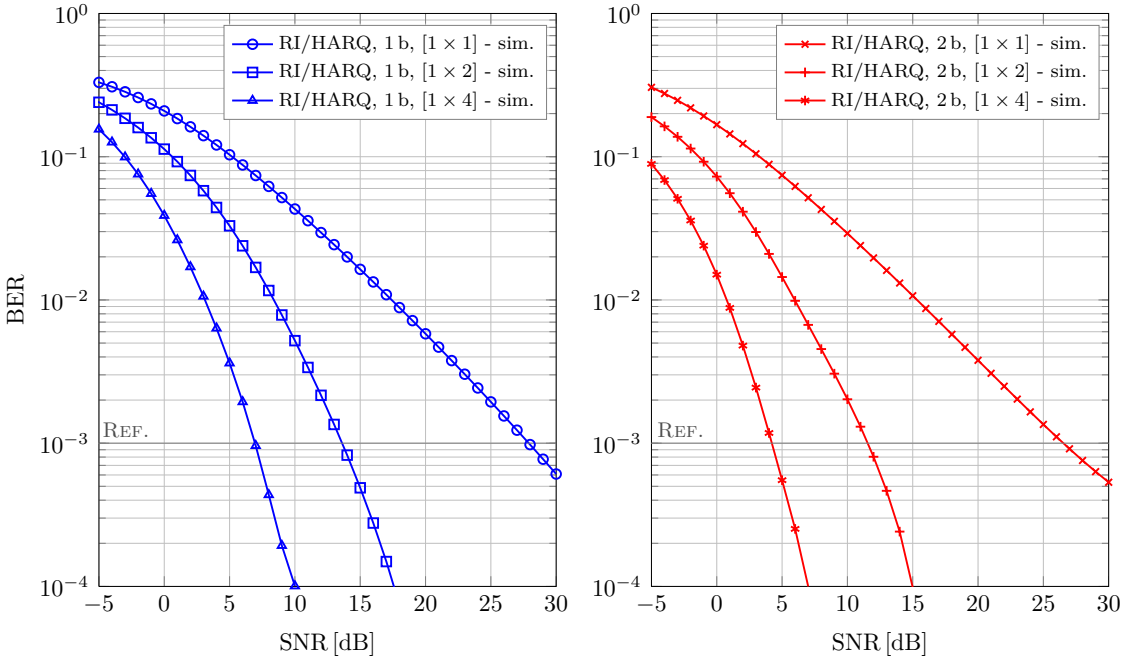

Fig. 3.19: BER of RI or HARQ-ARQ information transmitted via PUSCH, 1 bit codeword (left) and 2 bit codeword (right) in PedA channel, QPSK

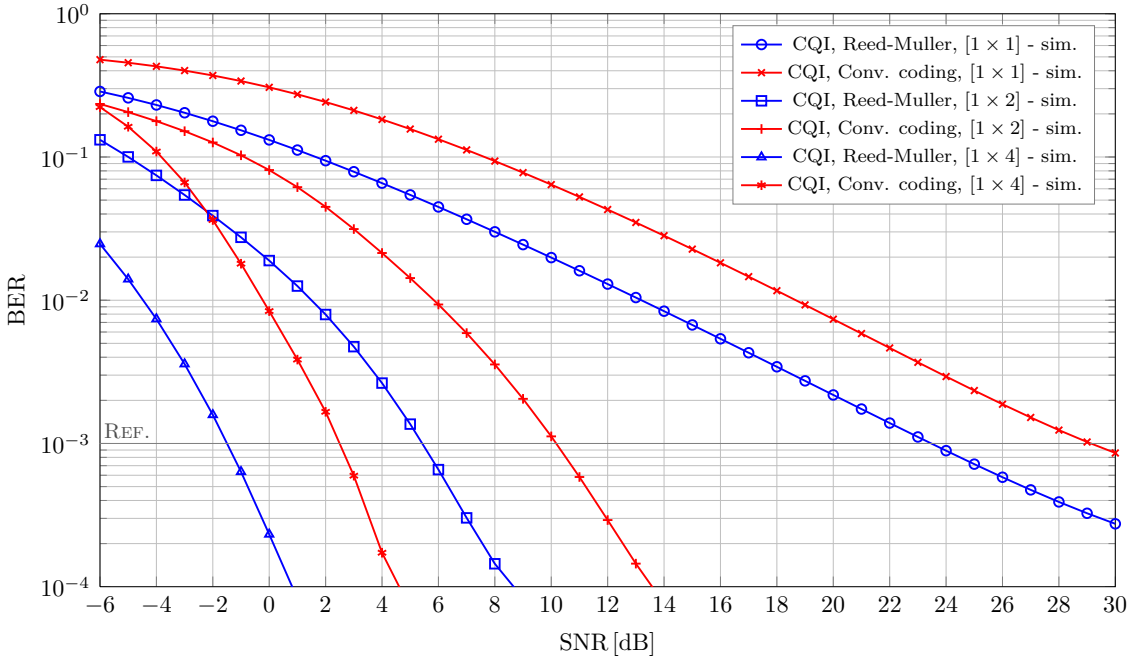

Fig. 3.20: BER of CQI/PMI information coded using Reed-Muller and Convolutional coding for the QPSK modulation scheme and different antenna configurations, in VehA channel

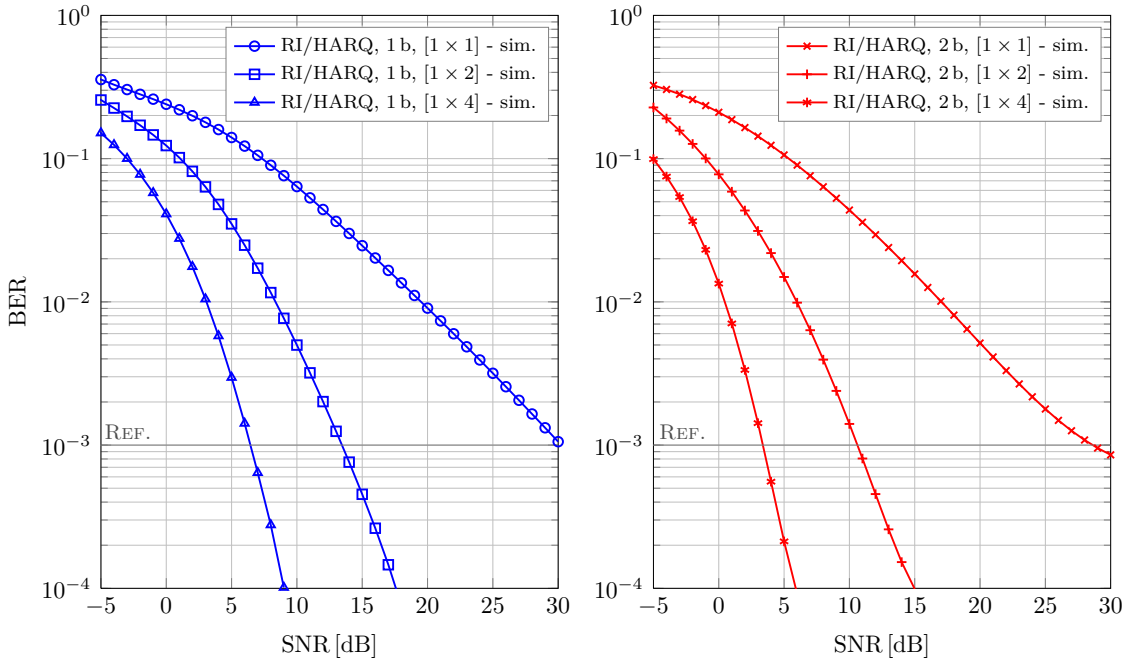

Fig. 3.21: BER of RI or HARQ-ARQ information transmitted via PUSCH, 1 bit codeword (left) and 2 bit codeword (right) in VehA channel, QPSK

3.3 Downlink Control Information Transmission

In this section, a detailed description of Downlink control information (DCI), Control format indicator (CFI) and Hybrid ARQ indicator (HI) signal processing in LTE downlink physical layer with emphasis on channel coding description is presented. Performance analysis results of mentioned control information are also presented. Mapping of transport to physical channels in downlink is depicted in Fig. 3.22.

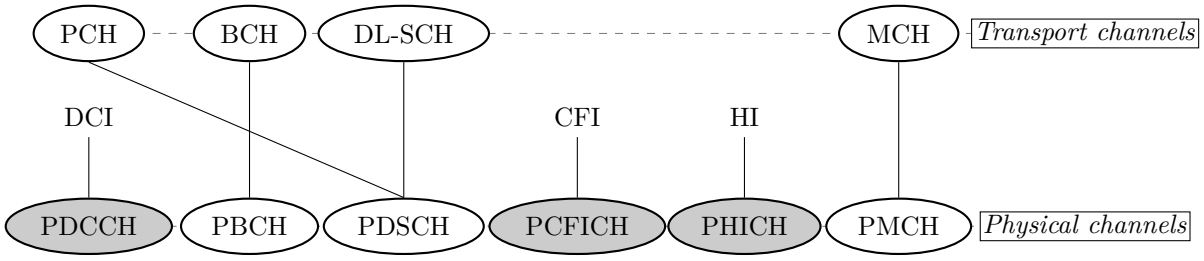

Fig. 3.22: Mapping transport to physical channels in LTE downlink

There is a triplet of traffic channels (PBCH, PDSCH and PMCH). Downlink control information (DCI), Control Format Indicator (CFI) and Hybrid ARQ Indicator (HI) are transmitted via a triplet of physical control channels, PDCCH, PCFICH and PHICH. As is obvious from the Fig. 3.22, the control information is not linked together with transport channels.

3.3.1 Physical Control Format Indicator Channel

Via this channel, the Control Format Indicator (CFI) is transmitted. The value stored in CFI determines the number of resource elements in the resource grid (in time domain) carrying the data of the PDCCH control channel. It determines the PDCCH control area in each subframe in downlink. PCFICH is transmitted in the first OFDM symbol in the resource grid [5].

Tab. 3.14: PCFICH channel block coding

CFI	CFI codeword $\mathbf{b} = [b_0, b_1, \ldots, b_{31}]$
1	$[0,1,1,0,1,1,0,1,1,0,1,1,0,1,1,0,1,1,0,1,1,0,1,1,0,1,1,0,1,1,0,1]$
2	$[1,0,1,1,0,1,1,0,1,1,0,1,1,0,1,1,0,1,1,0,1,1,0,1,1,0,1,1,0,1,1,0]$
3	$[1,1,0,1,1,0,1,1,0,1,1,0,1,1,0,1,1,0,1,1,0,1,1,0,1,1,0,1,1,0,1,1]$
4 (reserved)	$[0,0,0,0,0,0,0,0,0,0,0,0,0,0,0,0,0,0,0,0,0,0,0,0,0,0,0,0,0,0,0,0]$

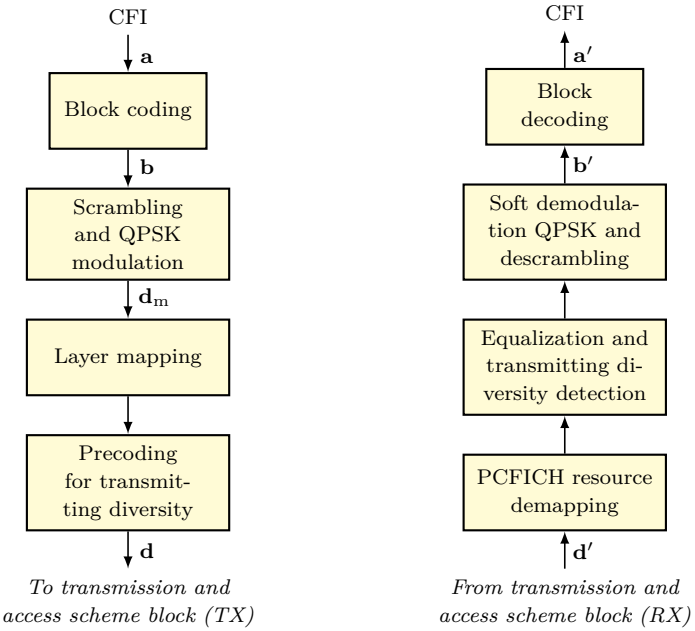

(a) Transmitting side (b) Receiving side

Fig. 3.23: Block scheme of the PCFICH channel coding, scrambling and modulation model (left) and channel decoding, descrambling and demodulation (right)

PCFICH Link Level Model

The CFI parameter takes values 1, 2 or 3 only. The block diagram of the PCFICH transmitting model is shown in Fig. 3.23. The first operation in the signal processing chain is channel coding. A bit sequence of 32 bits in length is assigned to each two-bit value stored in CFI according to Tab. 3.14. Thus, the code rate of PCFICH channel block coding equals 16.

A codeword $\mathbf{b}$ of 32 bits in length is scrambled with a pseudo-random scrambling sequence, which is unique for each cell, according to (3.4). The scrambled bits $\tilde{\mathbf{b}}$ are modulated by QPSK modulation. The modulation scheme used in PCFICH is depicted in Fig. 3.24.

Next, the vector of complex-value symbols $\mathbf{d}_{\mathrm{m}} = [d_{\mathrm{m}}(0), d_{\mathrm{m}}(1), \ldots, d_{\mathrm{m}}(D_{\mathrm{CFI}} - 1)]$ is mapped into ν-layers, dependant on the number of transmitting antennas, where $\nu = \{1, 2, 4\}$ and D_{CFI} are the number of modulated symbols in PCFICH. In the case of one transmitting antenna, layer mapping is not used and transmitting diversity precoding is not provided [46]. In the case of two transmitting antennas, layer mapping is provided in terms of

$$\mathbf{x} = \begin{cases} x^{(0)}(i) = d_{\mathrm{m}}(2i), \\ x^{(1)}(i) = d_{\mathrm{m}}(2i+1), \end{cases} \tag{3.22}$$

where $x^{(0)}(i)$ is the i-th symbol layer mapped to an antenna with index 0 and $x^{(1)}(i)$ is the i-th symbol layer mapped to an antenna with index 1. Transmitting diversity precoding is provided according to

$$\mathbf{d} = \begin{bmatrix} d^{(0)}(2i) \\ d^{(1)}(2i) \\ d^{(0)}(2i+1) \\ d^{(1)}(2i+1) \end{bmatrix} = \frac{1}{\sqrt{2}} \begin{bmatrix} 1 & 0 & \mathrm{j} & 0 \\ 0 & -1 & 0 & \mathrm{j} \\ 0 & 1 & 0 & \mathrm{j} \\ 1 & 0 & -\mathrm{j} & 0 \end{bmatrix} \begin{bmatrix} \mathrm{Re}\left(x^{(0)}(i)\right) \\ \mathrm{Re}\left(x^{(1)}(i)\right) \\ \mathrm{Im}\left(x^{(0)}(i)\right) \\ \mathrm{Im}\left(x^{(1)}(i)\right) \end{bmatrix}, \tag{3.23}$$

where $\mathbf{d}$ is a matrix of precoded, layer mapped and modulated symbols. Thus, precoded symbols $\mathbf{d}$ are time-mapped to two antennas in terms of the following diagram.

Ant. 0:	$x^{(0)}(i)$	$x^{(1)}(i)$	$x^{(0)}(i+1)$	$x^{(1)}(i+1)$	$\cdots$
Ant. 1:	$-x^{(1)}(i)^*$	$x^{(0)}(i)^*$	$-x^{(1)}(i+1)^*$	$x^{(0)}(i+1)^*$	$\cdots$

In the case of using four transmitting antennas, layer mapping is provided in terms of

$$\mathbf{x} = \begin{cases} x^{(0)}(i) = d_{\mathrm{m}}(4i), \\ x^{(1)}(i) = d_{\mathrm{m}}(4i+1), \\ x^{(2)}(i) = d_{\mathrm{m}}(4i+2), \\ x^{(3)}(i) = d_{\mathrm{m}}(4i+3). \end{cases} \tag{3.24}$$

Precoding for transmit diversity is provided according to equation (3.25).

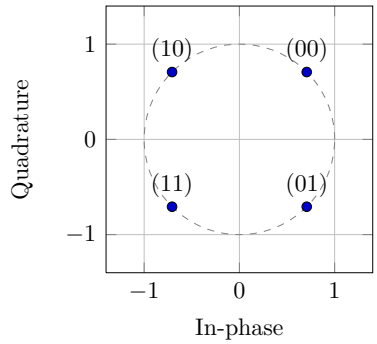

Fig. 3.24: QPSK modulation scheme used in PCFICH and PDCCH

$$\mathbf{d} = \begin{bmatrix} d^{(0)}(4i) \\ d^{(1)}(4i) \\ d^{(2)}(4i) \\ d^{(3)}(4i) \\ d^{(0)}(4i+1) \\ d^{(1)}(4i+1) \\ d^{(2)}(4i+1) \\ d^{(3)}(4i+1) \\ d^{(0)}(4i+2) \\ d^{(1)}(4i+2) \\ d^{(2)}(4i+2) \\ d^{(3)}(4i+2) \\ d^{(0)}(4i+3) \\ d^{(1)}(4i+3) \\ d^{(2)}(4i+3) \\ d^{(3)}(4i+3) \end{bmatrix} = \frac{1}{\sqrt{2}} \begin{bmatrix} 1 & 0 & 0 & 0 & \mathrm{j} & 0 & 0 & 0 \\ 0 & 0 & 0 & 0 & 0 & 0 & 0 & 0 \\ 0 & -1 & 0 & 0 & 0 & \mathrm{j} & 0 & 0 \\ 0 & 0 & 0 & 0 & 0 & 0 & 0 & 0 \\ 0 & 1 & 0 & 0 & 0 & \mathrm{j} & 0 & 0 \\ 0 & 0 & 0 & 0 & 0 & 0 & 0 & 0 \\ 1 & 0 & 0 & 0 & -\mathrm{j} & 0 & 0 & 0 \\ 0 & 0 & 0 & 0 & 0 & 0 & 0 & 0 \\ 0 & 0 & 0 & 0 & 0 & 0 & 0 & 0 \\ 0 & 0 & 1 & 0 & 0 & 0 & \mathrm{j} & 0 \\ 0 & 0 & 0 & 0 & 0 & 0 & 0 & 0 \\ 0 & 0 & 0 & -1 & 0 & 0 & 0 & \mathrm{j} \\ 0 & 0 & 0 & 0 & 0 & 0 & 0 & 0 \\ 0 & 0 & 0 & 1 & 0 & 0 & 0 & \mathrm{j} \\ 0 & 0 & 0 & 0 & 0 & 0 & 0 & 0 \\ 0 & 0 & 1 & 0 & 0 & 0 & -\mathrm{j} & 0 \end{bmatrix} \begin{bmatrix} \mathrm{Re}\left(x^{(0)}(i)\right) \\ \mathrm{Re}\left(x^{(1)}(i)\right) \\ \mathrm{Re}\left(x^{(2)}(i)\right) \\ \mathrm{Re}\left(x^{(3)}(i)\right) \\ \mathrm{Im}\left(x^{(0)}(i)\right) \\ \mathrm{Im}\left(x^{(1)}(i)\right) \\ \mathrm{Im}\left(x^{(2)}(i)\right) \\ \mathrm{Im}\left(x^{(3)}(i)\right) \end{bmatrix}, \tag{3.25}$$

Precoded symbols $\mathbf{d}$ are time-mapped to four antennas in terms of the following diagram (same resource elements in different antennas).

Ant. 0:	$x^{(0)}(i)$	$x^{(1)}(i)$	0	0	$\cdots$
Ant. 1:	0	0	$x^{(2)}(i)$	$x^{(3)}(i+1)$	$\cdots$
Ant. 2:	$-x^{(1)}(i)^*$	$x^{(0)}(i)^*$	0	0	$\cdots$
Ant. 3:	0	0	$-x^{(3)}(i)^*$	$x^{(2)}(i+1)^*$	$\cdots$

Complex symbols for each transmitting antenna are grouped to quaternary symbols, so-called symbol quadruplets, which are mapped to defined positions in the resource grid [47]. Furthermore, an IFFT operation with symbols in the resource grid is performed and CP is inserted.

After passing through the channel, CP is removed and FFT is performed. Signal processing on the receiving side is depicted in Fig. 3.23. In the resource demapping block, PCFICH symbols $\mathbf{d}'_{\mathrm{CFI}}$ are collected. When using more than one transmitting antenna, equalization and operations for transmitting diversity (TxD) detection is provided in terms of the following expressions which describe the situation for two transmitting and a single receiving antenna [2×1]. The transmission of modulated symbols $\mathbf{x}$, which are precoded using (3.23), via channel $\mathbf{H}$ ($\hat{\mathbf{H}}$ respectively) is described as

$$\mathbf{y} = \hat{\mathbf{H}}\mathbf{x} + \mathbf{n}, \tag{3.26}$$

where $\mathbf{y}$ denotes the vector of received symbols and $\mathbf{n}$ denotes the white Gaussian

noise (AWGN) vector. We can rewrite it as

$$\begin{bmatrix} y(i) \\ y(i+1)^* \end{bmatrix} = \underbrace{\begin{bmatrix} h_1(i) & -h_2(i) \\ h_2(i+1)^* & h_1(i+1)^* \end{bmatrix}}_{\mathbf{H}'} \begin{bmatrix} x(i) \\ x(i+1) \end{bmatrix} + \begin{bmatrix} n_1 \\ n_2^* \end{bmatrix}. \tag{3.27}$$

Here, the matrix of estimated channel coefficients $\hat{\mathbf{H}}$ is restructured to the so-called channel equivalent matrix $\mathbf{H}'$. The pseudo-inverse of channel equivalent matrix $(\mathbf{H}')^{-1}$ is used to determine received symbols $\hat{\mathbf{x}}$ according to

$$\hat{\mathbf{x}} = (\mathbf{H}')^{-1}\mathbf{y}. \tag{3.28}$$

Inverse TxD precoding for different antenna configurations are provided in a similar way.

Complex-value symbols are soft-demodulated using (3.17) and descrambled by pseudo-random sequence which is the same as on the transmitting side. Finally, PCFICH block decoding is provided in terms of Tab. 3.14 using majority logic vote and CFI is obtained.

Performance Analysis Results of CFI Transmission via PCFICH

The results of the PCFICH control channel transmission simulation and subsequent analysis of BER's dependence on the Signal to Noise Ratio (SNR) for investigated antenna configurations and models of the transmission channels used are listed in this section. The BER is calculated from the difference between two-bit CFI values obtained at the beginning and at the end of the transmission chain. The PCFICH BER curves arranged according to the investigated channel models (AWGN, Pedestrian B and Vehicular A) and available antenna configurations are shown in figures 3.25 to 3.27.

Tab. 3.15: PCFICH simulation parameters

Parameters	Description
Frame structure	FDD
Number of transmitted subframes	10000
System bandwidth	1.4 MHz
Cyclic prefix (CP)	normal
Subcarrier spacing	15 kHz
Channel estimation	perfect knowledge
Demodulation method	Soft-decision (LLR)
Antenna configuration [$N_{\mathrm{TX}} \times N_{\mathrm{RX}}$]	1×1, 2×1, 4×2

Tab. 3.16: SNR values at which the BER in PCFICH reaches the reference level 10^{-3} in different channel models

Antenna configuration	Minimal SNR value in dB for different channel type		
$[N_{TX} \times N_{RX}]$	AWGN	Pedestrian B	Vehicular A
1×1	−0.9 dB	6.5 dB	7.1 dB
2×1	−0.9 dB	3.4 dB	3.3 dB
4×2	−3.9 dB	−2.8 dB	−2.6 dB

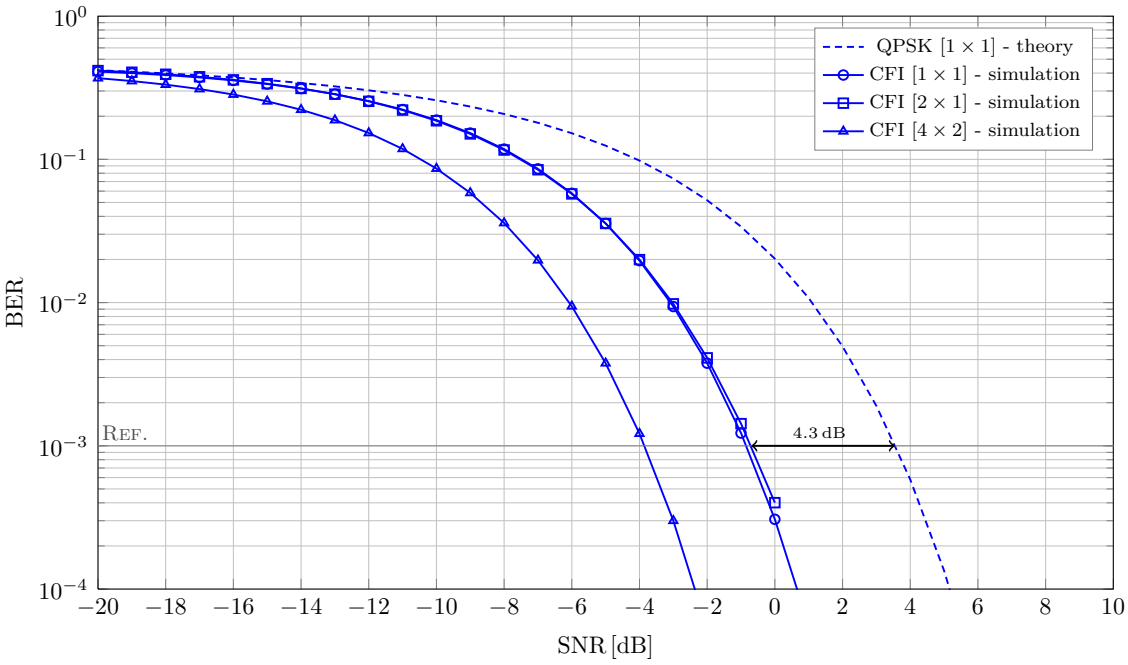

Fig. 3.25: BER of CFI information transmitted via PCFICH in AWGN channel, various antenna modes

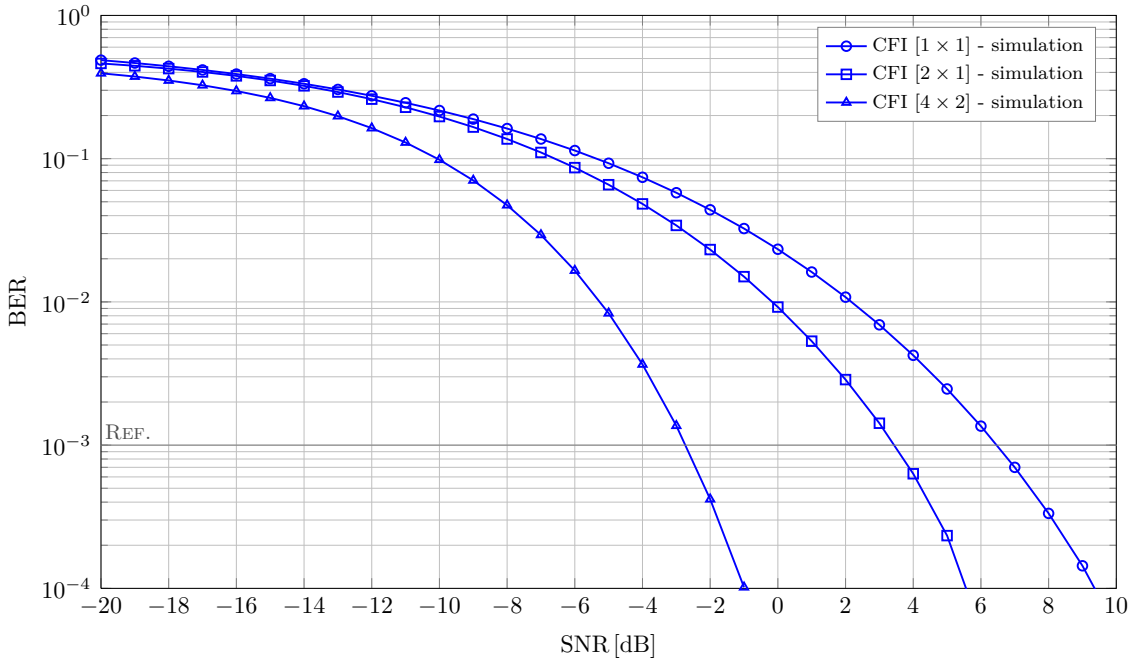

Fig. 3.26: BER of CFI information transmitted via PCFICH in Pedestrian B channel, various antenna modes

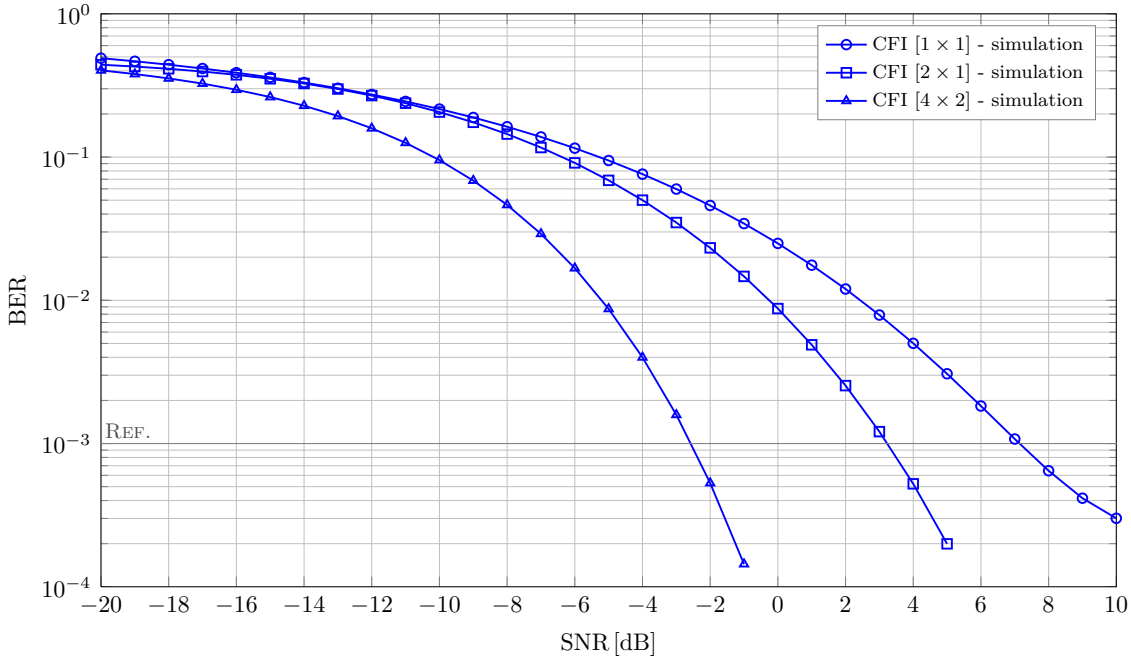

Fig. 3.27: BER of CFI information transmitted via PCFICH in Vehicular A channel, various antenna modes

Table 3.15 lists the main parameters of the simulation of PCFICH. The number of transmitted subframes equals 10000. SISO mode is a basic antenna mode and transmitting diversity is also investigated (antenna configuration $[2 \times 1]$ and $[4 \times 2]$). As was mentioned, simulations assume perfect knowledge of the transmission channel model and a single UE and single BS within a cell. Table 3.16 summarizes the results of PCFICH BER. The values of SNR are given at which the BER in the PCFICH channel reaches the reference level of 10^{-3}.

In Fig. 3.25, CFI BER in the AWGN channel model for the mentioned antenna configurations are shown. There is also depicted the curve of bit error probability of QPSK modulation in the OFDM system (without channel coding). The channel coding gain in the case of SISO mode in the AWGN model equals 4.3 dB. In AWGN it is obvious that using the transmitting diversity technique with two transmitting and single receiving antenna has the same results as in SISO mode. Diversity gain when $N_{\mathrm{TX}} = 4$ and $N_{\mathrm{RX}} = 2$ equals 3 dB. In Fig. 3.26 and 3.27 are shown BER CFI results in Pedestrian B and Vehicluar A channel model respectively. These results have similar curves as seen from the figures. The transmitting diversity technique gives a gain equalling 3 dB ($[2 \times 1]$) and 6 dB ($[4 \times 2]$) respectively.

3.3.2 Physical Downlink Control Channel

Physical Downlink Control Channel (PDCCH) is the most important control channel in downlink. It supports signalling for data channels in downlink and uplink. Via this channel Downlink Control Information (DCI) is transmitted. PDCCH supports various formats of DCI messages [39, 40]. They contain information about resource scheduling for downlink and uplink, Transmit Power Commands (TPC), etc.

PDCCH Link Level Model

The block diagram of the PDCCH channel coding, scrambling and modulation model in transmitting side is shown in Fig. 3.28. Individual DCI messages of different formats are channel coded. Cyclic redundancy check (CRC-16) of 16 bits in length is added to the DCI message. Afterwards, the CRC is scrambled with a Radio Network Temporary Identifier (RNTI) value and an antenna's mask if needed [8]. The next block in the processing chain is a convolutional coder with code rate $R = 1/3$. Convolutional coding is provided according to generating polynomials defined in (3.18). In the rate matching block, interleaving is provided and decreases the length of the coded DCI message.

These operations with all DCI messages are provided in parallel and these messages come into a PDCCH multiplexing block. The coded DCI messages are encapsulated into so-called Control Channel Elements (CCE). These elements are mapped into individual PDCCH formats (denoted as $\mathbf{b}$), see Tab. 3.17. This procedure is necessary because blind decoding technology is used on the receiving side. The PDCCH frame is scrambled in the same way as in the case of PCFICH.

Scrambled bits are modulated by QPSK modulation (see Fig. 3.24) and then form a block of complex-value symbols $\mathbf{d}_{\mathrm{m}}$ which are mapped into ν-layers according to (3.22) and (3.24) respectively, and precoding for transmit diversity is performed according to (3.23) and (3.25) respectively. These symbols, split into ν-parallel streams and mapped to the quadruplets of symbols, are interleaved using Free-quadratic Permutation Polynomial technology (QPP). When interleaving is performed, quadruplets are mapped into defined positions in the resource grid. The distribution of PDCCH quadruplets is given by the value in CFI. Furthermore,

Tab. 3.17: List of supported PDCCH formats

PDCCH format	Number of CCE's	Number of REG's	Number of PDCCH bits
0	1	9	72
1	2	18	144
2	4	36	288
3	8	72	576

complex-valued symbols $\mathbf{d}$ are transferred into the OFDMA transmitter. After passing through the channel, on the receiving side, inverse OFDMA operations are performed. In the resource demapping block, the matrix of PDCCH symbols $\mathbf{d}'_{\mathrm{PDCCH}}$ and the matrix of corresponding channel coefficients $\hat{\mathbf{H}}_{\mathrm{PDCCH}}$ are collected. Reverse sub-block interleaving is performed with both of these matrices. The modified symbols lead into the equalization, MIMO detector and soft-demodulation block. The

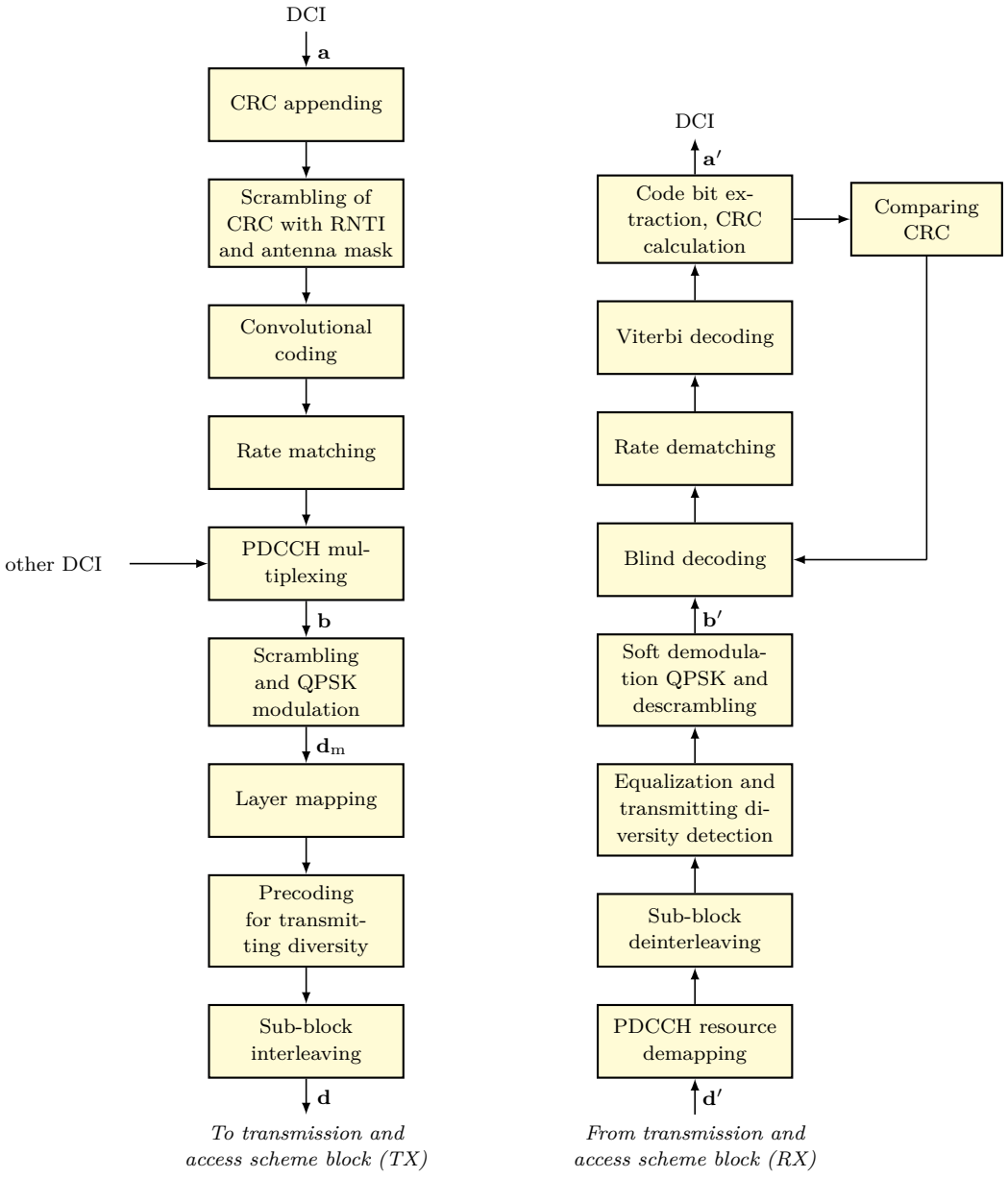

(a) Transmitting side

(b) Receiving side

Fig. 3.28: Block scheme of PDCCH channel coding, scrambling and modulation model (left) and channel decoding, descrambling and demodulation (right)

vector of demodulated bits is descrambled by the same cell-specific pseudo-random sequence as on the transmitting side and blind decoding is performed.

In the blind decoding block, the vector of input bits is scanned according to known lengths of the PDCCH formats (see Tab. 3.17). Output of the blind decoder block is up to 44 so-called PDCCH candidates. Each of these candidates subsequently enters blocks implementing channel decoding, rate dematching and Viterbi decoding. From these decoded bits, a new cyclic redundancy check is computed (CRC-16) and it is added mod 2 with cyclic redundancy check, which was received and we get a new value of RNTI′. In the event that both CRCs are the same, the system known value of RNTI and the new RNTI′ are identical and we have a searched DCI format. Another blind decoding is discontinued.

Performance Analysis Results of DCI Transmission via PDCCH

The results of the PDCCH control channel transmission simulation and subsequent analysis of BER's dependence on SNR for the investigated antenna configurations and models of transmission channels used are listed in this section. BER is calculated from the DCI value in bits (format 0 - test case set at the beginning of the simulation for performing the blind decoding faster) at the beginning and at the end of the transmission chain. Table 3.18 lists the main parameters of the simulation of PDCCH. The PDCCH BER graphs, arranged according to the investigated channel models, are shown in figures 3.29 to 3.31.

Summarized results of PDCCH BER are shown in Tab. 3.19. The values of SNR are given at which the BER in the PDCCH reaches the reference level 10^{-3}. BER of DCI transmitted using PDCCH in the AWGN channel model is shown in Fig. 3.29. In the figure we can see DCI BER curves arranged according to investigated antenna configurations together with theoretical bit error probability P_{b} curve of QPSK without channel coding in the OFDM system in AWGN. The difference of SNR value in SISO antenna mode where BER reaches the reference level 10^{-3}

Tab. 3.18: PDCCH simulation parameters

Parameters	Description
Frame structure	FDD
Number of transmitted subframes	10000
System bandwidth	1.4 MHz
Cyclic prefix (CP)	normal
Subcarrier spacing	15 kHz
Channel estimation	perfect knowledge
Demodulation method	Soft-decision (LLR)
Antenna configuration [$N_{\mathrm{TX}} \times N_{\mathrm{RX}}$]	1×1, 2×1, 4×2

and theoretical value is 7.5 dB. There is no difference between BER value for SISO antenna configuration and configuration with two transmitting and a single receiving antenna. The antenna configuration with four transmitting and two receiving antennas gives a gain equals 3 dB.

In Fig. 3.30 DCI BER in the Pedestrian B channel model is shown. The SNR value where BER reaches the reference level for SISO equals 17 dB. Transmitting diversity gives a gain equalling 6.8 dB and 5.1 dB respectively. In Fig. 3.27 are shown DCI BER curves in the Vehicular A channel model. Performance results are listed in Tab. 3.19.

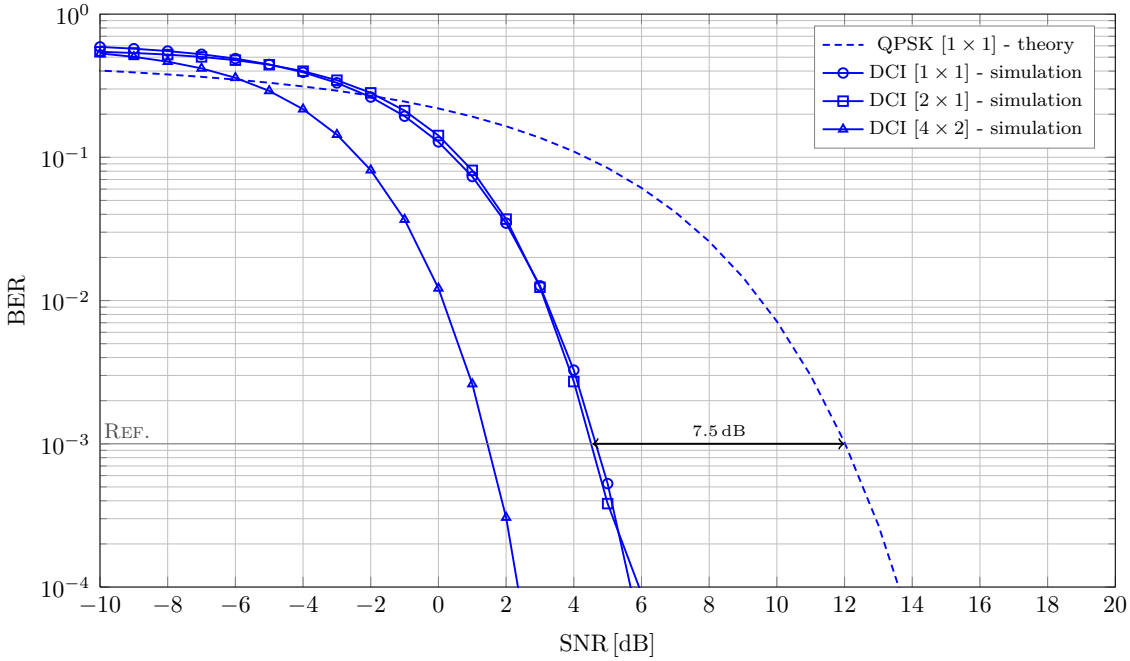

Fig. 3.29: BER of DCI (format 0) information transmitted via PDCCH in AWGN channel, various antenna modes

Tab. 3.19: SNR values at which the BER in PDCCH reaches the reference level 10^{-3} in different channel models

Antenna configuration	Minimal SNR value in dB for different channel type		
$[N_{TX} \times N_{RX}]$	AWGN	Pedestrian B	Vehicular A
1×1	4.5 dB	17.1 dB	17.5 dB
2×1	4.5 dB	10.6 dB	10.8 dB
4×2	1.5 dB	5.2 dB	5.1 dB

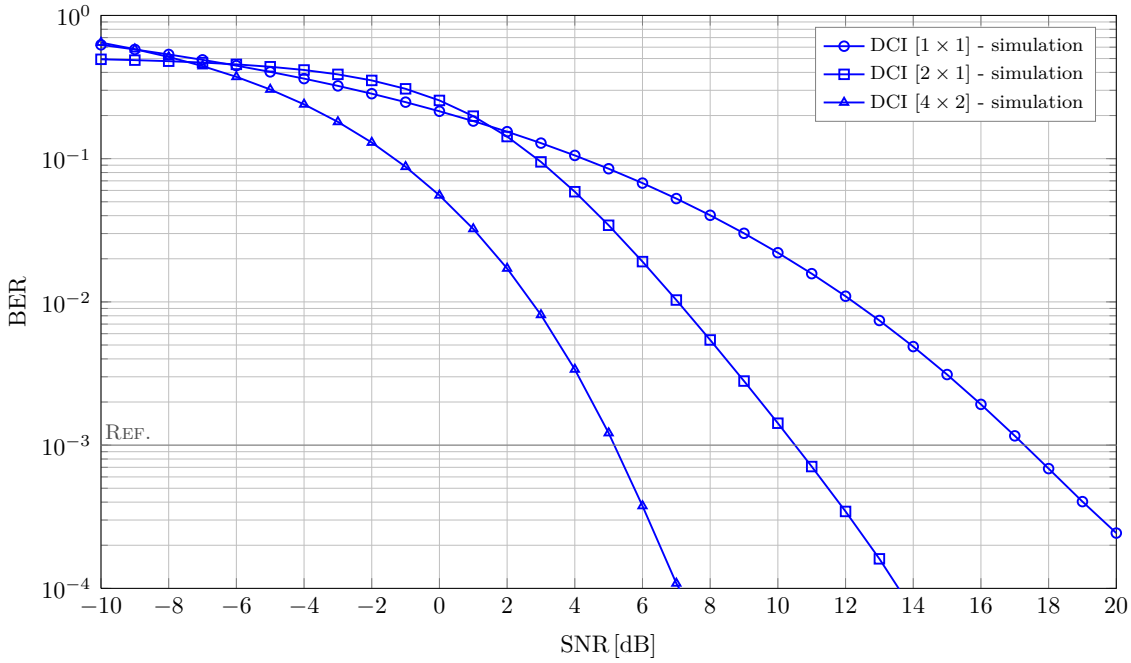

Fig. 3.30: BER of DCI (format 0) information transmitted via PDCCH in Pedestrian B channel, various antenna modes

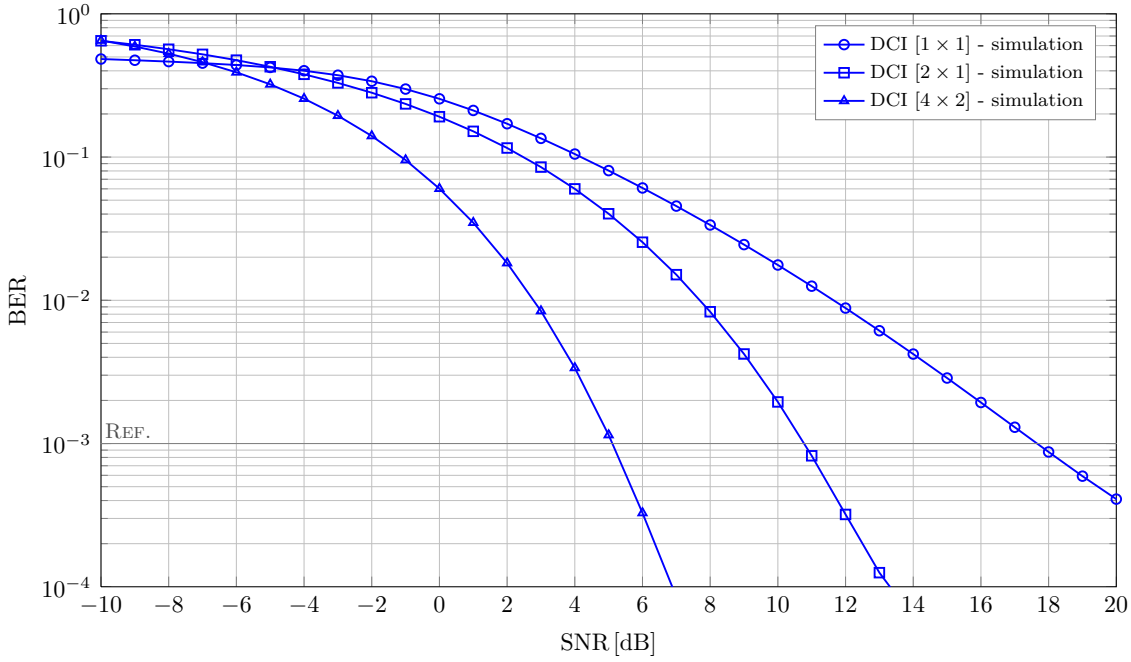

Fig. 3.31: BER of DCI (format 0) information transmitted via PDCCH in Vehicular A channel, various antenna modes

3.3.3 Physical Hybrid ARQ Indicator Channel

For transmitting user (traffic) data in the LTE (Release 8) communication standard in uplink direction PUSCH is used. Reliability of data transmission via PUSCH is achieved in two ways. The first, traffic data payload is coded by Turbo channel coding and the second, LTE employs a Hybrid Automatic Repeat Request (HARQ) technique [3, 8]. In uplink direction, synchronous adaptive HARQ is used. The New Data Indicator (NDI) and the corresponding HARQ indicator (HI) indicates whether the previous transmission in uplink was correct or if the received data was erroneous. A Physical HARQ Indicator Channel (PHICH) forms a feedback channel for HI transmission in downlink direction. An HI value of 0 represents nonacknowledgement (NACK) and an HI value of 1 represents acknowledgement (ACK) [6, 32]. One or up to eight HARQ Indicators forms a vector called PHICH message or PHICH.

For PUSCH transmissions in the subframe with index n, a UE determines the corresponding PHICH message in the subframe with index $n+k_{\mathrm{PHICH}}$, where $k_{\mathrm{PHICH}} = 4$ only for frame structure type 1 (FDD). The corresponding uplink and downlink subframes for frame structure type 1 is depicted in Fig. 3.32. The PHICH message with a single or multiple HARQ Indicators is mapped to the identical set of resource elements and form a PHICH group. The individual HI within the PHICH message is separated by eight different orthogonal sequences for normal CP length and four orthogonal sequences defined for extended CP length [8]. Identification of the PHICH resource is defined by a pair of parameters $(N_{\mathrm{PHICH}}^{\mathrm{group}}, N_{\mathrm{PHICH}}^{\mathrm{seq}})$, where $N_{\mathrm{PHICH}}^{\mathrm{group}}$ is the number of the PHICH groups and $N_{\mathrm{PHICH}}^{\mathrm{seq}}$ is the orthogonal sequence index within the PHICH group.

The number of PHICH groups is different for FDD and TDD frame structures. For an FDD frame structure (type 1), the number of PHICH groups is constant in all subframes and is defined by (3.29).

$$N_{\mathrm{PHICH}}^{\mathrm{group}} = \begin{cases} \left\lceil N_g \left(N_{\mathrm{RB}}^{\mathrm{DL}}/8 \right) \right\rceil & \ldots \text{normal CP} \\ 2 \left\lceil N_g \left(N_{\mathrm{RB}}^{\mathrm{DL}}/8 \right) \right\rceil & \ldots \text{extended CP} \end{cases} \tag{3.29}$$

Parameter $N_g \in \left\{ \frac{1}{6}, \frac{1}{2}, 1, 2 \right\}$ is a scaling factor and it is provided by higher layers. The index of the PHICH group $N_{\mathrm{PHICH}}^{\mathrm{group}}$ ranges from 0 to $N_{\mathrm{PHICH}}^{\mathrm{group}} - 1$. The parameter N_g

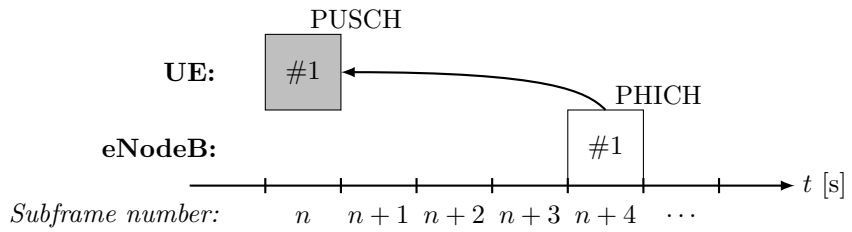

Fig. 3.32: PHICH delay in LTE FDD

is broadcasted in the Master information block (MIB) in downlink. A single PHICH group can contain up to 8 individual HIs (normal CP) according to the number of possible orthogonal sequences, Tab. 3.21.

PHICH Link Level Model

In the case of PHICH, emphasis during design was put on the overall simplicity of the channel coding and decoding process. The complete PHICH channel coding, modulation, scrambling and MIMO processing model is shown in Fig. 3.33. First, the individual HI message is channel coded by repetition coding with code rate $R = 1/3$, which results in a vector of bits $\mathbf{b}_{n_{\text{PHICH}}^{\text{seq}}} = [b_0, b_1, b_2]$ according to Tab. 3.20.

Using the repetition coder is very simple [48]. Triplicating the individual HI together with the modulation scheme and symbol spreading should provide better conditions for receiving. This type of signal processing in the channel coding block allows to use a simple version of the decoding mechanism – matched filter. The overall spreading factor can be defined as the multiplication of the repetition coder

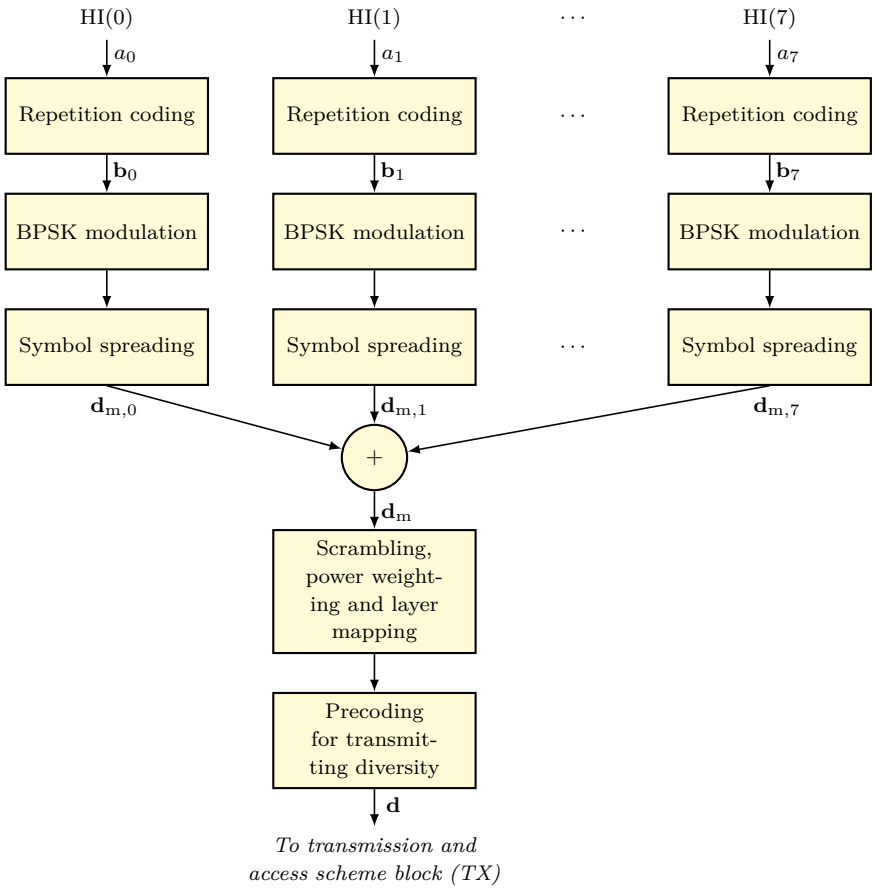

Fig. 3.33: Block scheme of the PHICH channel coding, scrambling and modulation model

Tab. 3.20: HARQ Indicator repetition channel coding

HI	HI codeword $\mathbf{b} = [b_0, b_1, b_2]$
0 (NACK)	$[0, 0, 0]$
1 (ACK)	$[1, 1, 1]$

code rate R and the orthogonal sequence spreading factor $N_{\mathrm{SF}}^{\mathrm{PHICH}}$. In the case of normal CP, the overall spreading factor equals 12. This value gives the length of the matched filter in the receiver.

Individual bits in HI codeword $\mathbf{b}$ are modulated using BPSK modulation and produce a vector of complex-valued symbols $\mathbf{z} = [z_0, z_1, z_2]$ as is depicted in Fig. 3.34. Each element of the $\mathbf{z}$ vector is symbol spread using the orthogonal sequence $\mathbf{w}$ (see Tab. 3.21) and form a vector of complex-valued symbols $\mathbf{d}_{\mathrm{m},n_{\mathrm{PHICH}}^{\mathrm{seq}}}$. The scheme of symbol spreading is illustrated in Fig. 3.35.

The above-mentioned operations are provided stepwise with individual HI. All of the processed symbol vectors $\mathbf{d}_{\mathrm{m},n_{\mathrm{PHICH}}^{\mathrm{seq}}}$ within one PHICH group are combined

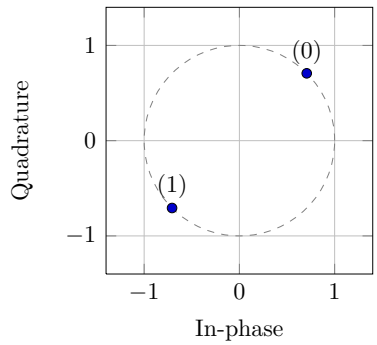

Fig. 3.34: BPSK modulation scheme used in PHICH

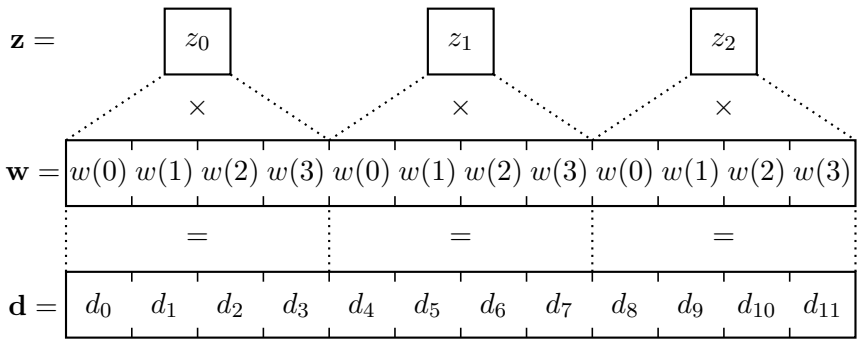

Fig. 3.35: Symbol spreading of individual modulated symbol $\mathbf{z}$

Tab. 3.21: Orthogonal sequences for PHICH (normal CP length)

Sequence index $n_{\mathrm{PHICH}}^{\mathrm{seq}}$	Orthogonal sequence $\left(N_{\mathrm{SF}}^{\mathrm{PHICH}}=4\right)$ $\mathbf{w}=\left[w(0),\ldots,w\left(N_{\mathrm{SF}}^{\mathrm{PHICH}}-1\right)\right]$
0	$[+1,+1,+1,+1]$
1	$[+1,-1,+1,-1]$
2	$[+1,+1,-1,-1]$
3	$[+1,-1,-1,+1]$
4	$[+\mathrm{j},+\mathrm{j},+\mathrm{j},+\mathrm{j}]$
5	$[+\mathrm{j},-\mathrm{j},+\mathrm{j},-\mathrm{j}]$
6	$[+\mathrm{j},+\mathrm{j},-\mathrm{j},-\mathrm{j}]$
7	$[+\mathrm{j},-\mathrm{j},-\mathrm{j},+\mathrm{j}]$

with the other corresponding $\mathbf{d}_{\mathrm{m},n_{\mathrm{PHICH}}^{\mathrm{seq}}}$ sequences. The superposition is defined by equation (3.30).

$$d_{\mathrm{m}}(n)=\sum_{n_{\mathrm{PHICH}}^{\mathrm{seq}}}^{\max\left(n_{\mathrm{PHICH}}^{\mathrm{seq}}\right)} d_{\mathrm{m},n_{\mathrm{PHICH}}^{\mathrm{seq}}}(n), \tag{3.30}$$

where $d_{\mathrm{m}}(n)$ is the n-th element of the resulting complex-valued vector $\mathbf{d}_{\mathrm{m}}$ after superposition combining, $d_{\mathrm{m},n_{\mathrm{PHICH}}^{\mathrm{seq}}}(n)$ is the n-th element of the individual symbol-spread vector $\mathbf{d}_{\mathrm{m},n_{\mathrm{PHICH}}^{\mathrm{seq}}}$ and n is the index of the element [5, 31].

In the case of $n_{\mathrm{PHICH}}>1$ the superposition process (3.30) creates different modulation schemes than BPSK. The resulting modulation scheme of the PHICH channel depends on the number of PHICHs within a single PHICH group. Constellation diagrams of these modulation schemes for n_{PHICH} from 1 to 8 are shown in Fig. 3.36. These modulation schemes are formed due to adding individual $d_{\mathrm{m},n_{\mathrm{PHICH}}^{\mathrm{seq}}}(n)$ and results in the vector $\mathbf{d}_{\mathrm{m}}$.

Every possible combination of logical values of **HI** vector, where

$$\mathbf{HI}=\left[\mathrm{HI}(0),\mathrm{HI}(1),\ldots,\mathrm{HI}\left(\max\left(n_{\mathrm{PHICH}}^{\mathrm{seq}}\right)\right)\right]=\left[a_0,a_1,\ldots,a_{\max\left(n_{\mathrm{PHICH}}^{\mathrm{seq}}\right)}\right]$$

and each combination of **HI** codewords have a characteristic pattern of modulation symbols. This fact is well used on the receiving side in the channel decoding process. As we can see in the constellation diagrams for $N_{\mathrm{PHICH}}^{\mathrm{seq}}=\{2,4,6,8\}$, a negative property indicates the possibility of the presence of a modulation symbol with zero transmitting power (in the origin of the x and y axes). On the transmitting side there is a resource element in the resource grid with zero power.

Channel coded information, represented by the symbol vector $\mathbf{d}_{\mathrm{m}}$ enter the block of cell-specific scrambling and there it is scrambled by using the cell-specific scrambling vector $\mathbf{c}$ and form the scrambled data vector according to (3.31)

$$\tilde{d}_{\mathrm{m}}(n)=d_{\mathrm{m}}(n)\times(1-2c(n)), \tag{3.31}$$

where $\tilde{d}_{\mathrm{m}}(n)$ is a modulated and scrambled symbol and $n = [0, 1, \ldots, 3N_{\mathrm{SF}}^{\mathrm{PHICH}} - 1]$. In the case where $N_{\mathrm{PHICH}}^{\mathrm{seq}} > 1$, it is necessary to perform power control by multiplying precoded symbols $\tilde{d}_{\mathrm{m}}(n)$ by the power weight coefficient $P_{\mathrm{weight}}^{\mathrm{PHICH}}$, according to Tab. 3.22.

The vector of scrambled and weighted symbols shall be mapped to ν-layers according to (3.22) and (3.24) and precoded. The layer mapping operation is provided in a similar way as in PCFICH and PDCCH [5]. The number of layers ν is defined by the system according to the number of transmitting antennas. In this block, the input matrix of layer mapped complex-valued symbols is precoded using SFBC and results to $\mathbf{d}$. Note that PHICH is transmitted through the same set of antenna ports as the Physical Broadcast Channel (PBCH). Furthermore, OFDMA operation in the transmitting side is provided. After passing through the channel, reverse OFDMA signal operation is performed.

On the receiving side which is depicted in Fig. 3.37, symbols corresponding with PHICH channel mapping are picked out from the resource grid together with estimated channel coefficients $\hat{\mathbf{H}}_{\mathrm{PHICH}}$. MIMO detection is performed according to the number of transmitting and receiving antennas. The cell-specific descrambling block provides an inverse operation with the same scrambling sequence as into the transmitting side. The last operation on the receiving side is channel decoding. Using repetition coding and the fact that every possible combination of HI codeword creates a characteristic pattern of symbols allows to provide channel decoding in a fast and effectively way. A bit valued pattern of possible combinations corresponding with HI bit value which is known on the receiving side. Received bits are compared with patterns of possible HI combinations and individual HI are determined using the simple majority vote technique [49].

Performance Analysis Results of HI Transmission via PHICH

A performance analysis was made by way of analyzing the BER of the PHICH and the results are presented in this section. The number of transmitted subframes was 5000 and 10000 (for simulations when $N_{\mathrm{PHICH}}^{\mathrm{seq}} > 1$). Normal CP length and Soft-sphere decoders (SSD) were used as is listed in Tab. 3.23. The first part of simulations was performed for $N_{\mathrm{PHICH}}^{\mathrm{seq}} = 1$ in AWGN, Pedestrian B and Vehicular A channel models with block fading [37]. The BER simulation results are presented depending on the antenna configurations.

Tab. 3.22: PHICH power weight coefficients according to the value of $N_{\mathrm{PHICH}}^{\mathrm{seq}}$

$N_{\mathrm{PHICH}}^{\mathrm{seq}}$	1	2	3	4	5	6	7	8
$P_{\mathrm{weight}}^{\mathrm{PHICH}}$	1	$\frac{1}{2}$	$\frac{1}{3}$	$\frac{1}{4}$	$\frac{1}{3\sqrt{2}}$	$\frac{1}{2\sqrt{5}}$	$\frac{1}{5}$	$\frac{1}{4\sqrt{2}}$

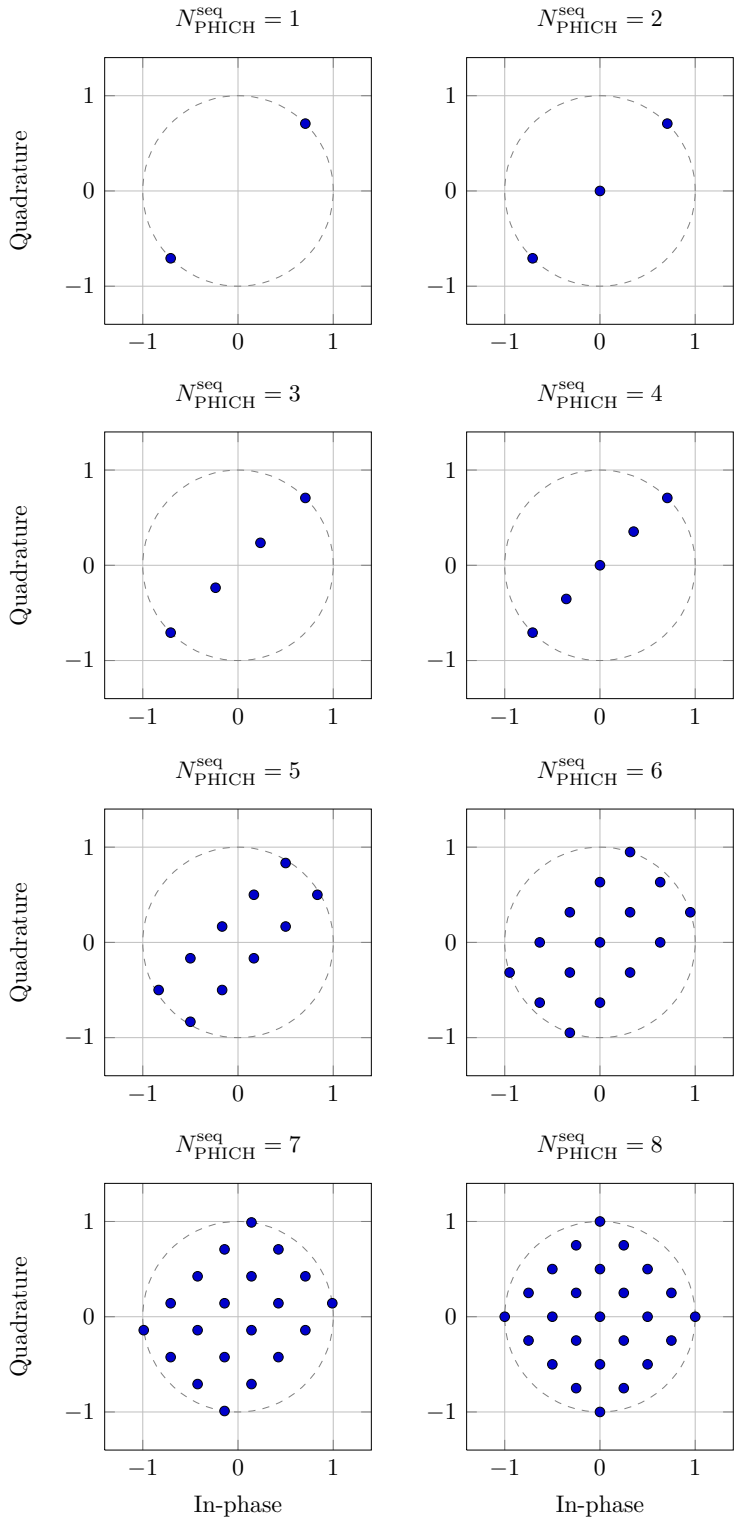

Fig. 3.36: PHICH modulation schemes after addition block

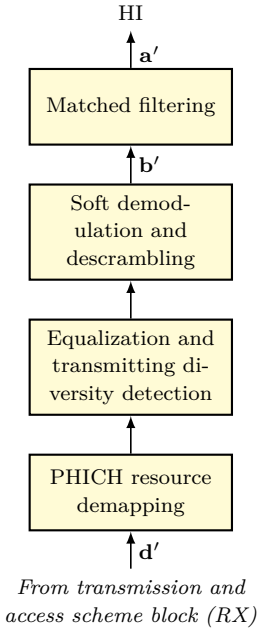

Fig. 3.37: Block scheme of PHICH channel decoding, descrambling and demodulation model

The PHICH BER curves according to the used channel models are shown in Figures 3.38–3.40. The simulations were provided for $N_{\mathrm{PHICH}}^{\mathrm{seq}} = 1$ and the orthogonal sequence with index $n_{\mathrm{PHICH}}^{\mathrm{seq}} = 0$ was used. The PHICH BER was calculated from a one bit HI value at the beginning and at the end of the transmission chain. The SNR reference level is given by the target quality value for NACK to ACK or ACK to NACK error (10^{-3}) [43]. The BER curves for the AWGN channel model are shown in Fig.3.38. There is no marked difference between the theoretical BPSK BER curve

Tab. 3.23: PHICH simulation parameters

Parameters	Description
Frame structure	FDD
Number of transmitted subframes	10000
System bandwidth	1.4 MHz
Cyclic prefix (CP)	normal
Subcarrier spacing	15 kHz
Channel estimation	perfect knowledge
Demodulation method	Soft-decision (LLR)
Antenna configuration $[N_{\mathrm{TX}} \times N_{\mathrm{RX}}]$	1×1, 2×1, 4×2
Number of PHICH sequences $N_{\mathrm{PHICH}}^{\mathrm{seq}}$	$\{1, 2, \ldots, 8\}$

Tab. 3.24: SNR values at which the BER in PHICH reaches the reference level 10^{-3} in different channel models for $N_{\mathrm{PHICH}}^{\mathrm{seq}} = 1$

Antenna configuration	Minimal SNR value in dB for different channel type		
$[N_{\mathrm{TX}} \times N_{\mathrm{RX}}]$	AWGN	Pedestrian B	Vehicular A
1×1	−1.2 dB	6.0 dB	6.9 dB
2×1	−1.6 dB	2.5 dB	2.3 dB
4×2	−4.4 dB	−3.2 dB	−3.0 dB

in the OFDMA system and BER HI curve for SISO antenna configuration. These results testify that the used repetition coding does not improve reception in this case and is used due to low overall complexity. The SNR reference value for the case of single transmitting and two receiving antennas is lower by 0.4 dB than the reference value in SISO mode. Using four transmitting and two receiving antennas gives a gain equalling 3 dB.

BER HI simulation results in Pedestrian B and Vehicular A channels are presented in Fig. 3.30 and Fig. 3.40 respectively. SNR reference values for abovementioned simulations are listed in Tab. 3.24.

The results of the PHICH simulation and BER analysis depending on SNR for the configuration with 1 transmitting and 1 receiving antenna and used AWGN channel model for different values of $N_{\mathrm{PHICH}}^{\mathrm{seq}}$ from 1 to 8 within a single PHICH group are shown in Fig. 3.41. The simulations were provided for orthogonal sequences with index equalling $n_{\mathrm{PHICH}}^{\mathrm{seq}} = \{0, 1, \ldots, 7\}$. The PHICH BER values were calculated from one up to eight bit length HI values at the beginning and at the end of the transmission chain in dependence on the number of PHICHs within a single PHICH group. Notice that the Minimal SNR value in dB for $n_{\mathrm{PHICH}} = 2$ is estimated from the trend of the curve. These simulation results are provided and shown for the configuration with the used AWGN channel model and SISO antenna mode only due to transparency.

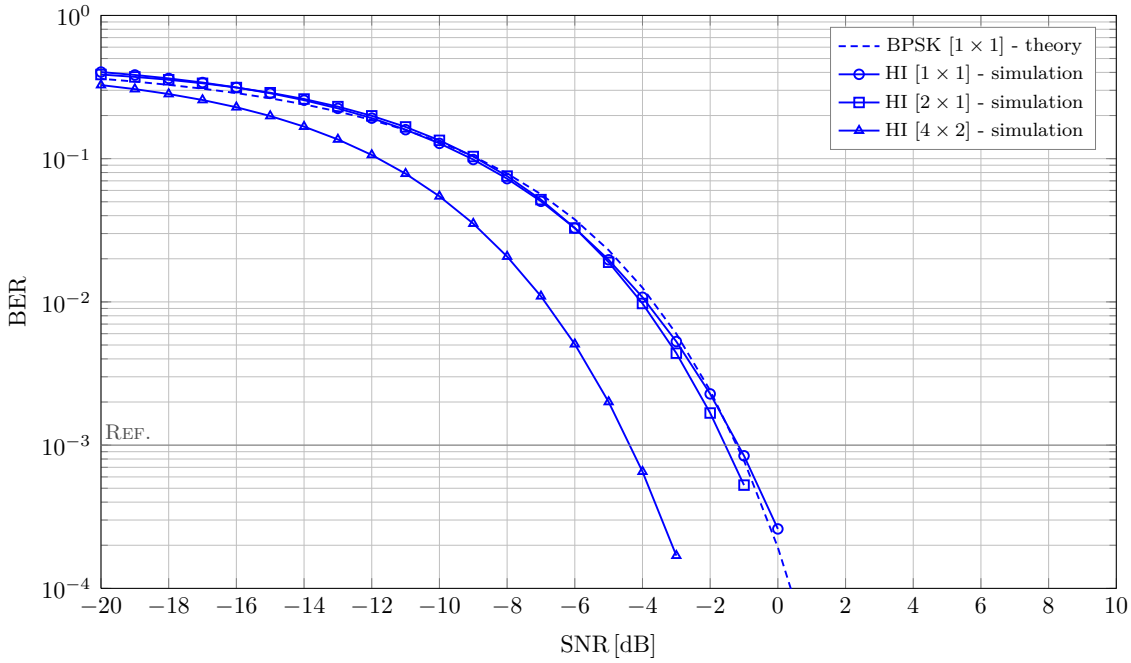

Fig. 3.38: BER of single HI information transmitted via PHICH in AWGN channel, various antenna modes

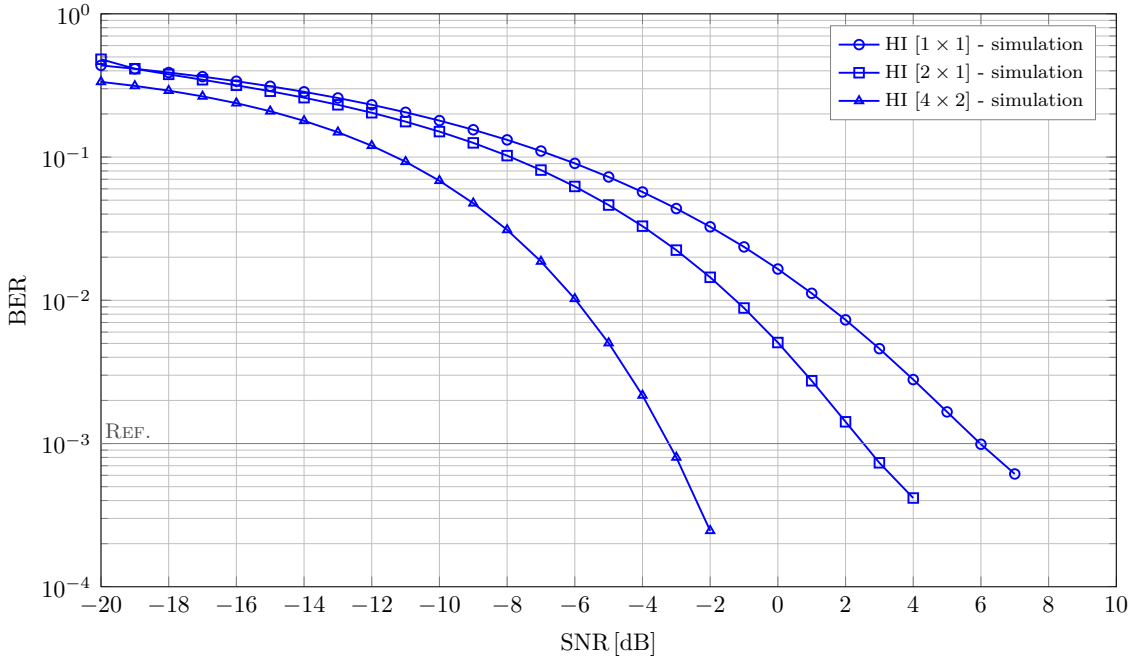

Fig. 3.39: BER of single HI information transmitted via PHICH in Pedestrian B channel, various antenna modes

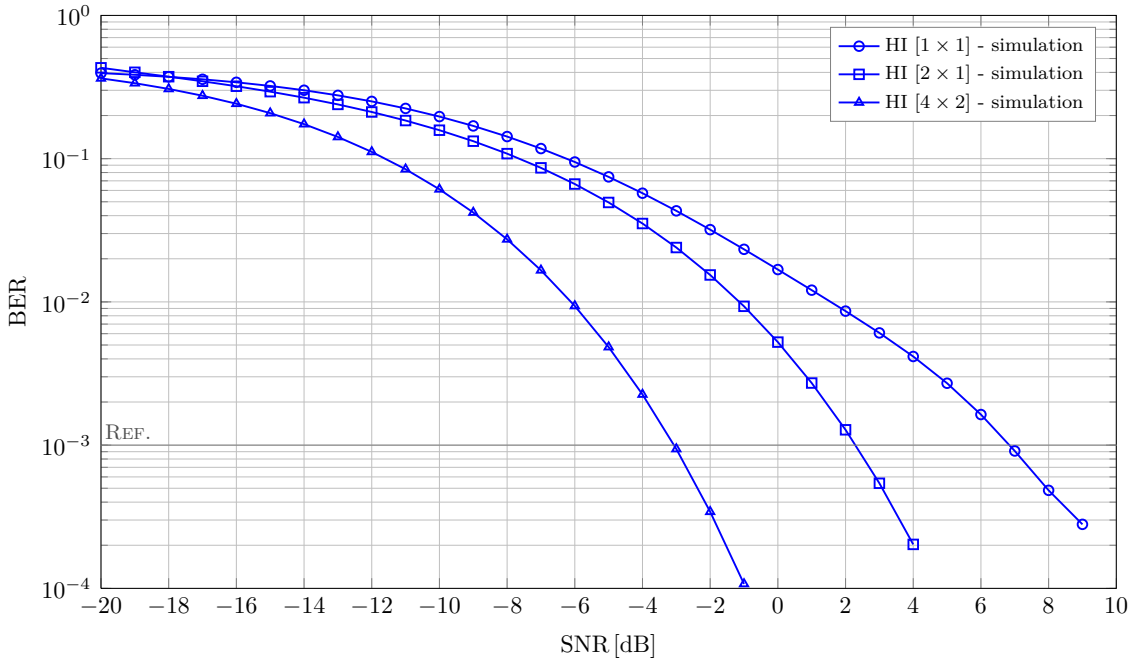

Fig. 3.40: BER of single HI information transmitted via PHICH in Vehicular A channel, various antenna modes

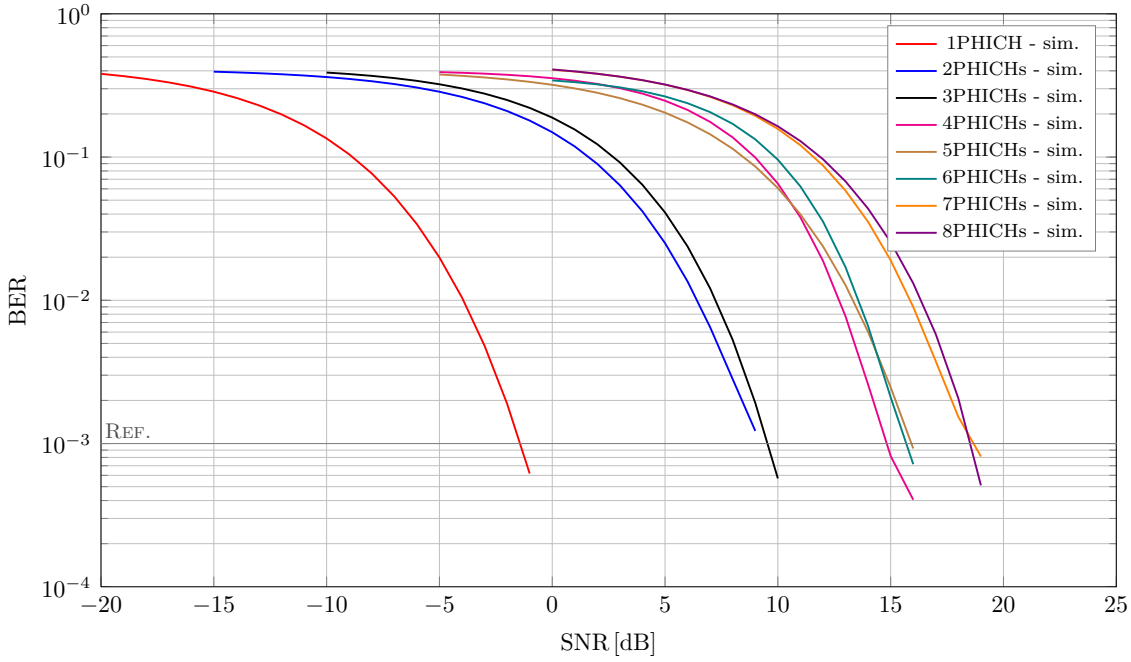

Fig. 3.41: BER of HI information within single PHICH group transmitted via PHICH in AWGN channel, SISO antenna mode

3.4 Summary

This chapter describes in detail the analysis of signal processing of LTE control channels in uplink and downlink. Link level simulations of control information transmissions were provided and results are presented for all possible system and antenna configurations in representative types of channel models. Control information link level simulation results were presented in journal [50], international journals [51, 52], international conferences [53–55] and student conference [56].

4 COEXISTENCE ANALYSIS IN UNLICENSED BANDS

Requirement on higher mobile data rates and growing number of mobile users brings a question how possible is to improve or extend the existing 3G/4G cellular networks. Corporations that develop mobile equipment and technology together with mobile operators brought some possibilities to innovate and improve user data throughput.

Qualcomm[1] and Huawei[2] company, self-containedly brought a study which uses unlicensed frequency bands for extending former LTE or LTE-Advanced standard [57, 58]. They have proposed utilization of unlicensed frequency bands for LTE or LTE Advanced. Licensed spectrum is the best choice for operators thanks to predictable behavior ensuring of Quality of Service (QoS), mobility and system control. Unfortunately, amount of available licensed spectrum is limited. Using of unlicensed spectrum brings unpredictable QoS and opportunistic usage for cellular standards. Thus, using of unlicensed frequency bands can be only applied as complementary to LTE and LTE Advanced, especially in pico or femtocells. Unfortunately the unlicensed spectrum is also occupied by varied wireless technology (Wi-Fi, Bluetooth, etc.). Due to these circumstances, it is necessary to investigate possibility of collisions and stability of LTE (Release 8) in unlicensed bands and perform coexistence analysis of control channels. Another reason for performing of coexistence analysis of LTE control channels in unlicensed bands is availability of the wide range of measuring devices to verify simulated results. Interference analysis results of LTE control channels in Industrial, Science and Medical band (ISM) are presented in this chapter.

4.1 Coexistence Scenario

Unlicensed frequency bands (or ISM bands) are reserved mainly for industrial, scientific and medical purposes other than telecommunications [59]. The ISM bands ($f < 10\,\text{GHz}$) and their frequencies are listed in Tab. 4.1. The most important ISM bands are 2.4 GHz and 5.8 GHz.

Nowadays, the mentioned frequency bands are used especially for Wireless Local Area Network (WLAN) or Wireless Personal Area Network (WPAN). Some mobile operators build picocells utilizing Wi-Fi technology as a support data pipeline in city centers or places with possibility of an occurrence of one-off high required data rates [60]. These supporting Wi-Fi networks are controlled centrally by operators and locally could bring higher data throughput than 3G/4G small cells. Qualcomm

[1] Qualcomm Incorporated is an American global semiconductor company which designs and markets wireless telecommunications products and services.

[2] Huawei Technologies Co. Ltd. is a Chinese multinational networking and telecommunications equipment and services company.

and Huawei brought an idea how to improve supporting Wi-Fi networks and take advantage of unlicensed bands and picocells in LTE or LTE Advanced cellular network.

General design principles and prerequisites for Unlicensed-LTE (U-LTE) are integration with licensed spectrum (aggregation licensed and unlicensed carriers brings better network performance, longer range and increasing capacity), minimum changes of LTE air-interface and ensuring coexistence in the unlicensed bands [58]. Unification of LTE network with common authentication, security and management is an advantage. There are two main approaches for U-LTE: First, *Supplemental downlink* (SDL) which increases throughput only in downlink (main option for LTE FDD), and the second, *Carrier aggregation* which increases throughput in both downlink and uplink (option for LTE TDD). Here, we will consider only SDL due to the developed LTE control channel simulator working only with subframe type 1 (FDD). According to Huawei concept for unlicensed secondary carrier design for FDD, there is adopted an option when primary cell (Pcell) FDD in downlink (data+control) is transmitted in licensed band and secondary cell (Scell) FDD in downlink (data+control) is transmitted in unlicensed band [58].

The Wi-Fi technology is used as an interfering wireless system in a simulation scenario. Wi-Fi networks work only in ISM bands. Mainly, Wi-Fi network built on IEEE 802.11n standard works in 2.4 GHz band [61]. Wi-Fi network built on IEEE 802.11n and IEEE 802.11ac works in 5 GHz band [62]. Both contemporary most popular Wi-Fi standards are based on OFDM modulation scheme and uses scalable bandwidths. In this chapter, there is discussed coexistence of control channels in LTE downlink and IEEE 802.11n in 2.4 GHz frequency band. LTE CCH coexistence simulator model is presented together with coexistence analysis results and measured results on a real mobile device in laboratory conditions in further text.

Tab. 4.1: List of unlicensed spectrum available for interested bands

Band [GHz]	Frequency range [MHz]	Bandwidth [MHz]
2.4	2400–2483.5	83.5
5.1	5150–5350	200
5.3	5350–5470	120
5.4	5470–5825	355
5.8	5725–5875	150
5.9	5850–5925	75

4.2 Simulation of LTE and IEEE 802.11n Coexistence

This section is focused on the simulations of inter-system interference analysis of LTE in the 2.4 GHz ISM band. The simulator for inter-system interference analysis is described here. As in the case of control information performance analysis in uplink (sec. 3.2) and downlink (sec. 3.3), presented interference (coexistence) analysis is performed as a link level. There are two main types of inter-system interference analysis:

1. **Co-channel inter-system interference analysis (CCI)** – the worst case in which the spectrum of the two signals (e.g. LTE and interfering IEEE 802.11n) are completely overlapped. It is an equivalent to the overlap of the two base-band signals. Influencing the systems is the greatest.

2. **Adjacent channel inter-system interference analysis (ACI)** – the case in which interfering signal is modulated to adjacent channel.

As was mentioned before, a lot of wireless standards simultaneously work in ISM band. The graphical representation of 2.4 GHz band Wi-Fi channels overlapping is shown in Fig. 4.1. Central frequencies of Wi-Fi channels are overlapped by two to four another Wi-Fi channels in this band. Due to this circumstances, the co-channel inter-system interference analysis (CCI) is considered only. Note, guard bands and requirements for Adjacent Channel Leakage Ratio (ACLR) for LTE and IEEE 802.11n are not defined in standards.

Useful and interfering signal are upconverted to ISM band with carrier frequency $f_c > 2.4\,\text{GHz}$ (bandpass signal). Upconversion of both signals to the ISM band is highly computationally and time-consuming process. It is necessary to perform the coexistence simulations in MATLAB using graphics processing units (GPU) and the NVIDIA CUDA technology [63]. Simulations are performed for all LTE physical control channels in downlink direction (PCFICH, PDCCH and PHICH) for LTE system bandwidth $B_{\text{sys}} = 1.4\,\text{MHz}$.

4.2.1 Link Level Model for Coexistence Simulations

Downlink control channel link level coexistence analysis model is depicted in Fig. 4.2. Useful LTE signal from transmitter (*victim*) is represented by LTE downlink physical layer model (TX) block. Parameters of investigated LTE system are listed in Tab. 4.2. Output OFDM signal $s(t)$ is filtered using Square-root raised cosine filter (SRRC) with Roll-off factor $\beta = 0.22$ and upconverted to the carrier frequency f_c. The amplitude and phase response of SRRC filter in frequency domain is depicted in Fig. 4.3. The upconverted real signal is transmitted to the channel model.

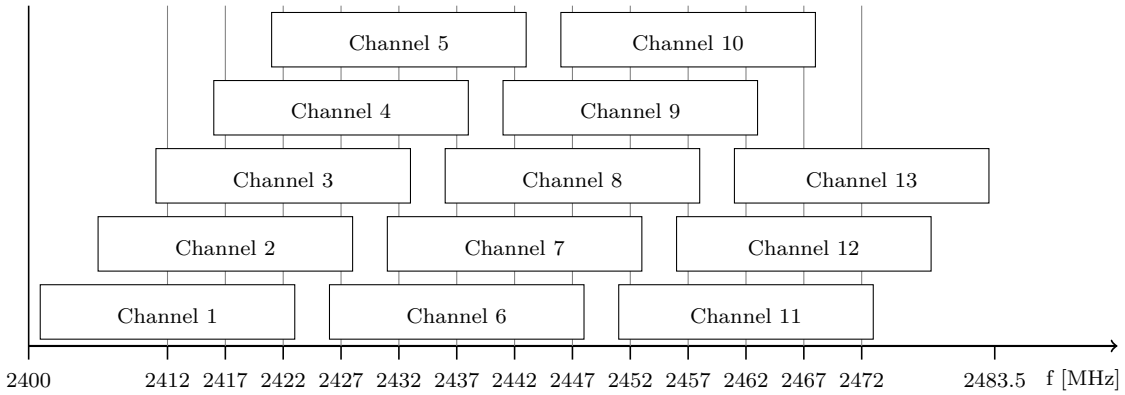

Fig. 4.1: Graphical representation of 2.4 GHz band channels overlapping

The channel model is represented by two signal adders. The interfering Wi-Fi signal (*aggressor*) is added to the useful LTE signal together with the noise vector **N**.

The interfering branch is modeled using the Interfering signal generator block that generates a baseband interfering signal according to IEEE 802.11n standard [61]. IEEE 802.11n in 2.4 GHz band uses a scalable bandwidths, 20 MHz and 40 MHz (extended). Wi-Fi bandwidth equaling to 20 MHz in all presented coexistence simulations. Parameters of interfering IEEE 802.11n system are listed in Tab. 4.3. Interfering IEEE 802.11n output signal is filtered using raised cosine filter with Roll-off factor $\beta = 0.1$ and not exceed defined spectral mask [64]. The interfering signal is upconverted to the carrier frequency f_{interf}. Finally, the output power of the interfering signal is set according to simulated Carrier to Interference Ratio (CIR) or Carrier to Noise and Interference Ratio (CNIR), respectively. Notice that the both upconverted signals are normalized to unitary power before adding process.

Tab. 4.2: Coexistence simulation parameters of LTE system

Parameters	Description
Frame structure	FDD
Number of transmitted subframes	500
System bandwidth	1.4 MHz
Cyclic prefix (CP)	normal
Subcarrier spacing	15 kHz
Channel model	AWGN
Channel estimation	no estimation needed
Evaluation type	BER and raw BER
Antenna configuration [$N_{\text{TX}} \times N_{\text{RX}}$]	1×1 (SISO only)
Investigated control channels	PCFICH, PDCCH and PHICH
Used unlicensed band	2.4 GHz

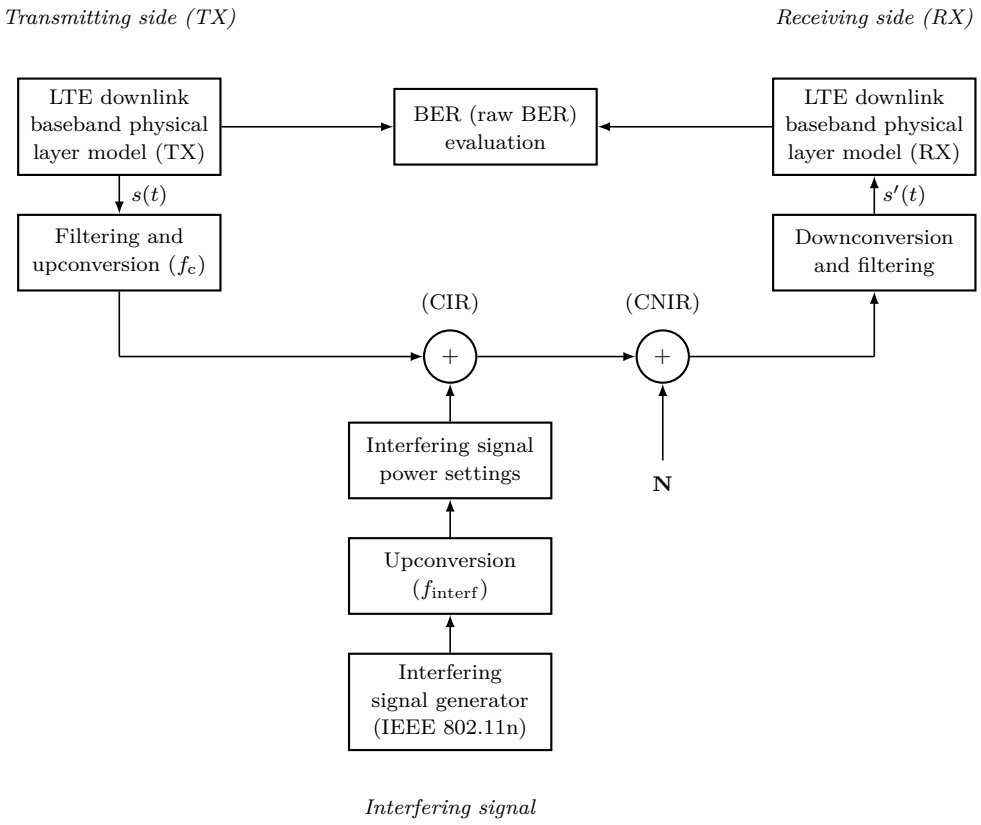

Fig. 4.2: Downlink control channel link level coexistence analysis model

The noise vector $\mathbf{N}$ is a background signal noise (LTE receiver input noise) modeled as AWGN with the power level N given by equation (4.1).

$$N = N_0 B = kTB, \tag{4.1}$$

where N_0 is noise power spectral density, B is bandwidth of LTE system, k is the Boltzmann's constant $k = 1.38 \times 10^{-23}\,\mathrm{J{\cdot}K^{-1}}$ and T is absolute temperature of the receiver input in Kelvin (here $T = 290\,\mathrm{K}$). For modeled LTE system we have $N_0 = -173.98\,\mathrm{dBm/Hz}$, if $B_{\mathrm{sys}} = 1.4\,\mathrm{MHz}$, N in dBm is defined as

$$N = N_0 + 10\log_{10}\left(1.4{\times}10^6\right) = -173.98 + 61.46 = -112.52\,\mathrm{dBm}. \tag{4.2}$$

The interfered signal from the channel leads to LTE downconversion block, where it is transposed to baseband and filtered using SRRC. Downconverted signal $s'(t)$ enters to the receiving LTE downlink physical layer model (RX) block. Vector of received modulation symbols belonging to physical control channels are picked up from the resource grid, channel decoded and enter to BER or raw BER evaluation block. Raw BER value (*uncoded BER, gross BER*) is defined as the BER value without considering of channel coding and interleaving.

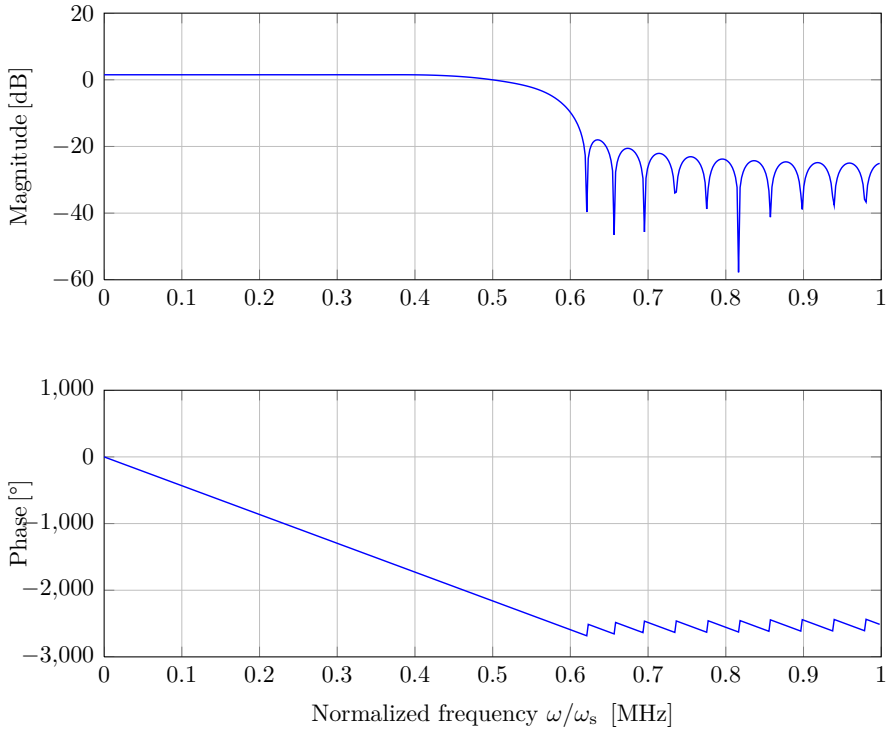

Fig. 4.3: Amplitude and phase response of LTE SRRC filter in frequency domain

4.2.2 Co-channel Inter-system Interference Analysis Results

As was mentioned, only the co-channel inter-system interference analysis simulation is performed. Both signals are upconverted to the first Wi-Fi channel in 2.4 GHz ISM band [65]. In this case, the carrier frequency of LTE signal is equaling to the carrier frequency of interfering IEEE 802.11n signal, $f_c = f_{interf} = 2412$ MHz. Simulated frequency spectrum of the useful (narrowband) and interfering signal (wideband) in the same ISM channel (co-channel) is depicted in Fig. 4.4.

Tab. 4.3: Coexistence simulation parameters of interfering IEEE 802.11n system

Parameters	Description
System bandwidth	20 MHz
Subcarrier spacing	312.5 kHz
FFT length	64
Number of data subcarriers	52
Number of pilot subcarriers	4
Modulation scheme	64QAM
Antenna configuration [$N_{TX} \times N_{RX}$]	1×1 (SISO)
Used unlicensed band	2.4 GHz

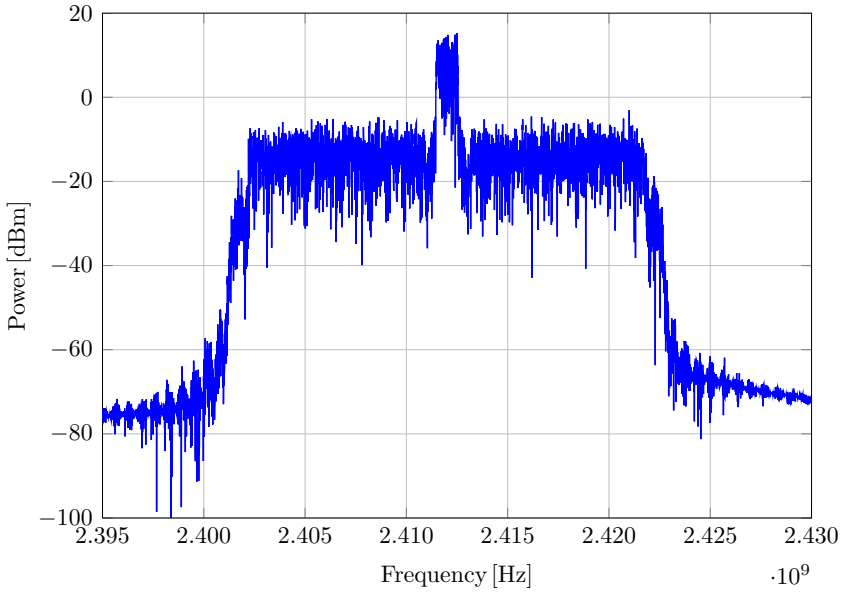

Fig. 4.4: Simulated power frequency spectrum of LTE and IEEE 802.11n signal (co-channel, CNIR = 16 dB)

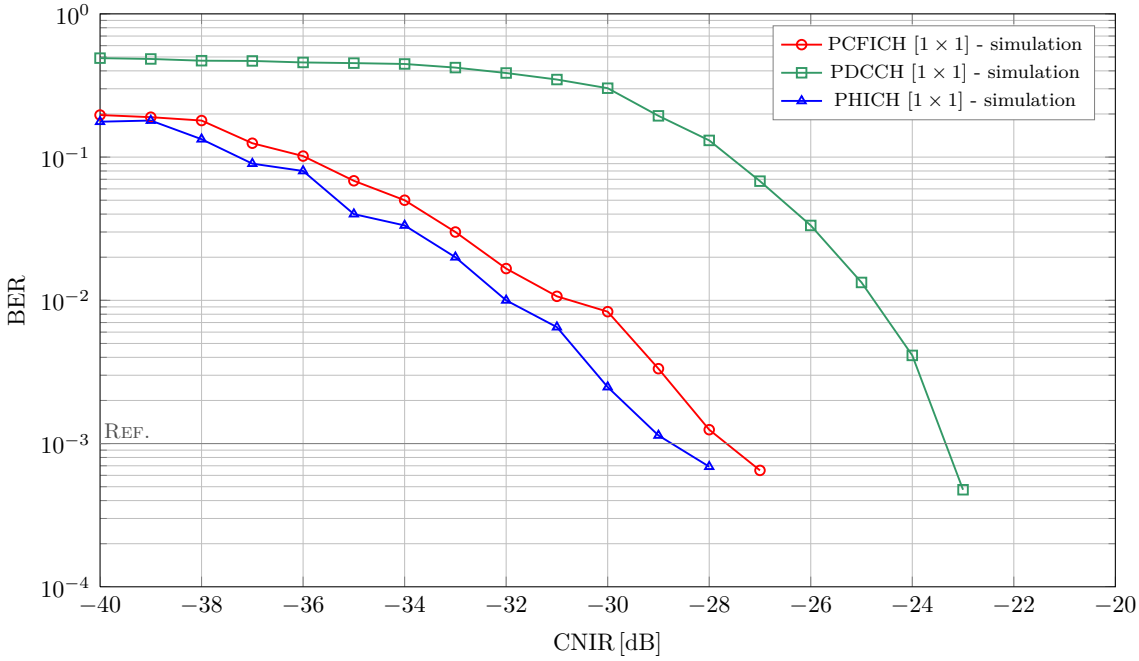

Fig. 4.5: Simulated BER results of co-channel inter-system interference in PCFICH, PDCCH and PHICH, SISO antenna mode

Overall overlapping of the LTE signal by the interfering IEEE 802.11n signal is obvious in the presented spectrum. Notice that LTE systemis always perfectly synchronized in simulation. Primary (PSS) and secondary (SSS) synchronization signal are not transmitted.

Figure 4.5 presents the simulated BER results of the co-channel inter-system interference in PCFICH, PDCCH and PHICH for SISO antenna mode. As in the case of baseband simulations, 21 bits in length PDCCH format 0 is transmitted, 2 bits in length CFI message in PCFICH channel is transmitted and single bit in length HI message ($n_{\mathrm{PHICH}} = 1$) within single PHICH group is transmitted in PHICH channel. BER reference level 10^{-3} is reached for CNIR value equals -23.2 dB for PDCCH channel. BER reference level is reached for CNIR -28.8 dB for PCFICH channel and -27.6 dB for PHICH channel. Presented value of CNIR in which BER reaches to the reference level 10^{-3} indicates very good resistance to interferences and ability to using of LTE system in ISM as Supplemental Downlink pipeline.

4.3 Measurement of LTE and IEEE 802.11n Coexistence

In this section, the simulation results presented in previous sections are experimentally verified using available devices in laboratory environment. The measured results are compared with the simulated ones and the created link level model is optimized in accordance with the obtained results.

4.3.1 Description of Measuring Workplace

The laboratory measurement is an illustrative case in order to verify BER results obtained using the simulations. The verification of the simulated results by measuring gives information about credibility of the provided simulations and it helps in a case of the link level model optimization. Measuring of LTE coexistence in real conditions and real devices gives the best insight into the issue. Only this type of measurement provides decisive information about the possibility of using LTE in the 2.4 GHz ISM band. In the Czech Republic, there are three providers of LTE network – T-Mobile, O2 and Vodafone (in various stages of testing or coverage of the area). Unfortunately, there is no possibility to measure on their devices.

The block diagram of the measuring workplace is depicted in Fig. 4.6. Two-channel signal generator Rohde & Schwarz SMU200A [66,67] creates the useful signal LTE with 1.4 MHz bandwidth and power level P_{C} as well as interfering Wi-Fi (IEEE 802.11n) signal with 20 MHz bandwidth and power level P_{I}. Both signals lead to Wilkinson splitter (designed for 2.4 GHz ISM band). Signals P_{C} and P_{I} are splitted keeping with power ratio $P_{\mathrm{C}}/P_{\mathrm{I}}$ to signal $P_{\mathrm{CI}} = P_{\mathrm{C}} + P_{\mathrm{I}}$. Signal attenuation caused by Wilkinson splitter and the coaxial cables is ignored. The splitted signal with the power level P_{CI} is led using coaxial cable to signal analyzer Rohde & Schwarz FSW26 [68, 69]. The power level of the thermal noise superimposed to the input of the

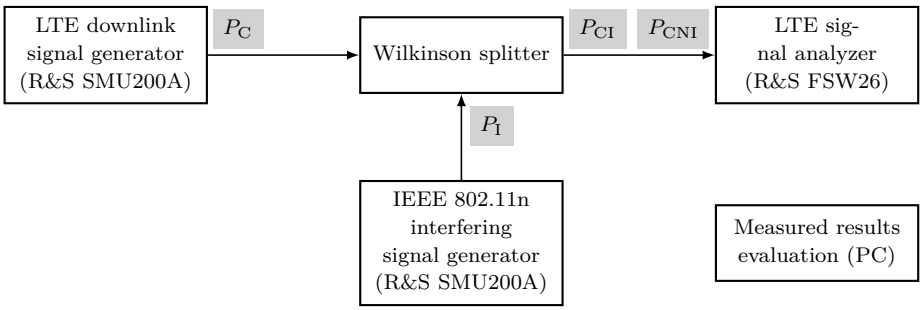

Fig. 4.6: Block scheme of workplace for measuring coexistence

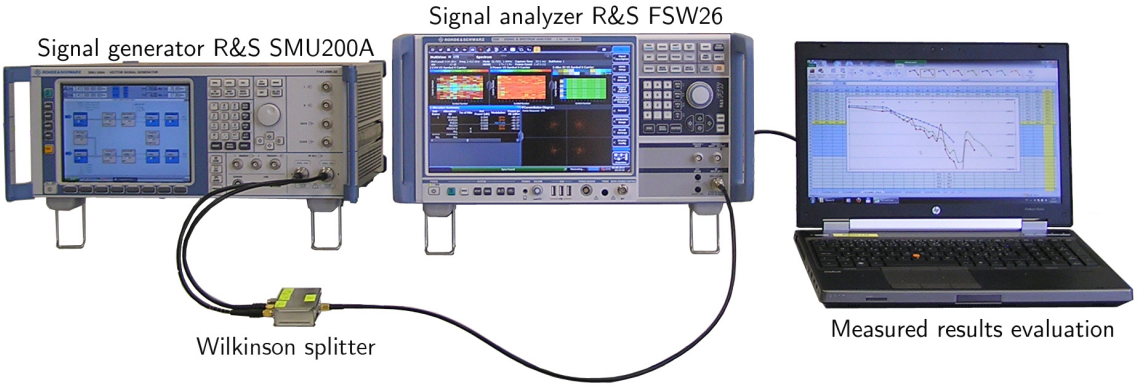

Fig. 4.7: Image of workplace for measuring coexistence

analyzer is defined by (4.2). The power level of the received signal on the input of the analyzer is $P_{\mathrm{CNI}} = P_{\mathrm{C}} + P_{\mathrm{N}} + P_{\mathrm{I}}$. The power level P_{CNI} is an equivalent to CNIR power ratio defined in simulations. The measuring workplace is depicted in Fig. 4.7.

Raw BER is an evaluation parameter of the measurement. Carrier to Noise and Interference Ratio (CNIR) is an independent variable. Raw BER is measured for all LTE control channels in downlink. The signal analyzer Rohde & Schwarz FSW26 supports measuring of raw BER depending on the allocation of resource elements (RE) using an Allocation summary feature. The Allocation summary feature allows measuring of Error Vector Magnitude (EVM) depending on the allocation of physical channels [70].

EVM is always normalized using reference signal constellation which is known in both measuring devices [67, 69]. EVM is evaluated according to equation (4.3).

$$\mathrm{EVM}_{\mathrm{RMS}} = \sqrt{\frac{\frac{1}{N}\sum_{k=1}^{N} e_k}{\frac{1}{N}\sum_{k=1}^{N}(I_k^2 + Q_k^2)}} = \sqrt{\frac{\frac{1}{N}\sum_{k=1}^{N}\left[(I_k - \bar{I}_k)^2 + (Q_k - \bar{Q}_k)^2\right]}{\frac{1}{N}\sum_{k=1}^{N}(I_k^2 + Q_k^2)}}, \tag{4.3}$$

where N is the number of considered modulation symbols, k is the index of modulation symbol ($k = 1, 2, \ldots, N$), $\sqrt{e_k}$ is error vector length (Euclidean distance between measured and reference modulation symbol), reference IQ values are defined as transmitted modulation symbols from signal generator $\mathbf{z}_{\mathrm{CCH}} = I + \mathrm{j}Q$ (sampled in ideal sampling time) and measured IQ values are defined as received modulation symbols $\mathbf{z}'_{\mathrm{CCH}} = \bar{I} + \mathrm{j}\bar{Q}$. Graphical representation of EVM is depicted in Fig. 4.8. Measured EVM values are converted to error bit probability P_{b} for better comparison of the simulated and measured results. Association between EVM and SNR (or CNIR) is defined in (4.4) [71].

$$\mathrm{SNR} \approx \frac{1}{\mathrm{EVM}^2}. \tag{4.4}$$

Obtained SNR is used to calculate of E_{b}/N_0 ratio according to equation (3.9) and P_{b} for PSK modulation is calculated according to equation (3.6).

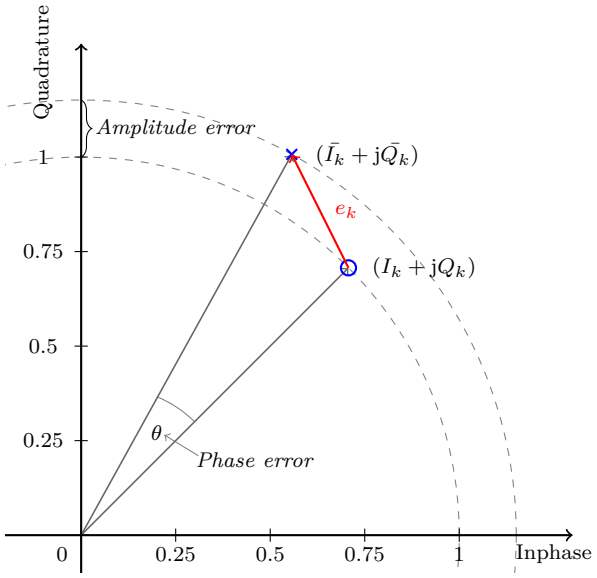

Fig. 4.8: Graphical representation of EVM

4.3.2 Settings of Measuring Devices

The useful signal as well as the interfering signal is generated using signal generator Rohde & Schwarz SMU200A. A snapshot of the signal generator configuration panel is depicted in Fig. 4.9. The useful LTE signal is generated in the branch A and the interfering signal is generated in the branch B. Frequency in both branches is set to 2412 MHz (see 4.2.2).

The maximal output signal power level of LTE base station (eNodeB) depends on a base station class according to the cell size [33, 72]. The maximal defined output signal power level in LTE Pico eNodeB is listed in Tab. 4.4. Thus, the maximal output power in Pico eNodeB for one transmitting port is equaling to 24 dBm.

Minimal reference sensitivity of LTE downlink receiver is not specified in 2.4 GHz ISM band. Due to this circumstances, it is necessary to estimate the reference sensitivity value for QPSK modulation scheme $P_{\mathrm{REFSENS}}^{\mathrm{QPSK}}$ [73]. Sensitivity values $P_{\mathrm{REFSENS}}^{\mathrm{QPSK}}$ defined for LTE-FDD and system bandwidth equals 1.4 MHz are listed in Tab. 4.5.

Tab. 4.4: LTE Pico eNodeB maximum output power

Base station class		Maximum output power
Pico eNodeB	24 dBm	(for one transmit antenna port)
	21 dBm	(for two transmit antenna ports)
	18 dBm	(for four transmit antenna ports)

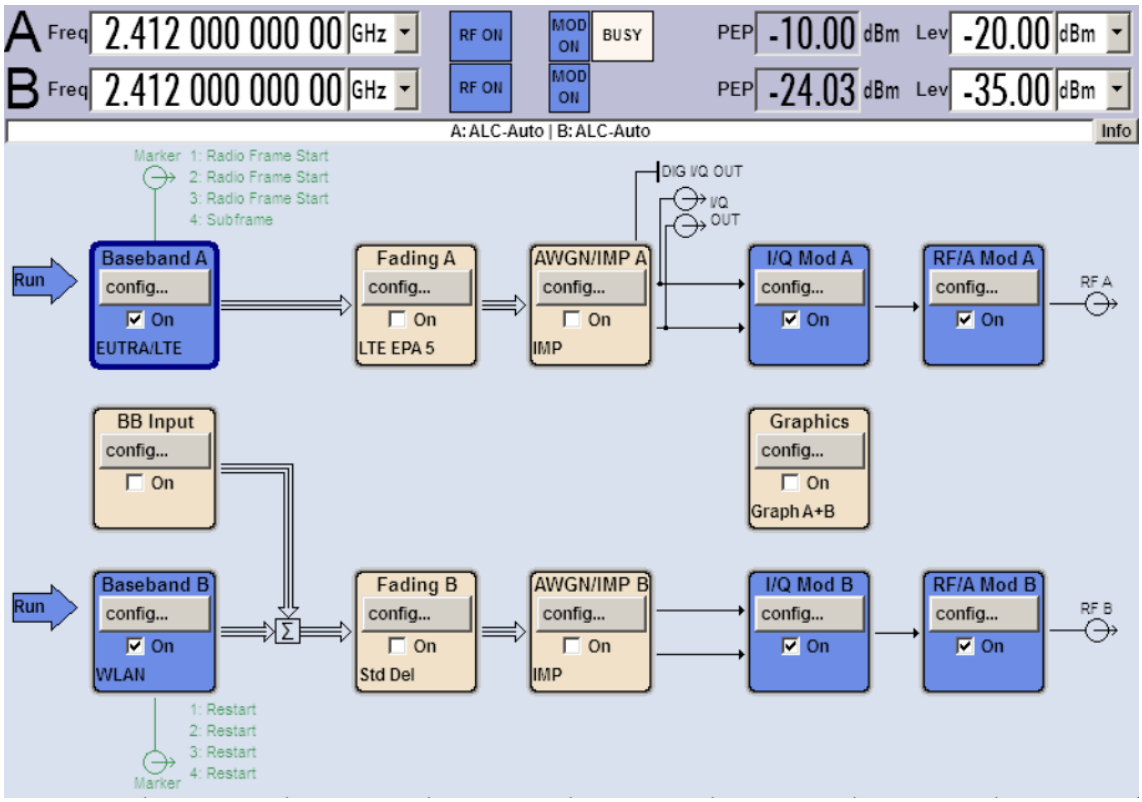

Fig. 4.9: Snapshot of the R&S SMU200A signal generator configuration panel

LTE-FDD channel 23 with bandwidth equals 20 MHz is closest to 2.4 GHz ISM band. Reference sensitivity for QPSK $P_{\mathrm{REFSENS}}^{\mathrm{QPSK}}$ is equaling to -104.7 dBm in this channel. This $P_{\mathrm{REFSENS}}^{\mathrm{QPSK}}$ value is below the noise level on the signal analyzer input, see (4.2). The dynamic range of input signal is greater than 100 dB. The maximal input power level of the signal analyzer is 30 dBm.

Tab. 4.5: LTE downlink user equipment reference sensitivity

FDD channel number	Channel frequency range [MHz]	$P_{\mathrm{REFSENS}}^{\mathrm{QPSK}}$
2	1850 – 1910	−102.7 dBm
3	1710 – 1785	−101.7 dBm
4	1710 – 1755	−104.7 dBm
5	824 – 829	−103.2 dBm
8	880 – 915	−102.2 dBm
12	699 – 716	−101.7 dBm
17	704 – 716	−102.2 dBm
23	2000 – 2020	−104.7 dBm
25	1850 – 1915	−101.2 dBm

Rohde & Schwarz devices have common measuring profiles defined for LTE-FDD in downlink direction [70]. Thank to usage of these profiles in the generator and the analyzer, it is not necessary to use synchronization. Necessary changes in the measuring profiles are listed in Tab. 4.6. The changes are made due to unification with the simulation settings.

4.3.3 Measured Results

Measured results of co-channel inter-system interference are presented in this section. Raw BER results are converted from EVM values and presented in dependency on CNIR values. Measured frequency spectrum of co-channel interference is depicted in Fig. 4.11. Snapshot of the signal analyzer display is depicted in Fig. 4.10. The display is separated into four parts. There is graphical representation of EVM for each resource block in single subframe (level of EVM is indicated using color graph), graphical representation of physical channels and signal allocation in single subframe, constellation diagram and allocation summary which gives a numeric value of EVM. Notice that the R&S FSW26 signal analyzer allows to customize the graphic environment.

Tab. 4.6: LTE-FDD measuring profile settings

Type of control channel	Parameter	Value
All	Number of transmitting antennas	1
	Number of receiving antennas	1
	Precoding	none
	Number of adjustable subframes	10
	Input attenuation	10 dB
PCFICH	Relative power	0 dB
	Scrambling state	yes
	PDCCH control region	2 OFDMA symbols
PDCCH	Relative power	0 dB
	Scrambling state	yes
	Number of bits	184
	Number of available REGs	23
	Number of available CCEs	2
	PDCCH format	0
	Number of PDCCHs	2
	Data source	PN9
PHICH	Duration	normal
	N_g	1
	Power mode	constant
	Relative power	−3.01 dB
	ACK/NACK pattern group	[1xxxxxxx]

Measuring of co-channel inter-system interference in 2.4 GHz ISM band is provided for CNIR values from -30 to -5 dB. Synchronization failure is occured for CNIR values lower than -8 dB (non-detection of primary and secondary synchronization signal). This fact has a minimum impact to the measurement.

The measured and simulated results of co-channel inter-system interference in PCFICH depending on CNIR are shown in Fig. 4.12. The simulated PCFICH raw BER values are calculated from 32 bits in length CFI codewords at the beginning and at the end of the transmission chain (16 resource elements, QPSK modulation). Simulated PCFICH CNIR reference value at which the raw BER reaches 10^{-3} is equaling to -19.3 dB. Measured PCFICH CNIR reference value is -15.8 dB. The difference between simulated and measured CNIR reference value is 3.5 dB.

The measured and simulated results of co-channel inter-system interference in PDCCH depending on CNIR are shown in Fig. 4.13. The simulated PDCCH raw BER values are calculated from 184 bits in length DCI codewords at the beginning and at the end of the transmission chain (72 resource elements, QPSK modulation). Simulated PDCCH CNIR reference value is equaling to -18.1 dB. Measured PDCCH CNIR reference value is equaling to -17.2 dB. The difference between simulated and measured CNIR reference value is 0.9 dB.

The measured and simulated results of co-channel inter-system interference in PHICH for $n_{\mathrm{PHICH}} = 1$ within single PHICH group depending on CNIR are shown in Fig. 4.14. The simulated PHICH raw BER values are calculated from 12 bits in length HI codewords at the beginning and at the end of the transmission chain (12 resource elements, BPSK modulation). Simulated PHICH CNIR reference value is equaling to -21.45 dB. Measured PHICH CNIR reference value is equaling to -19.8 dB. The difference between simulated and measured CNIR reference value is 1.7 dB.

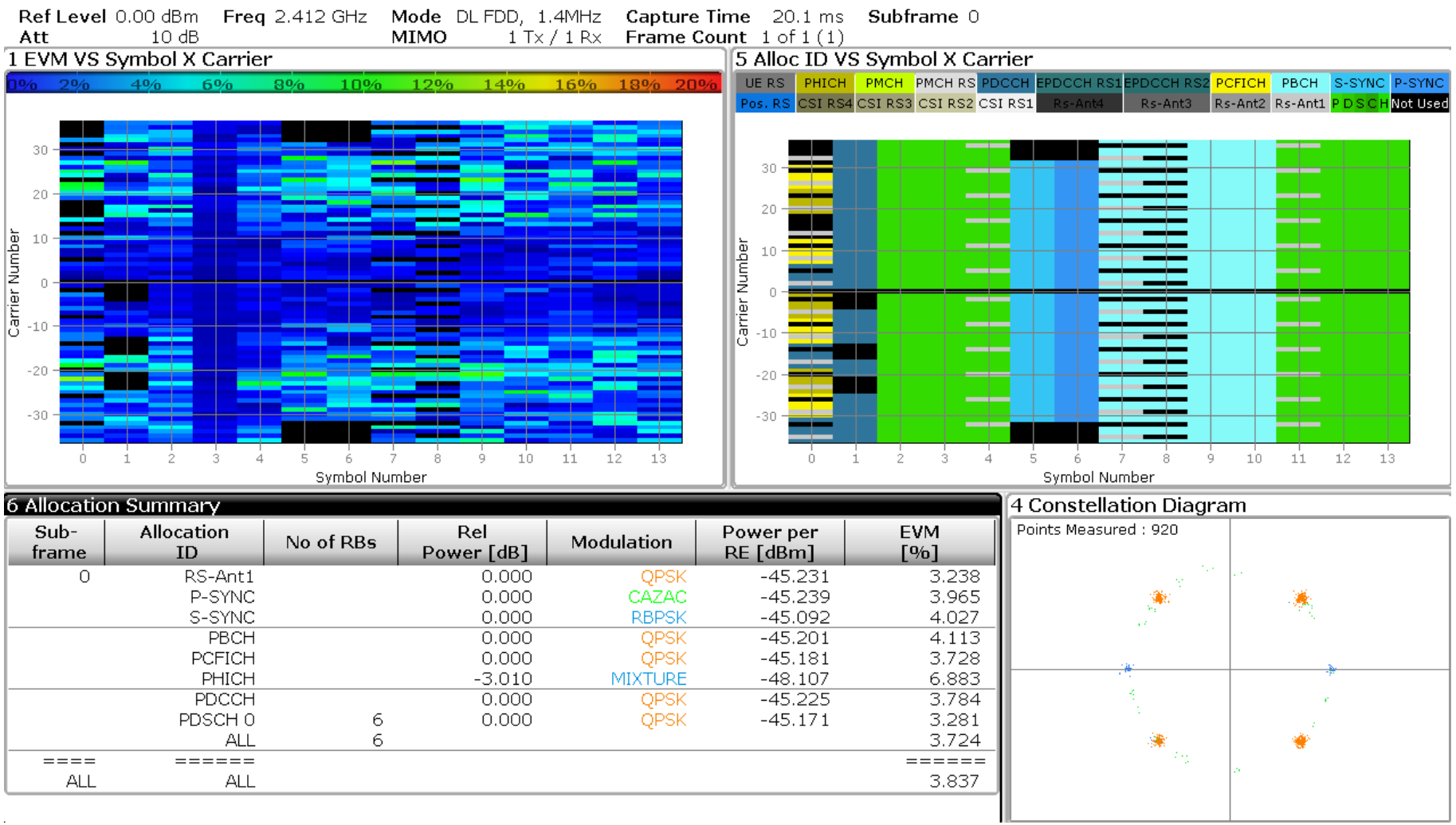

Sub-frame	Allocation ID	No of RBs	Rel Power [dB]	Modulation	Power per RE [dBm]	EVM [%]
0	RS-Ant1		0.000	QPSK	-45.231	3.238
	P-SYNC		0.000	CAZAC	-45.239	3.965
	S-SYNC		0.000	RBPSK	-45.092	4.027
	PBCH		0.000	QPSK	-45.201	4.113
	PCFICH		0.000	QPSK	-45.181	3.728
	PHICH		-3.010	MIXTURE	-48.107	6.883
	PDCCH		0.000	QPSK	-45.225	3.784
	PDSCH 0	6	0.000	QPSK	-45.171	3.281
	ALL	6				3.724
====	======					======
ALL	ALL					3.837

Fig. 4.10: Snapshot of the R&S FSW26 signal analyzer display (co-channel inter-system coexistence analysis scenario)

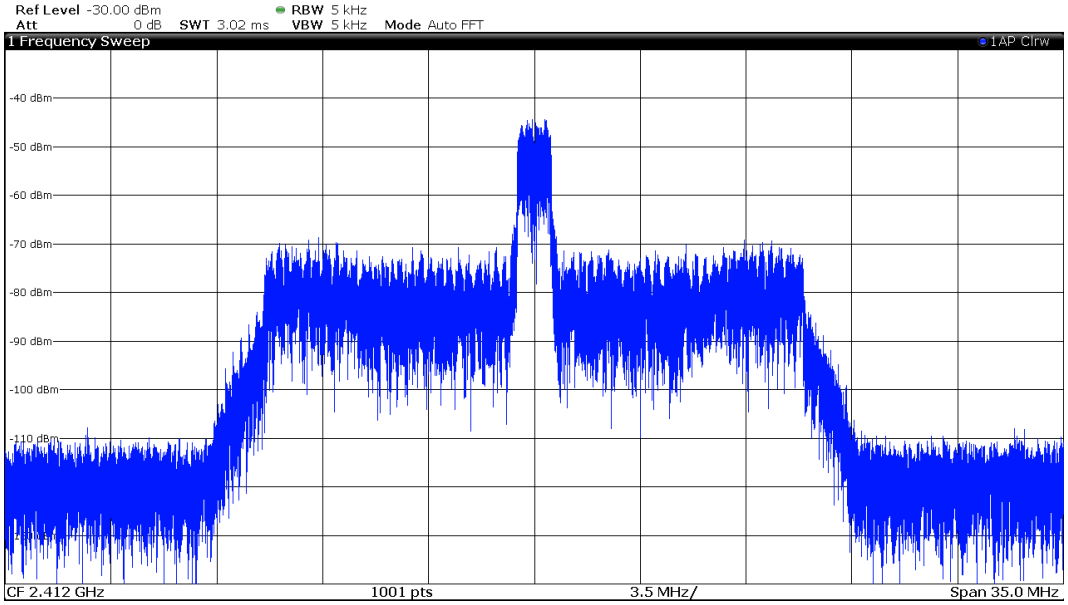

Fig. 4.11: Example of measured spectrum of co-channel inter-system coexistence analysis scenario (CNIR = 30 dB)

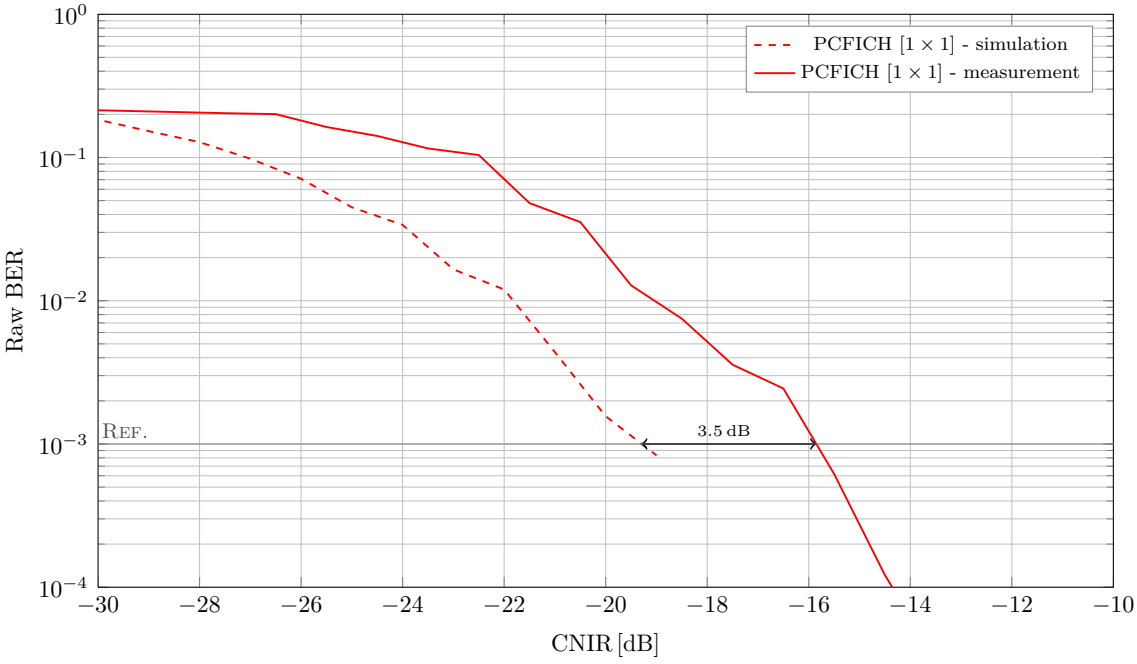

Fig. 4.12: Measured and simulated results of co-channel inter-system interference (raw BER) in PCFICH, SISO antenna mode

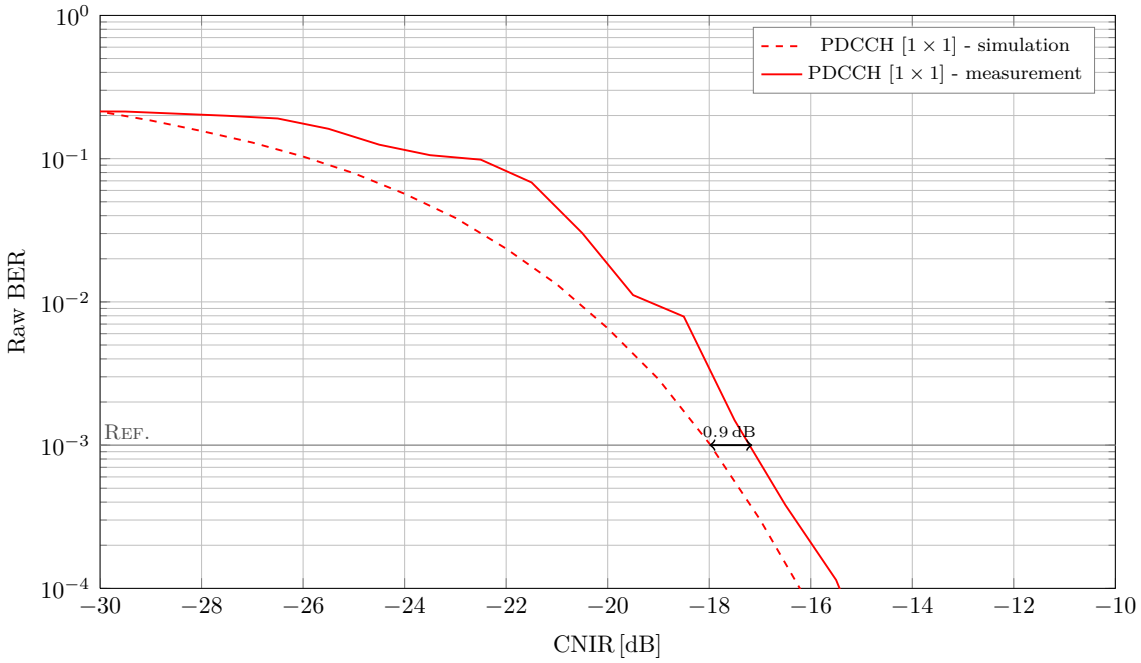

Fig. 4.13: Measured and simulated results of co-channel inter-system interference (raw BER) in PDCCH, SISO antenna mode

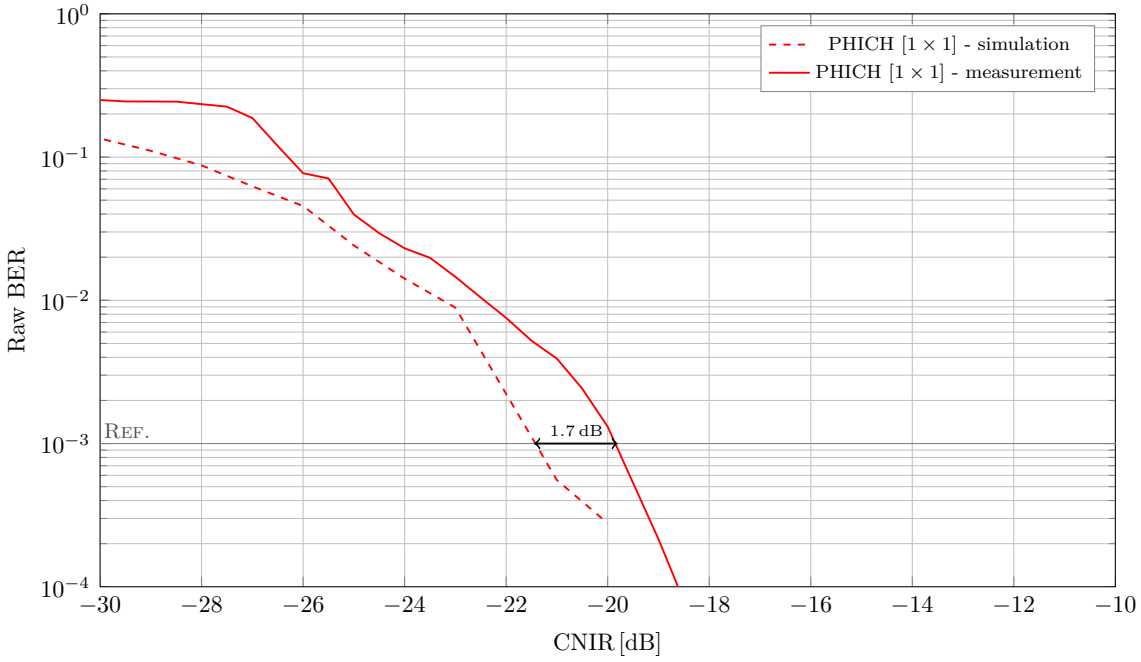

Fig. 4.14: Measured and simulated results of co-channel inter-system interference (raw BER) in PHICH, SISO antenna mode

4.4 Summary

This chapter described in detail LTE and Wi-FI co-channel inter-system interference analysis in 2.4 GHz ISM band and presented simulation and measurement results. Presented coexistence scenario has a pair of LTE transmitter and receiver in downlink direction and single interfering Wi-Fi transmitter. Simulations were performed as a passband in MATLAB environment on a personal computer using GPU with CUDA technology. Simulated BER values indicates a very good performance of all LTE physical control channels in downlink in the case of co-channel inter-system interferences. CNIR reference values in which the BER of transmitted control information is equaling to 10^{-3} are within the range of -29 to -23 dB.

A measurement of raw BER and a comparison with simulated raw BER values was also performed. The measurement of co-channel inter-system coexistence was accomplished in laboratory environment using Rohde & Schwarz measuring devices according to the same scenario as in the case of the simulation. The comparison of the simulated and measured raw BER results indicates minimal differences. Further, the simulator was optimized according to the results of the initial measurement. The measured results also indicate very high resistance of LTE control channels against interference in 2.4 GHz ISM band. Sec. 4.3 also presents a basic operating manual for measuring of EVM (raw BER) value of LTE control channels. The results of co-channel interference analysis of LTE control channels and Wi-Fi in 2.4 GHz ISM band have never been presented (August, 2014).

5 RECOMMENDATION FOR OPERATION

Recommendations for reliable operation and low BER of the LTE control information in uplink and downlink are listed in this chapter. The following general recommendations for operation refer to the U-LTE coexistence analysis results (Chap. 4). Preconditions are Pico eNodeB, 2.4 GHz ISM band and co-channel inter-system interference.

- It is necessary to keep the power level of the interfering system in the 2.4 GHz ISM band which was determined by the Czech Telecommunication Office (radiated power level $P_{\text{out}} < 100$ mW EIRP, power spectral density 10 dBm/MHz maximally), channel spectral mask and U-LTE receiver sensitivity level [73,74]

- Wi-Fi systems based on the IEEE 802.11b/g standard should not be used in the same Picocell area as U-LTE. The channel spectral mask defined for IEEE 802.11b/g is not strict as in the case of IEEE 802.11n [75]. It causes higher undesirable power emissions to adjacent channels.

- It is necessary to keep a guard band between separated U-LTE and Wi-Fi channels (this requirement has not been standardized).

- It is recommended to use multiple-antenna technology in U-LTE (transmitting diversity in downlink and receiving diversity in uplink). It is also appropriate to use beamforming technology and recent antenna arrays in picocells.

- Carrier to Noise and Interference Ratio (CNIR) should be higher than or equal to -20 dB (referring to U-LTE power level, see Sec. 4.2.2).

The following detailed recommendations for operation refer to LTE control channel simulations in baseband (Sec. 3.2 and 3.3).

- It is appropriate to send HARQ-ACK information in uplink using PUCCH format 1A or 2A.

- CQI information should be transmitted using PUSCH encapsulated into short segments (Reed-Muller channel coding).

- The RI and HARQ-ACK information should be transmitted using the PUSCH placeholder technique with the 64QAM modulation scheme.

- It is appropriate to use transmitting diversity in downlink at least with antenna configuration [4×2] and [2×2] (especially in fading channels).

6 CONCLUSION

The aim of the thesis is an investigation of the signal processing in the LTE physical control channels, creation of mathematical models and performing baseband simulations in AWGN and fading channels as well as a coexistence analysis. The next aim is creation of a scenario for coexistence analysis of LTE and an interfering system. Results of the coexistence analysis simulation should be compared with measured coexistence results. At last, recommendations for reliable operation of LTE should be specified.

Signal processing of control information in LTE in uplink (PUCCH, PUSCH) and downlink (PCFICH, PDCCH, PHICH) is described in Chap. 3. The simulator of control information transmission was created in the MATLAB simulation environment. Simulations of control information transmission were performed as a baseband in AWGN and fading channels for different system settings. The influence of MIMO technology on receiving performance of control information especially in fading channels was examined. The performance results were qualitatively evaluated.

Chapter 4 is focused on the coexistence of the LTE system and different wireless or cellular standards in a shared frequency band. The concept of using LTE in unlicensed bands (U-LTE concept) is presented and discussed as well as the coexistence scenario. The coexistence scenario deals with using LTE in 2.4 GHz ISM unlicensed band only. The co-channel inter-system interference is considered in the scenario as the worst possible type of interference. It represents the state when broadcasting in the picocell is not controlled. The IEEE 802.11n was chosen as an interfering wireless standard for 2.4 GHz ISM band. The scenario is created according to the newest information presented by the world's leading manufacturers of microchips for mobile applications. The LTE coexistence simulator was also created in MATLAB environment. The details of the created simulator are presented in Sec. 4.2 as well as the coexistence analysis simulation results (co-channel inter-system interference). Notice that mentioned coexistence simulations are performed as a passband (f_c>2.4 GHz). This highly computationally demanding problem was computed using a graphical processing unit (GPU) and CUDA NVIDIA technology.

Section 4.3 is focused on verifying the simulated coexistence results using a measurement of LTE devices in a laboratory. Measurement is performed according to the coexistence scenario presented in Sec. 4. A signal generator Rohde & Schwarz SMU200A generates the useful LTE signal as well as the interfering Wi-Fi signal. A modern measuring device Rohde & Schwarz FSW26 is used as a receiver and analyzer of the LTE signal. The simulated and the measured raw BER results are compared and the difference between them is no more than 3.5 dB in the case of PCFICH. Afterwards, the simulator is optimized according to previously measured results.

The recommendations for an optimized operation of the LTE system are presented in Chapter 5. Reliable operation of LTE is maintained via low bit error rates in the control channels. It can be noted that Quality of Service in shared bands should be ensured mainly by cooperating eNodeBs and mobile operators.

Application of LTE in the unlicensed frequency bands and its coexistence with former wireless standards is a contemporary topic. An analysis of interference influence on the LTE control channels in ISM band has not been found in journals or conferences yet (state up to August, 2014). This thesis presents a comprehensive analysis of the bit error rates in LTE control channels in baseband and passband (2.4 GHZ ISM band). All simulation results were presented in two international journals [51, 52], international conferences [53–55], student conference [56] and journal [50]. Moreover, the LTE uplink control information simulator created in MATLAB is available for free [76].

Hereafter, a complex system level and link level performance analysis of interference influence on the control channels of LTE system in 2.4 GHz and 5 GHz ISM band should be performed. The system level analysis could bring novel algorithms to network management in 2.4 GHz ISM bands.

REFERENCES

[1] S. Sesia, I. Toufik, and M. Baker, *LTE - The UMTS Long Term Evolution: From Theory to Practice*. Wiley, 2009. [Online]. Available: http://books.google.cz/books?id=beIaPXLzYKcC

[2] "Requirements for Evolved UTRA (E-UTRA) and Evolved UTRAN (E-UTRAN), Release 8," 3rd Generation Partnership Project, Version 8.0.0 TS 25.913, Dec. 2009. [Online]. Available: http://www.3gpp.org/ftp/Specs/archive/25_series/25.913/25913-800.zip

[3] "Evolved universal terrestrial radio access (E-UTRA); LTE physical layer - general description, Release 8," 3rd Generation Partnership Project, Version 8.3.0 TS 36.201, Mar. 2009. [Online]. Available: http://www.3gpp.org/ftp/Specs/archive/36_series/36.201/36201-830.zip

[4] M. Andersson, A. Wolfgang, C. Orlenius, and J. Carlsson, *Long Term Evolution - 3GPP LTE radio and cellular technology*. CRC press, 2009, ch. Measuring performance of 3GPP LTE terminals and small base stations in reverbation chambers, pp. 415–460.

[5] "Evolved universal terrestrial radio access (E-UTRA); LTE physical channels and modulation, Release 8," 3rd Generation Partnership Project, Version 8.9.0 TS 36.211, Dec. 2009. [Online]. Available: http://www.3gpp.org/ftp/Specs/archive/36_series/36.211/36211-890.zip

[6] F. Khan, *LTE for 4G mobile broadband: air interface technologies and performance*, 1st ed. Cambridge, United Kingdom: Cambridge University Press, 2009.

[7] E. Dahlman, S. Parkvall, J. Sköld, and P. Beming, *3G Evolution: HSPA and LTE for mobile broadband*. Oxford, United Kingdom: Academic Press, 2007.

[8] "Evolved universal terrestrial radio access (E-UTRA); LTE physical layer - multiplexing and channel coding, Release 8," 3rd Generation Partnership Project, Version 8.8.0 TS 36.212, Dec. 2009. [Online]. Available: http://www.3gpp.org/ftp/Specs/archive/36_series/36.212/36212-880.zip

[9] B. Priyanto, H. Codina, S. Rene, T. B. Sorensen, and P. Mogensen, "Initial performance evaluation of DFT-spread OFDM based SC-FDMA for UTRA LTE uplink," in *Vehicular Technology Conference, 2007. VTC2007-Spring. IEEE 65th*, 2007, pp. 3175–3179. [Online]. Available: http://ieeexplore.ieee.org/stamp/stamp.jsp?tp=&arnumber=4213078

[10] G. Berardinelli, L. Ruiz de Temino, S. Frattasi, M. Rahman, and P. Mogensen, "OFDMA vs. SC-FDMA: performance comparison in local area IMT-A scenarios," *Wireless Communications, IEEE*, vol. 15, no. 5, pp. 64–72, 2008. [Online]. Available: http://ieeexplore.ieee.org/stamp/stamp.jsp?tp=&arnumber=4653134

[11] H. Marcelino, Z. Hua-shen, and G. Yanbin, "Performance analysis of OFDMA system in next generation wireless communication networks," in *Computer Science and Information Technology (ICCSIT), 2010 3rd IEEE International Conference on*, vol. 8, 2010, pp. 335–339. [Online]. Available: http://ieeexplore.ieee.org/stamp/stamp.jsp?tp=&arnumber=5564799

[12] F. Rezaei, M. Hempel, and H. Sharif, "A comprehensive performance analysis of LTE and Mobile WiMAX," in *Wireless Communications and Mobile Computing Conference (IWCMC), 2012 8th International*, 2012, pp. 939–944. [Online]. Available: http://ieeexplore.ieee.org/stamp/stamp.jsp?tp=&arnumber=6314331

[13] A. Elnashar and M. El-Saidny, "Looking at LTE in practice: A performance analysis of the LTE system based on field test results," *Vehicular Technology Magazine, IEEE*, vol. 8, no. 3, pp. 81–92, 2013. [Online]. Available: http://ieeexplore.ieee.org/stamp/stamp.jsp?tp=&arnumber=6568955

[14] C. Mehlführer, M. Wrulich, J. C. Ikuno, D. Bosanska, and M. Rupp, "Simulating the Long Term Evolution physical layer," in *17th European Signal Processing Conference (EUSIPCO 2009)*, Glasgow, United Kingdom, Aug. 2009. [Online]. Available: http://publik.tuwien.ac.at/files/PubDat_175708.pdf

[15] *LTE Downlink Link Level Simulator*, Vienna University of Technology, Vienna, Austria. [Online]. Available: http://www.nt.tuwien.ac.at/ltesimulator/

[16] S. Thiruvengadam and L. Jalloul, "Performance analysis of the 3GPP LTE physical control channels," *EURASIP Journal on wireless communications and networking*, vol. 2010, no. 914934, 2010. [Online]. Available: http://jwcn.eurasipjournals.com/content/2010/1/914934

[17] J. Liu, R. Love, K. Stewart, and M. Buckley, "Design and analysis of LTE Physical Downlink Control Channel," in *Vehicular Technology Conference, 2009. VTC Spring 2009. IEEE 69th*, 2009, pp. 1–5.

[18] P. Frenger, H. Koorapaty, and J.-C. Guey, "Evaluation of control channel performance with adaptive radio unit activation in LTE," in *Vehicular Technology Conference, 2012. VTC Spring 2012. IEEE 75th*, 2012, pp. 1–5.

[19] F. Rezaei, M. Hempel, and H. Sharif, "LTE PHY performance analysis under 3GPP standards parameters," in *Computer Aided Modeling and Design of Communication Links and Networks (CAMAD), 2011 IEEE 16th International Workshop on*, 2011, pp. 102–106. [Online]. Available: http://ieeexplore.ieee.org/stamp/stamp.jsp?tp=&arnumber=5941095

[20] M. Suarez and O. Zlydareva, "LTE transceiver performance analysis in uplink under various environmental conditions," in *Ultra Modern Telecommunications and Control Systems and Workshops (ICUMT), 2012 4th International Congress on*, 2012, pp. 84–88. [Online]. Available: http://ieeexplore.ieee.org/stamp/stamp.jsp?tp=&arnumber=6459780

[21] N. Hou, K. Niu, Z. He, and S. Sun, "Test and performance analysis of PUSCH channel of LTE system," in *Microwave, Antenna, Propagation and EMC Technologies for Wireless Communications (MAPE), 2013 IEEE 5th International Symposium on*, 2013, pp. 110–114. [Online]. Available: http://ieeexplore.ieee.org/stamp/stamp.jsp?tp=&arnumber=6689964

[22] D. Wang, S. Yang, Y. Liao, and Y. Liu, "Efficient receiver scheme for LTE PUCCH," *Communications Letters, IEEE*, vol. 16, no. 3, pp. 352–355, 2012.

[23] I. L. J. Da Silva, A. L. F. De Almeida, F. R. P. Cavalcanti, R. Baldemair, and S. Falahati, "A new multi-user receiver for PUCCH LTE format 1," in *Signal Processing Advances in Wireless Communications (SPAWC), 2010 IEEE Eleventh International Workshop on*, 2010, pp. 1–5.

[24] T. Chaitanya and E. Larsson, "Improving 3GPP-LTE uplink control signaling performance using complex-field coding," *Vehicular Technology, IEEE Transactions on*, vol. 62, no. 1, pp. 161–171, 2013. [Online]. Available: http://ieeexplore.ieee.org/stamp/stamp.jsp?tp=&arnumber=6287064

[25] D. Khan and B. Priyanto, "Performance evaluation of frequency hopping schemes in UTRA-LTE uplink," in *Student Paper, 2008 Annual IEEE Conference*, 2008, pp. 1–5. [Online]. Available: http://ieeexplore.ieee.org/stamp/stamp.jsp?tp=&arnumber=4460562

[26] S. Donthi and N. Mehta, "Performance analysis of user selected subband channel quality indicator feedback scheme of lte," in *Global Telecommunications Conference (GLOBECOM 2010), 2010 IEEE*, 2010, pp. 1–6.

[27] Z. Bečvář and P. Mach, "Modelování bezdrátových sítí v prostředí MATLAB," 2010, přednáška KTT FE ČVUT v Praze.

[28] *Communiaction System Toolbox: Bit Error Rate (BER). MATLAB 2012a: Project documentation*, MathWorks Inc., 2012. [Online]. Available: http://www.mathworks.com/help/toolbox/comm/ug/bsvzixi.html

[29] B. Wojtowicz, "Open LTE: free simulation tool," version 00.08.01.2013. [Online]. Available: http://openlte.sourceforge.net/

[30] G. Piro, L. Grieco, G. Boggia, F. Capozzi, and P. Camarda, "Simulating LTE cellular systems: An open-source framework," *Vehicular Technology, IEEE Transactions on*, vol. 60, no. 2, pp. 498–513, 2011. [Online]. Available: http://telematics.poliba.it/index.php/en/tools/97-tools/tools/158-lte-sim

[31] *4G Evolution Lab - LTE and LTE-Advanced Toolbox and Blockset - LTE Toolbox User Guide: Hybrid Automatic Repeat Request Indicator Channel*, Steepest Ascent, Glasgow, United Kingdom, 2008. [Online]. Available: http://www.steepestascent.com/

[32] H. Holma and A. Toskala, *LTE for UMTS: OFDMA and SC-FDMA based radio access*, 1st ed. New York: Wiley and Sons, 2009.

[33] "Evolved Universal Terrestrial Radio Access (E-UTRA); Base Station (BS) radio transmission and reception," 3rd Generation Partnership Project, Version 8.13.0 TS 36.104, Jul. 2012. [Online]. Available: http://www.3gpp.org/ftp/Specs/archive/36_series/36.104/36104-8d0.zip

[34] *MATLAB documentation*, R2012b ed., MathWorks Inc., U.S. [Online]. Available: http://www.mathworks.com/help/matlab/

[35] H. Myung, J. Lim, and D. Goodman, "Single carrier FDMA for uplink wireless transmission," *Vehicular Technology Magazine, IEEE*, vol. 1, no. 3, pp. 30–38, Sept 2006. [Online]. Available: http://hgmyung.googlepages.com/SingleCarrierFDMA_VTmagSep06.pdf

[36] A. Saadani, S. Wendt, P. Gelp, and D. Duponteil, "A tapped delay line model of multipath channel for CDMA systems," in *Control, Communications and Signal Processing, 2004. First International Symposium on*, March 2004, pp. 783–786.

[37] "Selection procedures for the choice of radio transmission technologies of the UMTS," ETSI, Tech. Rep. 101.112, Nov. 1997. [Online]. Available: http://www.etsi.org/deliver/etsi_tr/101100_101199/101112/03.01.00_60/tr_101112v030100p.pdf

[38] Orthogonal Frequency-Division Multiple Access. Wikipedia. [Online]. Available: http://en.wikipedia.org/wiki/Orthogonal_frequency-division_multiple_access

[39] "Evolved universal terrestrial radio access (E-UTRA); LTE physical layer procedures, Release 8," 3rd Generation Partnership Project, Version 8.8.0 TS 36.213, Sep. 2009. [Online]. Available: http://www.3gpp.org/ftp/Specs/archive/36_series/36.213/36213-880.zip

[40] C. Johnson, *Long Term Evolution in bullets*, 1st ed. Northampton, England: LTE Bullets, 2010.

[41] Y. Wen, W. Huang, and Z. Zhang, "CAZAC sequence and its application in LTE random access," in *Information Theory Workshop, 2006. ITW '06 Punta del Este. IEEE*, 2006, pp. 544–547.

[42] M. Pesavento and W. Mulder, "LTE tutorial, part 1: LTE basics." in *Femto forum plenary*, Reading, United Kingdom, Jun. 2010.

[43] "Evolved universal terrestrial radio access (E-UTRA) and Evolved universal terrestrial radio access network (E-UTRAN); Overall description; Stage 2," 3rd Generation Partnership Project, Version 8.12.0 TS 36.300, Mar. 2010. [Online]. Available: http://www.3gpp.org/ftp/Specs/archive/36_series/36.300/36300-8c0.zip

[44] N. Kolehmainen, J. Puttonen, P. Kela, T. Ristaniemi, T. Henttonen, and M. Moisio, "Channel quality indication reporting schemes for UTRAN Long Term Evolution downlink," in *Vehicular Technology Conference, 2008. VTC Spring 2008. IEEE*, 2008, pp. 2522–2526.

[45] Y.-H. Nam and J. Zhang, "Method and system for mapping HARQ-ACK bits," US Patent WO/2011/159 131, 2011. [Online]. Available: http://patentscope.wipo.int/search/en/WO2011159131

[46] I. G. Kim, Y. Han, Y.-H. Kim, and S. C. Bang, "Transmit diversity and multiplexing methods for 3G-LTE downlink control channels," in *Vehicular Technology Conference, 2006. VTC-2006 Fall. 2006 IEEE 64th*, Sept 2006, pp. 1–4. [Online]. Available: http://ieeexplore.ieee.org/xpl/articleDetails.jsp?arnumber=4109475

[47] P. Hosein, "Resource allocation for the LTE Physical Downlink Control Channel," in *GLOBECOM Workshops, 2009 IEEE*, Nov 2009, pp. 1–5. [Online]. Available: http://ieeexplore.ieee.org/xpl/login.jsp?tp=&arnumber=5360730

[48] D. J. Mackay, "Error correcting codes for the binary symmetric channel: Repetition codes," Information Theory, Pattern Recognition & Neural Networks Information Theory, 1997. [Online]. Available: http://www.inference.phy.cam.ac.uk/mackay/itprnn/1997/l1/node6.html

[49] L. Pullum, *Software Fault Tolerance Techniques and Implementation.* Artech House, 2001. [Online]. Available: http://books.google.cz/books?id=hqXvxsO5xz8C

[50] J. Milos, S. Hanus, and P. Kejik, "Bitová chybovost v řídicím kanálu PCFICH systému LTE," *Elektrorevue*, vol. 2012, pp. 1–5, Jan. 2012.

[51] J. Milos and S. Hanus, "Performance analysis of PCFICH and PDCCH LTE control channels," *Radioenegineering*, vol. 2, pp. 445–451, 2014.

[52] J. Milos and S. Hanus, "Analysis of LTE physical Hybrid ARQ control channel," *Advances in Electrical and Computer Engineering*, no. 2, pp. 97–100, May 2014. [Online]. Available: http://www.aece.ro/displaypdf.php?year=2014&number=2&article=16

[53] J. Milos and S. Hanus, "Performance analysis of PCFICH and PDCCH LTE control channel," in *ICDT 2013 The Eighth International Conference on Digital Telecommunications*, vol. 1. Venice: IARIA Journal, 2013, pp. 32–37.

[54] J. Milos and S. Hanus, "Simulation of UCI transmission via PUCCH in LTE uplink," in *24th International Conference Radioelektronika*, Bratislava, 2014, pp. 1–4.

[55] J. Milos, S. Hanus, and M. Slanina, "Analysis and simulation of aperiodically reported signaling in LTE uplink," in *37th International conference on telecommunications and signal processing.* Berlin: TSP, July 2014.

[56] J. Milos, "Performance analysis of PCFICH LTE control channel," in *Proceedings of the 18th Conference STUDENT EEICT*, vol. 3, 2012, pp. 19–23.

[57] "Extending LTE Advanced to unlicensed spectrum," Qualcomm Incorporated, White paper, Dec. 2013. [Online]. Available: http://www.qualcomm.com/media/documents/files/white-paper-extending-lte-advanced-to-unlicensed-spectrum.pdf

[58] "U-LTE: Unlicensed Spectrum Utilization of LTE," Huawei, White paper, Feb. 2014. [Online]. Available: http://www.huawei.com/ilink/en/download/HW_327803

[59] "Article 1 - terms and definitions," life.itu.ch, Oct. 2009. [Online]. Available: http://life.itu.ch/radioclub/rr/art01.htm

[60] "LTE Small Cell v.s. WiFi User Experience," Huawei, White paper, 2013. [Online]. Available: www.huawei.com/ilink/en/download/HW_323974

[61] *802.11n, Part 11: Wireless LAN Medium Access Control (MAC) and Physical Layer (PHY) Specifications*, IEEE Computer Society Std., Oct. 2009. [Online]. Available: http://standards.ieee.org/getieee802/download/802.11n-2009.pdf

[62] "802.11ac technology introduction," Rohde & Schwarz, White paper, Dec. 2013. [Online]. Available: http://cdn.rohde-schwarz.com/dl_downloads/dl_application/application_notes/1ma192/1MA192_7e_80211ac_technology.pdf

[63] "NVIDIA CUDA Parallel Programming and Computing Platform," August 2014. [Online]. Available: http://www.nvidia.com/object/cuda_home_new.html

[64] A. Zubow and R. Sombrutzki, "Reinvestigating channel orthogonality-adjacent channel interference in IEEE 802.11n networks," Tech. Rep., 2011. [Online]. Available: http://sar.informatik.hu-berlin.de/research/publications/SAR-PR-2011-14/aci_80211n_.pdf

[65] List of WLAN channels. Wikipedia. [Online]. Available: http://en.wikipedia.org/wiki/List_of_WLAN_channels

[66] "R&S SMU200A Vector Signal Generator Specifications," Rohde & Schwarz GmbH & Co KG, Tech. Rep. 08.00, January 2012. [Online]. Available: http://cdn.rohde-schwarz.com/pws/dl_downloads/dl_common_library/dl_brochures_and_datasheets/pdf_1/SMU_dat-sw-en.pdf

[67] *R&S SMU200A Vector Signal Generator Operating Manual*, 1st ed., Rohde & Schwarz GmbH & Co KG, 2012. [Online]. Available: http://cdn.rohde-schwarz.com/pws/dl_downloads/dl_common_library/dl_manuals/gb_1/s/smu200a_1/RS_SMU200A_Operating.pdf

[68] "R&S FSW Signal and Spectrum Analyzer Specifications," Rohde & Schwarz GmbH & Co KG, Tech. Rep. 10.00, March 2014. [Online]. Available: http://cdn.rohde-schwarz.com/pws/dl_downloads/dl_common_library/dl_brochures_and_datasheets/pdf_1/FSW_dat-sw_en_5214-5984-22_v1000.pdf

[69] *R&S FSW Signal and Spectrum Analyzer User Manual*, 1st ed., Rohde & Schwarz GmbH & Co KG, 2014. [Online]. Available: http://cdn.rohde-schwarz.com/pws/dl_downloads/dl_common_library/dl_manuals/gb_1/f/fsw_1/FSW_UserManual_en_19.pdf

[70] *R&S FSW-K10x (LTE Downlink) LTE Downlink Measurement Application User Manual*, 1st ed., Rohde & Schwarz GmbH & Co KG, 2014. [Online]. Available: http://cdn.rohde-schwarz.com/pws/dl_downloads/dl_common_library/dl_manuals/gb_1/f/fsw_1/FSW_K10x_LTE_DL_UserManual_en_07.pdf

[71] R. Shafik, S. Rahman, and R. Islam, "On the extended relationships among EVM, BER and SNR as performance metrics," in *Electrical and Computer Engineering, 2006. ICECE '06. International Conference on*, Dec 2006, pp. 408–411. [Online]. Available: http://ieeexplore.ieee.org/xpl/abstractCitations.jsp?arnumber=4178493&tag=1

[72] "Evolved Universal Terrestrial Radio Access (E-UTRA); Radio Frequency (RF) requirements for LTE Pico Node B," 3rd Generation Partnership Project, Version 9.0.0 TR 136.931, May 2011. [Online]. Available: http://www.etsi.org/deliver/etsi_tr/136900_136999/136931/09.00.00_60/tr_136931v090000p.pdf

[73] "Evolved Universal Terrestrial Radio Access (E-UTRA); User Equipment (UE) radio transmission and reception," 3rd Generation Partnership Project, Version 10.3.0 TS 136.101, June 2011. [Online]. Available: http://www.etsi.org/deliver/etsi_ts/136100_136199/136101/10.03.00_60/ts_136101v100300p.pdf

[74] "Všeobecné oprávnění č. VO-R/12/06.2010-9 k využívání rádiových kmitočtů a k provozování zařízení pro širokopásmový přenos dat v pásmech 2,4 GHz až 66 GHz," Czech Telecommunication Office, Prague, č. VO-R/12/06.2010-9 65 372/2010-613, June 2010. [Online]. Available: http://www.ctu.cz/cs/download/oop/rok_2010/vo-r_12-06_2010-09.pdf

[75] IEEE 802.11a/b/g WLAN spectral masks. [Online]. Available: http://www.rfcafe.com/references/electrical/wlan-masks.htm

[76] J. Milos and S. Hanus, "LTE-UL- CCH; LTE uplink control information simulator," March 2013. [Online]. Available: http://www.urel.feec.vutbr.cz/index.php?page=software

LIST OF ABBREVIATIONS

3GPP	3rd Generation Partnership Project
ACI	adjacent inter-system interference analysis
ACK	acknowledgement indicator
ACLR	Adjacent Channel Leakage Ratio
ADC	analog to digital converter
AWGN	Additive White Gaussian Noise
BER	bit error ratio
BLER	block error ratio
BPSK	Binary Phase Shift Keying
BS	base station
CCE	Control Channel Element
CCH	control channels
CCI	co-channel inter-system interference analysis
CFI	Control Format Indicator
CIR	Carrier to Interference Ratio
CP	cyclic prefix
CNIR	Carrier to Noise and Interference Ratio
CQI	Channel Quality Indicator
CRC	Cyclic redundancy check
CUDA	Compute Unified Device Architecture
DC	direct current
DCI	Downlink Control Information
DFT	Discrete Fourier Transform
DMRS	Demodulation Reference Symbols
DVB-T	Digital Video Broadcasting — Terrestrial
E-UTRAN	Evolved-UMTS Terrestrial Radio Access Network
EVM	Error Vector Magnitude
FDD	Frequency Division Duplex

FFT	Fast Fourier Transform
FPGA	field-programmable gate array
GPL	general public license
GPU	graphics processing unit
GSM	Global System for Mobile Communications
HARQ	Hybrid Automatic Repeat Request
HI	Hybrid ARQ Indicator
HSPA+	Evolved High-Speed Packet Access
HSxPA	High-Speed Packet Access
IDFT	Inverse Discrete Fourier Transform
IEEE	Institute of Electrical and Electronics Engineers
IFFT	Inverse Fast Fourier Transform
IMT	International Mobile Telecommunications
IP	Internet Protocol
ISM	Industry, Science and Medical radio bands
ITU-R	International Telecommunication Union Radiocommunication Sector
LLR	log-likelihood ratio
LLS	link level simulations
LTE	Long Term Evolution
MIMO	Multiple input multiple output
MME	Mobility Management Entity
MRC	Maximal Ratio Combining
NACK	nonacknowledgement indicator
NDI	New Data Indicator
OFDM	Orthogonal Frequency Division Multiplex
OFDMA	Orthogonal Frequency Division Multiple Access
PAPR	Peak to Average Power Ratio
PBCH	Physical Broadcast Channel
PCFICH	Physical Control Format Indicator Channel

PDCCH	Physical Downlink Control Channel
PDF	Probability density function
PDSCH	Physical Downlink Shared Channel
PedA/B	Pedestrian A/B
PHICH	Physical Hybrid ARQ Indicator Channel
PHY	physical layer
PMCH	Physical Multicast Channel
PMI	Precoding Matrix Indicator
PRACH	Physical Random Access Channel
PSS	Primary Synchronization Signal
PUCCH	Physical Uplink Control Channel
PUSCH	Physical Uplink Shared Channel
QAM	Quadrature Amplitude Modulation
QoS	Quality of Service
QPP	Quadratic Permutation Polynomial
QPSK	Quadrature Phase Shift Keying
RB	resource block
RE	resource element
RF	radio frequency
RI	Rank Indicator
RNTI	Radio Network Temporary Identifier
RRC	Radio Resource Control
RS	reference signal
RX	receiver/receiving
RxD	receiving diversity
SC-FDMA	Single Carrier-Frequency Division Multiple Access
SDL	Supplemental Downlink
SFN	Single Frequency Network
SISO	Single input single output

SLS	system level simulations
SNR	Signal to Noise Ratio
SR	Scheduling Request
SRRC	square-root raised cosine
SRS	Sounding Reference Signal
SSD	soft-sphere decoders
SSS	Secondary Synchronization Signal
TDD	Time Division Duplex
TDL	Tapped delay line
TPC	Transmit Power Commands
TV	television
TX	transmitter/transmitting
TxD	transmitting diversity
UCI	Uplink Control Information
UE	user equipment
UMTS	Universal Mobile Telecommunications System
VehA/B	Vehicular A/B
WCDMA	Wideband Code Division Multiple Access
WiMAX	Worldwide Interoperability for Microwave Access
WLAN	Wireless Local Area Network
WPAN	Wireless Personal Area Network
WRC	World Radiocommunication Conference

LIST OF SYMBOLS

α	cyclic shift of Zadoff-Chu sequence
β	Roll-off factor of raised cosine filter
Δf_{sc}	subcarrier frequency spacing
$\mathbf{a}$	control information before channel coding
$\mathbf{a}'$	vector of control information after channel decoding
$\mathbf{b}$	vector of bits after channel coding
$\mathbf{b}'$	vector of bits before channel decoding
$\tilde{\mathbf{b}}$	vector of scrambled bits
B_{sys}	LTE system bandwidth
B_{DL}	LTE downlink used system bandwidth
B_{UL}	LTE uplink used system bandwidth
$\mathbf{c}$	cell-specific pseudo-random sequence
$\mathbf{d}$	vector of modulated symbols in transmitter
$\mathbf{d}'$	vector of modulated symbols in receiver
e_k	error vector
erfc ()	complementary error function
E_{b}	signal energy per bit
f_{b}	codeword bit rate
f_{c}	carrier frequency
f_{cr}	chip rate
f_{interf}	carrier frequency of interfering signal
$\mathbf{F}$	vector of application data in PUSCH
G	generating polynomial
$\mathbf{G}$	vector of multiplexed bits in PUSCH
$\mathbf{H}$	matrix of channel coefficients
$\hat{\mathbf{H}}$	matrix of estimated channel coefficients
k_{PHICH}	PHICH transmitting offset in a time domain
$\mathbf{K}$	interleaving matrix in PUSCH

$L(b)$	log-likelihood ratio of the transmitted bit b
M	number of constellation points in modulation scheme
M_{bit}	vector length in bits
M_{symb}	number of modulation symbols in PUSCH
$M_{\mathrm{sc}}^{\mathrm{PUSCH}}$	scheduled number of PUSCH subcarriers
n_{s}	slot number
n_{oc}	orthogonal sequence index in PUCCH
$n_{\mathrm{PHICH}}^{\mathrm{seq}}$	orthogonal sequence index within PHICH group
$\mathbf{N}$	noise vector (AWGN)
N_0	noise power spectral density
N_g	PHICH group scaling factor
N_{RX}	number of receiving antennas
N_{TX}	number of transmitting antennas
N_{symb}	number of OFDM symbols in a resource block
N_{sc}	number of subcarriers
N_{FFT}	FFT size
N_{RB}	number of resource blocks
$N_{\mathrm{sc}}^{\mathrm{RB}}$	number of subcarriers in a resource block
$N_{\mathrm{RE}}^{\mathrm{RB}}$	number of resource elements in a resource block
$N_{\mathrm{RB}}^{\mathrm{UL/DL}}$	number of resource blocks in uplink or downlink
$N_{\mathrm{seq}}^{\mathrm{PUCCH}}$	length of the Zadoff-Chu sequence
$N_{\mathrm{SF}}^{\mathrm{PUCCH}}$	PUCCH spreading factor
$N_{\mathrm{PHICH}}^{\mathrm{group}}$	number of PHICH groups
$N_{\mathrm{PHICH}}^{\mathrm{seq}}$	number of orthogonal sequences within PHICH group
$N_{\mathrm{SF}}^{\mathrm{PHICH}}$	PHICH orthogonal sequence spreading factor
P_{b}	bit error probability
P_{C}	power level of useful signal
P_{I}	power level of interfering signal
$P_{\mathrm{weight}}^{\mathrm{PHICH}}$	PHICH weighting coefficient

$P_{\mathrm{REFSENS}}^{\mathrm{QPSK}}$	receiver reference sensitivity of QPSK modulation scheme
Q_m	number of bits per modulation symbol in PUSCH
$\mathbf{Q}_{\mathrm{CQI}}$	CQI codeword in PUSCH
$\mathbf{Q}_{\mathrm{HARQ}}$	HARQ codeword in PUSCH
$\mathbf{Q}_{\mathrm{RI}}$	RI codeword in PUSCH
$r_{u,v}^{(\alpha)}$	Zadoff-Chu sequence
$\bar{r}_{u,v}$	base sequence
σ^2	noise variance of baseband signal
$s(t)$	transmitted baseband OFDM signal
$s'(t)$	received baseband OFDM signal
S_i	ideal constellation point of bit with index i
$S(n_{\mathrm{s}})$	scrambling sequence used in PUCCH
T	absolute temperature of receiver input
T_{cp}	cyclic prefix duration
T_{d}	duration of examined data symbols
T_{mb}	OFDM symbol main body duration
T_{rf}	radio frame duration
T_{s}	sample time
T_{sf}	subframe duration
T_{slot}	slot duration
T_{symb}	OFDM symbol duration
$w_{n_{\mathrm{oc}}}$	spreading orthogonal sequence
$\mathbf{x}_n$	vector of n modulated symbols before N-DFT operation
$\tilde{\mathbf{x}}_m$	vector of symbols after IFFT operation
$\hat{\mathbf{x}}$	vector of received symbols after inverse precoding
$\mathbf{X}$	vector of modulated symbols after N-DFT operation
$\tilde{\mathbf{X}}$	vector of modulated symbols after N-DFT operation mapped to subcarriers
$\mathbf{y}$	vector of MIMO precoded symbols
$\mathbf{z}$	matrix of complex-valued symbols

A APPENDIX

Tab. A.1: Outdoor to indoor and pedestrian test environment Tapped Delay Line parameters

Tap	Channel A		Channel B		Doppler
	Rel. delay [ns]	Avg. power [dB]	Rel. delay [ns]	Avg. power [dB]	spectrum
1	0	0	0	0	Classic
2	110	−9.7	200	−0.9	Classic
3	190	−19.2	800	−4.9	Classic
4	410	−22.8	1200	−8.0	Classic
5	-	-	2300	−7.8	Classic
6	-	-	3700	−23.9	Classic

Tab. A.2: Vehicular test environment, high antenna, Tapped Delay Line parameters

Tap	Channel A		Channel B		Doppler
	Rel. delay [ns]	Avg. power [dB]	Rel. delay [ns]	Avg. power [dB]	spectrum
1	0	0	0	−2.5	Classic
2	310	−1.0	300	0	Classic
3	710	−9.0	8900	−12.8	Classic
4	1090	−10.0	12900	−10.0	Classic
5	1730	−15.0	17100	−25.2	Classic
6	2510	−20.0	20000	−16.0	Classic

CURRICULUM VITAE

Personal	
Name	Jiří Miloš
Born	June 13th 1986 in Uherské Hradiště
Citizenship	Czech Republic
Contact	milosjiri@gmail.com
Education	
2010 – 2014	Brno University of Technology Department of Radio Electronics Doctoral's degree, Electronics and Communications Thesis: *Models of control channels in the LTE system*
2008 – 2010	Brno University of Technology Department of Radio Electronics Master's degree, Electronics and Communications Thesis: *Signal Processing in ZigBee System*
2005 – 2008	Brno University of Technology Department of Teleinformatics Bachelor's degree, Teleinformatics Thesis: *Cryptographic Methods of Data Security*
Experience	
09/2011 – 01/2012	Study stay at ESIEE Paris, France Topic: *Models of the LTE Physical Layer* Supervisor: prof. Geneviève Baudoin
Additional	
Languages	Czech, English
Specialization	mobile communications, wireless systems, simulation of communication systems, signal processing, electronics and measurement